Polytechnic University of Marche
Faculty of Engineering

A dissertation for the degree of Philosophiae Doctor
In Civil, Environmental, Building Engineering and Architecture

---

Monitoring and Self-diagnosis of Civil Engineering Structures: Classical and Innovative Applications

PhD Dissertation of:
Alessio Pierdicca

Supervisor
Prof. Stefano Lenci

Curriculum Supervisor
Prof. Stefano Lenci

XXIX Edition
November 2016

Abstract

Extreme events like explosions and earthquakes may have a deep impact on building safety. Seismic regions must live with these tragic events, so that continuous monitoring of structure health conditions is necessary in many cases.

Structural Health Monitoring (SHM) represents a powerful tool for the evaluation of dynamic behavior of monitored structures. Until a few years ago these techniques were widely employed especially in mechanical, aeronautical and aerospace engineering.

Nowadays, the reduction of equipment costs, the new generation of data acquisition systems, together with the continuous improvement of computational analysis have made it possible to apply SHM also to civil structures without strategic importance. SHM has moved from large infrastructures like bridges, dams and skyscrapers to historical heritage and residential buildings.

In this background, the present work tries to examine different aspects of SHM applications, especially referred to ordinary buildings.

Using Operational Modal Analysis (OMA) techniques, several civil structures have been monitored through a wired network sensor, in order to obtain the dynamic behavior in operating conditions. The relevant data collection provides a useful tool for calibrating the accuracy and sensitivity of similar SHM case studies.

Specific attention is focused in another important issue in civil and in mechanical engineering: detection of structural damages. Through a numerical approach, a new method for damage localization and quantification is proposed.

Besides the traditional wired acquisition system a Wireless Sensor Network (WSN) has been developed. The issues related to the usage of low-cost sensors and new generation data acquisition tools for non-destructive structural testing are discussed. Using the WSN an historical masonry building has been monitored, showing the positive results obtained following the Ambient Vibration Survey (AVS).

Sommario

Eventi estremi come esplosioni o terremoti possono avere un profondo impatto nella sicurezza degli edifici. Le zone sismiche devono convivere con questi tragici eventi, per questo monitorare in maniera continua le condizioni di salute di una struttura è necessario e auspicabile in molti casi.

Il monitoraggio strutturale (Structural Health Monitoring – SHM) rappresenta un potente strumento per la valutazione del comportamento dinamico della struttura monitorata. Fino a pochi anni fa queste tecniche erano impiegate prevalentemente in ambito meccanico, aeronautico e nell'ingegneria aerospaziale.

Al giorno d'oggi, la riduzione dei costi della strumentazione, sistemi di acquisizione dati di nuova generazione e l'incremento continuo dell'efficienta nelle analisi numeriche hanno reso possibile l'applicazione di queste tecniche anche a strutture civili ordinarie.

Le tecniche di monitoraggio strutturale vengono applicate non solo in grandi infrastrutture come ponti, dighe o grattacieli, ma anche in strutture storiche o edifici residenziali.

In questo contesto questa tesi tenta di esaminare differenti aspetti del monitoraggio strutturale, in particolar modo riferite a edifici ordinari.

Attraverso tecniche Output-Only (Operational Modal Analysis – OMA) sono state monitorate diverse strutture civili con reti di sensori cablate, al fine di ottenere il comportamento dinamico strutturale nelle reali condizioni opertive.

Particolare attenzione è stata focalizzata in un altra importante tematica dell'ingegneria strutturale: il danneggiamento strutturale. Attraverso un approccio numerico viene presentato un nuovo metodo per la localizzazione e quantificazione del danno a seguito di un evento sismico.

In alternativa alla classica rete cablata, è stato sviluppato un sistema di acquisizione con sensori wireless (Wireless Sensor Network – WSN). I principali risultati ottenuti con questa applicazione vengono riportati nella presente tesi, unitamente al design dei sensori low-cost. Con l'ausilio della sensoristica sviluppata è stato monitorato un edificio storico in muratura, mostrando i risultati positivi ottenuti a seguito della campagna di acquisizione di rumore ambientale (Ambient Vibration Survey -AVS).

Contents

List of Figures

List of Tables

Chapter 1
Introduction

In recent years the preservation of buildings and their structural safety are becoming topics of growing interest, encouraging the development of new methods and procedures for structural monitoring [1]. SHM is a set of techniques and methodologies for detection, localization, characterization and quantification of damaging phenomena. These techniques are used, among others, to predict the residual life of the structure before it reaches its collapse [2,3]. In fact, following the evolution of structural damage over time is crucial to understand if the damage mechanism has stopped and if the structure still has adequate resistance.

Seismic analyses for structural interventions are frequently performed using simplified numerical models that try to best reproduce the real dynamic behavior of the building. Often these models are not sufficiently refined and do not represent the real structure well enough. Destructive controls and structural surveys increase the knowledge of the structure, but are often not sufficient to understand the dynamic properties of the building.

Due to the many uncertainties about construction systems - material properties, modelling techniques, analysis methods and successive past interventions - the evaluation of structural behavior is a difficult task. These uncertainties can be the cause of completely wrong results.

SHM techniques solve these aspects. It is defined as the use of in-situ, non-destructive sensing and analysis of structural characteristics in order to identify if damage has occurred, to define its location and to estimate its severity, to evaluate its consequences on residual life of the structure.

Nowadays the reduction of equipment cost and the increase of computational performances have made the dynamic identification process widely used in civil engineering, particularly in existing buildings. These techniques can be applied for calibration of structural models of buildings to be used for repair-oriented design, rehabilitation and retrofit works, and the structural monitoring of the building by observing changes of its dynamic behavior in time.

Operational Modal Analysis (OMA) concerns the possibility of describing structural dynamics at small vibration amplitudes in real operating conditions with unknown excitation inputs (e.g., wind force) [4]. The importance of this issue comes from the fact that for identification of large civil structures, applying known excitation forces is costly, if not infeasible [5,6]. Moreover, output only algorithms are the best option for an online monitoring system, which can monitor vibrations of a structure constantly, without the application of a measurable input to the system.

1.1 Why SHM for civil applications

"Can theoretical models correctly represent the real dynamic properties of structures?" and "How to identify and quantify the evolution of damage?" are key questions which this research proposes to answer.

The methodology normally used to solve these issues is SHM. The procedure involves: observation of a structure in a specific period using periodic measurements; extraction of specific features of the measured variables; analysis of the characteristics detected to determine the state of health of the structure. For these reasons the environmental and operating conditions have to be determined choosing the type of variable to be monitored (choice of sensors, position, data acquisition system, etc.) and the method of data acquisition (continuous, periodically, only after extreme events, etc.).

The goal of SHM is to improve safety and reliability of infrastructure systems by detecting damage before it reaches a critical state and allow rapid post-event assessment.

Early detection of damage is a fundamental task from a safety and economic point of view. Traditionally, damage detection is performed through periodic maintenance and post-event visual inspection by qualified personnel. Visual inspections impose high costs and inconvenience on structural system owners and users alike. In buildings, for instance, visual inspections may require the removal of non-structural components such as ceiling tiles, partition walls, and fire proofing. In addition, such resources (qualified inspectors) may not be immediately available after a damaging event, especially for dense urban areas, prolonging expensive downtime.

The SHM system solution offers precise information which helps engineers and managers assess the state-of-health of their structures, and if needed, target specific regions to inspect.

The dynamic behavior of civil structures can be obtained by experimental tests conducted using know input. This procedure is called Experimental Modal Analysis (EMA). It allows the identification of dynamic properties of structures by applying input-output modal identification procedures. Traditional EMA, however, suffers some limitations, such as:

- Need of an artificial excitation in order to measure Frequency Response Functions (FRF). In some cases, such as large civil structures, it is very difficult or even impossible to provide adequate excitation;
- Artificial loading is usually expensive;
- External excitation is affected by the risk of damaging the structure.

As a consequence, in the last decades increasing attention has been focused on Operational Modal Analysis. OMA is based on measurements affecting only the response of the structure in operational conditions and subject to ambient excitation in order to extract modal characteristics. It is also called "ambient", or "output-only" modal analysis. OMA is very attractive due to a number of advantages with respect to traditional EMA:

- testing is fast and cheap to conduct;
- no excitation equipments are needed, nor boundary condition simulation;
- it does not interfere with the normal use of the structure;

- it allows identification of modal parameters which are representative of the whole system in its actual operational conditions;
- operational modal identification by output-only measurements can be used also for vibration-based structural health monitoring and damage detection of structures.

On the other hand, typical drawbacks are related to a signal-to-noise ratio in measured data much lower than in the case of controlled tests in lab environment. Thus, very sensitive equipment and careful data analysis are needed.

The appeal of these techniques motivated the presented dissertation in investigating the dynamic behavior of civil structures through OMA procedures.

1.2 Thesis outline

In the present thesis, Structural Health Monitoring procedures and Operational Modal Analysis techniques for civil structures are investigated.

The first step was to study the state-of-the-art of SHM, both regarding long and short-term monitoring to try and understand the role that SHM can play in the protection and in the maintenance of ordinary buildings (**Chapter 2**). **Chapter 3** provides a breakdown of research in Operational Modal Analysis process and the methodology used for the measuring campaign. An extensive literature review of OMA procedures is carried out, describing their theoretical background.

An overview of equipment and measurement instruments for the identification process in output-only conditions is addressed in **Chapter 4**. In this chapter, the hardware component (sensors, data acquisition hardware) characteristics and some practical issues are described in detail, in order to define the parameters to consider for a proper choice of hardware to be used for ambient vibration tests.

In **Chapter 5**, the damage detection theme is addressed and a complete literature of damage indexes is discussed. Through a case study, an integrated novel approach is proposed for the diagnosis of structures after a seismic event. The leading idea of this approach is to provide an estimation of the health and remaining life of monitored structures and to detect and quantify the damage, some of the crucial issues of SHM.

The reliability and high versatility of OMA techniques, which do not require knowledge about the excitation that causes structural vibrations, is demonstrated by applying them to a number of different case studies (**Chapter 6**). For each of them a modal model is obtained and dynamic parameters are extracted. Experimental data are also validated by performing suitably tuned numerical models. They allow the enhancing of structural aspects of the monitored buildings, characterizing the different parameters and boundary conditions that deeply influence the structural dynamic.

Finally, **Chapter 7** investigates an alternative way to perform dynamic measurements: Wireless Sensor Networks (WSN). With respect to a wired solution a WSN is usually a flexible solution with minor associated costs, especially if the network is composed of cheap devices (e.g., MEMS sensors). On the other hand, new problems should be considered: the synchronization between sensor nodes, the short transmission distance, the optimization of energy consumption and the selection of adequate low-cost sensors. In this framework, this Chapter details the main results obtained in the context of a masonry building monitored with WSN, with the aim of obtaining an accurate numerical model that simulates

the dynamic behavior of the whole structure. The device prototype is assembled and tested, showing the sensor design, the performances and the synchronization method.

Conclusions of the present research work are summarized in **Chapter 8**. Furthermore, open issues and suggestions for future research in the field of vibration-based structural health monitoring are also given.

Chapter 2
Structural Health Monitoring: State of art

2.1 Introduction to SHM

The most important objective in civil and earthquake engineering is to provide a structure with a proportionate margin of safety against damage due especially to significant events such as earthquakes. For this reason a control of the health condition of the structure becomes advisable and necessary for the safety of buildings [7].

In the most general terms, damage can be defined as changes introduced into a system that adversely affect its current or future performance [1]. Implicit in this definition is the comparison between two different states of the system, the initial, or undamaged state, and the ultimate, or damaged state.

The process of implementing a damage identification strategy for mechanical systems (aerospace, civil, engineering infrastructure, etc.) is referred to as SHM. This process involves the observation of a structure or mechanical system over time using periodically spaced measurements, the extraction of damage-sensitive features from these measurements and the statistical analysis of these features to determine the current state of system health.

The basic idea is that modal parameters, such as frequencies, mode shapes and modal damping, are based on the physical properties of the whole structure such as mass, damping and stiffness. So when a structure is exposed to damage the corresponding modal properties are changed. This approach is commonly called **Vibration-Based SHM**.

SHM is a very multidisciplinary field, where a number of different skills (seismology, electronic and civil engineering, computer science, signal theory) work together in order to increase performance and reliability of this field of research.

The first application of dynamic techniques based on the study of vibration was the rotating machinery. During the 1970s and 1980s, vibration-based damage identification methods were used for offshore platforms. This damage identification problem is fundamentally different from that of rotating machinery because the location of damage is unknown and because a large part of the structure is not readily accessible for measurement.

The aerospace community began to study the use of vibration-based damage identification during the late 1970s and early 1980s in conjunction with the development of the space shuttle.

The civil engineering community has studied vibration-based damage assessment of bridge structures and buildings since the early 1980s. Modal properties and quantities derived from these properties have been the primary features used to identify damage in bridge structures. Environmental and operating condition variability and the physical size presents significant challenges to bridge monitoring application.

Nowadays SHM techniques are widely used in civil applications and information obtained from this discipline can be useful for: (i) maintenance or structural safety evaluation of existing structures; (ii) rapid evaluation of conditions of damaged structures

after an earthquake; (iii) estimation of residual life of structures; (iv) repair and retrofitting of structures; (v) maintenance, management or rehabilitation of historical structures.

2.2 SHM Classifications

The damage state of a system can be described as a five-step process along the lines of the process discussed in Rytter (1993) to answer the following questions [5]:

(i) Existence. Is there damage in the system?
(ii) Location. Where is the damage in the system?
(iii) Type. What kind of damage is present?
(iv) Extent. How severe is the damage?
(v) Prognosis. How much useful life remains?

Answers to these questions in the order presented represent increased knowledge of the damage state.

The main category of classification for damage identification distinguishes between methods based on time dependent strategies. They are characterized as short-term, long-term, periodic, continuous, and triggered monitoring [8].

- **Short-term monitoring** can be used to examine the state of the structure at a specific point in time. This is a typical measure if an inspection shows a deficiency or damage in the structure and the safety is questioned. These types of monitoring are often used to evaluate a change. If several short-term monitoring measures are repeated frequently over an extended period it will be defined as periodic long-term monitoring.
- **Long-term monitoring** definition states that continuous monitoring of a structure is considered to be "long term" when the monitoring is carried out over a period of years-to-decades. Preferably, long-term monitoring should be carried out over the life of the structure. Recent advances in sensor technology, data acquisition, computer power, communication systems, data and technologies now makes it possible to construct this type of system. Long-term monitoring should be considered if the monitored quantity changes slowly (e.g. temperature) or if the loads are not predictable (e.g. natural hazards such as floods, hurricanes or earthquakes).
- **Periodic, continuous or triggered monitoring**. In long-term monitoring the collection of data is periodic when data is collected at regular time intervals. Continuous monitoring is used when rapid changes due to stochastic events are expected. Triggered periodic monitoring is when data collection is triggered by a specific event, e.g. when a measured parameter exceeds a threshold. The sampling interval for each data collection depends on the dynamic nature of the studied phenomena. A typical application for triggered monitoring is measurements of earthquake time histories.

Another important classification of SHM approach is based on the width of the structure involved.

- **Local monitoring** is the observation of local phenomenon, such as strain or crack opening. Local monitoring is not able to determine the health of the whole structure.

Still, in combination with global monitoring methods, local monitoring approach can be a useful to evaluate the severity of detected damages.

- **Global monitoring** is defined as the observation of global phenomena of structures. A typical application is the monitoring of modal parameters, such as frequencies, mode shapes and damping of the structure and to correlate the test results with the outcome of FE-analysis. The challenge is then to create a "damaged" FE-model so that the monitored results comply with the FE-analysis.

The last fundamental classification is based on the sampling rate of the measurement.

- **Static monitoring** is used for measurements of phenomena such as deflection, inclination, settlements, crack widths, temperature, and humidity. These are quasi-static since they vary slowly over the time.
- **Dynamic monitoring** is performed with a much higher sampling rate compared to static monitoring. It is usually used for measurements of accelerations in order to control the dynamic structural response.

For long-term SHM, the output of this process is periodically updated. Under an extreme event, such as an earthquake, SHM is used for rapid condition screening. This screening could provide, in near real-time, reliable information about system performance during such extreme events and the subsequent integrity of the system.

2.3 SHM applications

In conjunction with evolution, miniaturization and cost reductions of digital computing hardware developments, SHM has received considerable attention in the technical literature and practical applications. There are many real-life SHM studies in the USA, Japan, Hong Kong and Europe. New advances in sensor and information technologies and the wide use of the Internet make SHM a promising technology for better management of such civil infrastructures. Large-scale, real-life studies have been presented at a number of specialty conferences and workshops.

SHM for civil implementation can assist in the planning during the construction phase. The main objective for applying SHM to new structures is to provide feedback during erection and construction. Monitoring may help to manage safety risks during construction, as incomplete structural systems are typically vulnerable and exposed to accidents and hazards. Design of instrumentation and data acquisition for monitoring the construction process is best accomplished before the construction drawings and specifications are finalized. In fact, it is highly desirable to integrate monitoring directly into the design specifications. In this manner, the validity of the assumptions made during design calculations regarding the forces, reactions, displacements and drifts that a structure is expected to experience during its construction can be checked and confirmed. If the measurements indicate a need to modify the erection and construction, appropriate steps may be taken in a timely manner. Monitoring may therefore help to mitigate the uncertainties. The risk of constructing a structure with undesirably high forces, deformations and any other initial defects may be controlled. In addition, the design of fabrication monitoring before the start of construction may serve as an excellent measure for checking and mitigating any omission or errors in the executive drawings.

SHM is also a useful tool for evaluating the health conditions of existing buildings. It allows to make decisions for continued use, maintenance/repair/retrofit of aged or

damaged structures. SHM application may be made in the case of existing structures that exhibit premature aging, distress and performance problems. Some structures may lack sufficient system reliability due to undesirable construction details. In this case, the challenge would be to design a retrofit that would provide a significant enhancement of the system reliability. The analysis and interpretation of such data would provide critical information about the current load and responses as well as remaining fatigue life.

SHM can also be applied to large populations of similar types of structures. This kind of approach offers great promise for the implementation of structures by fully and systematically capitalizing on the common threads in the behavior of structures types. The science of statistical sampling, applied in conjunction with structural identification and structural health monitoring, would permit civil structures to be grouped into populations with similar behaviors. Some representative parameters can be monitored to evaluate the performance and health. Any findings such as root causes for damage and deterioration obtained from the SHM applications can be considered for the entire population when large-scale decisions are to be made.

2.4 SHM general methods

For any SHM application, it is imperative to properly-define the needs, requirements, expectations and constraints of the monitoring project. The expected outcome of the monitoring program should be clearly identified and analyzed, providing answers to specific questions such as load rating, structural behavior or performance.

As clearly summarized by Catbas F.L et al. [9], once the overall objectives and expectations are established, the following critical issues need to be considered (Fig.2.1).

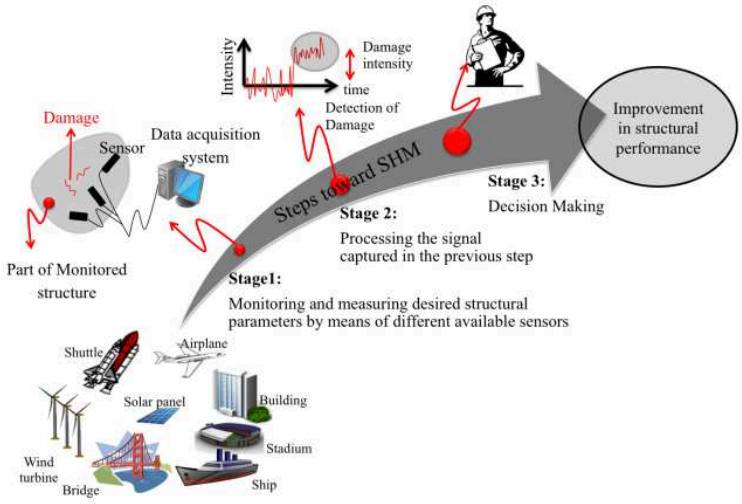

Figure 2.1 Simplified representation of stages involved in SHM process [10]

Structural system characterization. Characterization leads to a deep understanding of the structure and the objectives of the monitoring application. First, a thorough review is to be conducted using any relevant design information and drawings. Development of

analytical or Finite Element Models (FEM) for simulation of structural response is to be considered for structural characterization. These models also assist in the design of the monitoring project. Such models may be further refined and calibrated using SHM data to reflect actual conditions and mechanisms, and can serve as a baseline for evaluating future changes in the condition, performance and health of the structure.

Identifying the measurements. Based on the SHM objectives and characterization of the system, measurement needs have to be identified. The individual mechanical, chemical, electrical, and optical parameters that will characterize the phenomena of interest are to be evaluated. These parameters can include forces, stresses, displacements, rotations, vibrations, distortions and strains, environmental parameters such as temperature, humidity, precipitation, wind speed and direction, traffic quantities, images, etc. Some parameters may be static in nature, while others may be dynamic.

Sensing and data acquisition system selection. A detailed set of installation specifications should be prepared for each type of sensor and data acquisition component that will be used. These specifications should detail the methods and techniques to be used for installing and configuring the sensors and data acquisition components, and a methodology for verifying that they are working correctly.

Data quality assurance, processing and archival. Developing appropriate methods for data quality assurance, processing and archival purposes represent the major information technology related challenges for SHM applications. There are many possible sources of error and uncertainty in the field that can affect the reliability of measurements. Therefore, it is often desirable to have the methods developed and implemented at multiple levels of the signal path for quality assurance.

Data presentation and decision-making. The final step in the design process is to develop criteria for interpreting and presenting the monitor data and for making subsequent decisions. A monitoring system should generally only display data that have been synthesized to a form that is meaningful and can be easily understood. In a long-term structural health monitoring application, the system should be able to interpret the measurement data, compare the result with some predetermined set of criteria, and make a decision in an automated manner. The simplest example is to program a health monitoring system to issue an alert when the measurement data indicate that some behavior has exceeded a particular threshold value.

The procedure can be used to forecast the lifetime of the structure that was useful for the so-called Process of Prognosis, in order to predict the remaining life of the structure examined.

Chapter 3
Output-Only Modal Identification

3.1 Introducing OMA

The dynamic behavior of physical systems is often described by defining an ideal constant-parameter linear system (also known as Linear Time-Invariant—LTI—system, Fig.3.1). A system is characterized by constant parameters if all its fundamental properties are invariant with respect to time. Moreover, it shows a linear mapping between input and output if the response characteristics are additive and homogeneous.

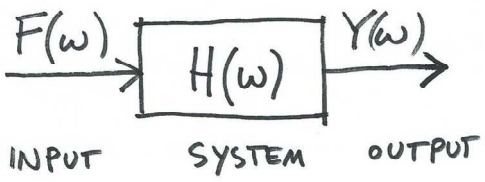

Figure 3.1 Schematic illustration of LTI system

For real structures, the validity of the linearity assumption depends not only on the characteristics of the structure, but also on the magnitude of the input. Physical systems typically show non-linear response characteristics when the magnitude of the applied load is large. However, for the applications of our interest, the response of many structures can be reasonably assumed to be linear, since ambient excitation yields small amplitude vibrations.

From a general point of view, the dynamics of a civil structure, like any mechanical system, can be described in terms of its mass, stiffness, and damping properties, or in terms of its vibration properties (natural frequencies, damping ratios, and mode shapes) or in terms of its response to a standard excitation.

Other descriptors of the dynamics of constant-parameter linear systems are defined in terms of their response to “standard” excitations. When the excitation is represented by a unit impulse input, the dynamics of the system can be described by its impulse response function (IRF). When the excitation is a unit-amplitude sinusoidal force applied at every frequency in a given range, another descriptor is obtained: it is the so-called frequency response function (FRF) defined over the considered range of frequency.

Consider for simplicity a Single Degree of Freedom (SDOF) system (the concepts can be easily extended to general MDOF systems by appropriate matrix notation). For any arbitrary input $f(t)$, the output of the SDOF system $y(t)$ is given by the following convolution integral of the IRF $h(\tau)$ with the input:

$$y(t) = \int_0^\infty h(\tau) f(t-\tau)\, dt \qquad 3.1$$

Alternatively, a physically realizable and stable LTI system can be described by the FRF $H(\omega)$. The convolution integral reduces to a simple multiplication when it is expressed in terms of the FRF and the Fourier Transforms of the input $F(\omega)$ and the output $Y(\omega)$:

$$Y(\omega) = H(\omega)F(\omega) \tag{3.2}$$

By solving the equations of motion when harmonic forcing is applied, the complete solution is described by a single matrix known as the Frequency Response Matrix $\boldsymbol{H(\omega)}$.

The system characteristics are completely contained in $H(\omega)$, which can be easily computed from:

$$H(\omega) = \frac{Y(\omega)}{F(\omega)} \tag{3.3}$$

This procedure is called Experimental Modal Analysis (EMA) and is usually performed when both the input and the output signals are known.

For a random excitation, a different approach is required. In this case the input is unknown and the only known variable is the output $Y(\omega)$. Moreover, when both excitation and response are described by random process, neither excitation nor response signals can be subjected to a valid Fourier Transform calculation and another approach must be found. As input is unknown, it is assumed to be a stationary zero mean Gaussian white noise: this assumption implies that input is characterized by a flat spectrum in the frequency range of interest and, therefore, it gives a broadband excitation, so that all modes are excited. As a consequence, the output spectrum contains full information about the structure, since all modes are equally excited.

For these reasons it is necessary to introduce and define different identification approaches. This procedure, previously introduced, is called Operational Modal Analysis (OMA).

OMA techniques are based on the following assumptions:

- **Linearity**: the response of the system to a certain combination of inputs is equal to the same combination of the corresponding outputs;
- **Stationarity**: the dynamic characteristics of the structure do not change over time, that is to say, coefficients of differential equations describing the problem are constant with respect to time;
- **Observability**: test setup must be defined in order to be able to measure the dynamic characteristics of interest (nodal point must be avoided in order to detect a certain mode).

OMA is the base for a number of applications: in particular, it is currently used in vibration-based structural health monitoring systems, founded on the relation between damage and changes in structural properties, such as mass, damping and stiffness.

The general procedure involves three stages. First, to identify the appropriate type of model (the **Spatial Model**) in terms of mass, stiffness and damping properties. Second, an analytical modal analysis of the Spatial Model is performed. It describes the structural behavior as a set of natural frequencies with corresponding vibration mode shapes and modal damping factors (the **Modal Model**). The third stage is characterized by the analysis of the structural vibration under given excitation conditions to describe the **Response**

Model. This will depend not only upon the properties of the structure but also on the nature and magnitude of the imposed excitation.

Processing of the Modal Model passes through the following steps:

- **planning and execution of tests** (proper location of sensors and, eventually, of actuators; selection of data acquisition parameters; eventual application of external excitation);
- **data processing and identification of modal parameters** (filtering, decimation, windowing; extraction of modal parameters);
- **validation of the modal model**.

Once the modal model has been found, it can be used for different purposes. A first approach is based on the observation that **changes in structural properties have consequences on natural frequencies.** However, their relatively low sensitivity to damage requires high accuracy of measurements in order to obtain reliable results. Significant changes in modal frequencies could not necessarily imply presence of damage, because of the effects of some environmental factors such as temperature changes. A variation of about 5% seems to be necessary to detect damage with confidence.

Damage can be detected through **mode shape changes**. A number of applications are reported in the literature but the most popular ones are based on some indexes such as Modal Assurance Criterion (MAC) [11].

Another important application of system identification, which is in some way related to the issues of monitoring and damage prognosis, is **force reconstruction**: in fact, knowledge of loads acting on structures gives opportunities in the field of structural health assessment and of estimation of the remaining lifetime. In many practical applications it is impossible to measure forces resulting, as an example, from wind or traffic directly. Therefore, they can be determined only indirectly from dynamic measurements. All these methods require system identification as a first step for load estimation.

The last main application of results of modal analysis concerns **model updating**. The extracted modal parameters can be used to validate or enhance numerical models. In fact, FE models are usually affected by errors and uncertainties. If a quite accurate model is available and there is some a-priori knowledge about characteristics of the structure or materials, it is possible to carry out sensitivity analyses on the remaining uncertain parameters in order to identify the values associated to the “best model”. Usual applications of FE model updating aim at identifying material properties or boundary conditions. Several techniques for model updating exist, including manual tuning of the update parameters. The updated model can be used for damage detection purpose [12] or for evaluation of short-term impact of natural hazardous events (earthquakes) or rehabilitation and retrofitting works.

In the next sections, after a short review about models of vibrating structures, the basic theory underlying the different OMA methods will be presented.

3.2 Structural Dynamics Models

3.2.1 Equation of motion and structural dynamic properties

The dynamic behavior of a structure can be represented either by a set of differential equations in time domain, or by a set of algebraic equations in frequency domain. Equations of motion (Fig 3.2) are traditionally expressed in time domain, thus obtaining, for a general MDOF system, the following set of linear second order differential equations expressed in matrix form:

$$[M]\{\ddot{v}(t)\} + [C]\{\dot{v}(t)\} + [K]\{v(t)\} = \{f(t)\} \quad 3.4$$

where $\ddot{v}(t)$, $\dot{v}(t)$ and $v(t)$ are the vectors of acceleration, velocity, and displacement, respectively; $[M]$, $[C]$, and $[K]$ denote the mass, damping, and stiffness matrices; $f(t)$ is the forcing vector.

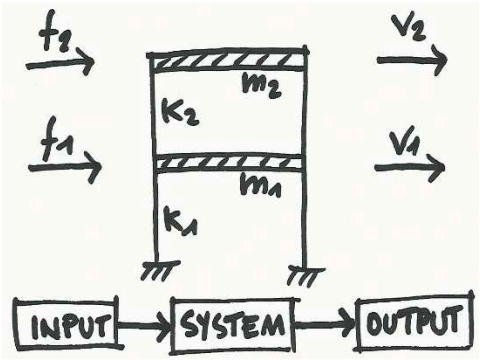

Figure 3.2 Schematic illustration of MDOF system

It describes the dynamics of the N-DOF discrete DOFs of the structure and it is usually referred to as the spatial model. The definition of the spatial model (of mass, stiffness, and damping properties) is the first step in theoretical analyses and it usually requires a large number of DOFs (some order of magnitude larger than the number of DOFs required for an accurate experimental model) in order to adequately describe the dynamic behavior of the structure.

Frequencies, damping and mode shapes are obtained by the associated homogeneous equation:

$$[M]\{\ddot{v}(t)\} + [C]\{\dot{v}(t)\} + [K]\{v(t)\} = 0 \quad 3.5$$

in addition, the solution is harmonic:

$$v = \varphi e^{\lambda t} \quad 3.6$$

Eigenproblem associated to $[M]$, $[C]$, and $[K]$ matrix is obtained by substituting (3.6) in (3.5):

$$(M\lambda^2 + C\lambda + K)\varphi = 0 \tag{3.7}$$

Through the calculation of (3.7) N eigenvalues and N eigenvectors, in general complex entities, are obtained. Usually eigenvalues λ can be rewritten as [13]:

$$\lambda_j = -\omega_j \xi_j + i\omega\sqrt{1 - {\xi_j}^2} \tag{3.8}$$

Where ω_j is the jth natural frequency in undamped system, and ξ_j is the associated modal damping.

3.2.2 State space models

State space-models are used to convert the second order problem, stated by the differential equation of motion (3.4) in matrix form, into two first order problems, defined by the so-called "**state equation**" and "**observation equation**". The state equation can be obtained by the second order equation of motion and can be conveniently given by:

$$\dot{x}(t) = A_c x(t) + B_c u(t) \tag{3.9}$$

obtained by introducing in (3.4) the state vector $x(t)$, the "**state matrix**" A_c, the "**input influence matrix**" B_c and the external force vector $u(t)$ defined as follows:

$$x(t) = \begin{bmatrix} v(t) \\ \dot{v}(t) \end{bmatrix}$$

$$A_c = \begin{bmatrix} 0 & I \\ -M^{-1}K & -M^{-1}C \end{bmatrix}$$

$$B_c = \begin{bmatrix} 0 \\ M^{-1} \end{bmatrix}$$

$$u(t) = \begin{bmatrix} 0 \\ f(t) \end{bmatrix}$$

where the subscript "$_c$" denotes continuous time. The system (3.8) is composed by 2N first-order differential equation.

Real structures are characterized by an infinite number of DOFs which becomes a finite but large number in finite element models, where lumped systems are considered. However, in a practical vibration test, this number decreases from hundreds and hundreds to a few tens or even less. Thus, by assuming that measurements are taken at "L" locations and that the sensors are either accelerometers, velocimeters and displacement transducers in the most general case, the state equation can be associated with the **observation equation**:

$$y(t) = C_a \ddot{v}(t) + C_v \dot{v}(t) + C_d v(t) \tag{3.10}$$

where $y(t)$ is the **vector of the outputs**, C_a, C_v and C_d are the **output location matrices** for acceleration, velocity and displacement respectively.

Combining equations (3.4) and (3.10) the following equation can be written:

$$y(t) = C_c x(t) + D_c u(t) \tag{3.11}$$

obtained by introducing the following definitions:

$$C = [C_d - C_a M^{-1} K \quad C_v - C_a M^{-1} C]$$

$$D = C_a M^{-1}$$

$$u(t) = \left[\frac{0}{f(t)}\right]$$

where C_c is the "**output influence matrix**" (*Lx2N*) and D_c is the "**direct transmission matrix**" (*LxN*). The direct transmission matrix disappears if no accelerometers are used for output measurements.

By combining equations (3.9) and (3.11), the **classical continuous-time state-space model** is obtained:

$$\begin{aligned} \dot{x}(t) &= A_c x(t) + B_c u(t) \\ y(t) &= C_c x(t) + D_c u(t) \end{aligned} \tag{3.12}$$

Since experimental tests yield measurements taken at discrete time instants while equations (3.12) are expressed in continuous time, the state space model must be converted to discrete time. By choosing a certain fixed sampling period Δt, the continuous-time equations can be discretized and solved at all discrete time instants $t = k\Delta t, k \epsilon N$ obtaining the **discrete-time state-space model formulation:**

$$\begin{aligned} x_{k+1} &= A x_k + B u_k \\ y_k &= C x_k + D u_k \end{aligned} \tag{3.13}$$

Where $x_k = x_k(\Delta t)$ is the discrete-time state vector yielding the sampled displacements and velocities, u_k and y_k are the sampled input and output, $[A]$ is the discrete state matrix, $[B]$ is the discrete input matrix, $[C]$ is the discrete output matrix and $[D]$ is the direct transmission matrix.

Once the state space model has been constructed, the modal parameters can be extracted by the eigendecomposition of the system matrix $[A]$, as described in Section 3.4.2.

3.3 Characterization of Output-Only techniques

Even if most of OMA techniques are derived from traditional EMA procedures, they are developed in a stochastic framework, due to the assumptions about input. Such assumptions have some consequences: first, modal participation factors cannot be computed as the input is unknown; moreover, due to the assumptions on input, OMA techniques are always of a multiple input type.

Modal identification methods can be first of all classified according to the domain for implementation. Parameter estimation methods directly based on time histories of the output signals are referred to as **time domain methods**. Methods based on Fourier transform of signals are, instead, referred to as **frequency domain methods**.

Time domain methods are, in fact, usually better conditioned than the frequency domain counterpart. This is mainly related to the effect of the powers of frequencies in frequency domain equations. Moreover, time domain methods are usually more suitable for handling noisy data, and they avoid most signal processing errors if applied directly to raw time domain data. On the other hand, in noisy measurement conditions, averaging is easier and more efficient in the frequency domain.

A second distinction is between **parametric** and **non-parametric methods**; if a model is fitted to data, the technique is called parametric. These procedures are more complex and computationally demanding compared to non-parametric ones, but they usually show better performance with respect to the faster and easier non-parametric techniques which, however, give a first insight into the identification problem.

A third distinction is between **Single Degree Of Freedom (SDOF)** and **Multiple Degree Of Freedom (MDOF) methods**. If in a certain frequency band only one mode is assumed to be important, the parameters of this mode can be determined separately, leading to the so-called SDOF methods. Even if these methods are very fast and characterized by a low computational burden, the SDOF assumption is a reasonable approximation only if the modes of the system are well decoupled. MDOF methods are, therefore, necessary when dealing with close-coupled modes or even coincident modes.

The last distinction is among **covariance-driven** and **data-driven methods**: in the first case correlation functions are estimated from the measured responses before carrying out modal identification; in the second case modal analysis is carried out directly on the raw data.

3.3.1 OMA in frequency domain

The easiest method for modal parameter estimation from output-only data is the **Basic Frequency Domain (BFD)** technique [14], also called the Peak-Picking method. The name of the method is related to the fact that natural frequencies are determined as the peaks of the Power Spectral Density (PSD) plots, obtained by converting the measured data to the frequency domain by the Discrete Fourier Transform (DFT). The BFD technique is a SDOF method for OMA: in fact, it is based on the assumption that, around a resonance, only one mode is dominant.

The BFD technique works well when damping is low and modes are well-separated: if these conditions are violated it may lead to erroneous results. Another important drawback is that the selection of eigenfrequencies can become a subjective task if the spectrum peaks are not very clear. Moreover, eigenfrequencies are estimated on a local basis (local

estimate) by looking at single spectra. The last drawback is the need of a fine frequency resolution in order to obtain a good estimation of the natural frequency.

The **Enhanced Frequency Domain Decomposition (FDD)** technique [15] is an extension of the BFD technique. The input x(t) and the output y(t) can be written in the form:

$$\left[G_{yy}(\omega)\right] = [H(\omega)]^{*}[G_{xx}(\omega)][H(\omega)]^{T} \tag{3.14}$$

where $\left[G_{yy}(\omega)\right]$ is the "*r x r*" input PSD matrix, "*r*" is the number of inputs, $[G_{xx}(\omega)]$ "*l x l*" output PSD matrix, *"l"* is the number of outputs, $[H(\omega)]$ is the "*l x r*" FRF matrix, and the superscripts * and *"T"* denote complex conjugate and transpose respectively. The FRF matrix can be expressed in a typical partial fraction form in terms of poles λ_k and residues $[R_k]$:

$$[H(\omega)] = \frac{[Y(\omega)]}{[X(\omega)]} = \sum_{k=1}^{n} \frac{[R_k]}{j\omega - \lambda_k} + \frac{[R_k]^{*}}{j\omega - \lambda_k{}^{*}} \tag{3.15}$$

$$\lambda_k = -\sigma_k + j\omega_{dk} \tag{3.16}$$

being *"n"* the number of modes, λ_k the pole of the kth mode, σ_k the modal damping (decay constant) and ω_{dk} the damped natural frequency of the kth mode. $[R_k]$ is the residue, and it is given by:

$$[R_k] = \{\phi\}_k \{\gamma\}_k^T \tag{3.17}$$

where $\{\phi\}_k$ is the mode shape vector and $\{\gamma\}_k^T$ is the modal participation vector.

Combining equations (3.14) and (3.15) and assuming that input is random both in time and space and has a zero mean white noise distribution (that is to say, its PSD matrix is a constant: : $[G_{xx}(\omega)] = [C]$), the output PSD matrix can be written as:

$$\left[G_{yy}(\omega)\right] = \sum_{k=1}^{n} \sum_{s=1}^{n} \left[\frac{[R_k]}{j\omega - \lambda_k} + \frac{[R_k{}^{*}]}{j\omega - \lambda_k{}^{*}}\right] [C] \left[\frac{[R_s]}{j\omega - \lambda_s} + \frac{[R_s{}^{*}]}{j\omega - \lambda_s{}^{*}}\right] \tag{3.18}$$

As reported in [15] the estimate of the output PSD $\widehat{G_{yy}}(\omega)$ know at discrete frequency $\omega = \omega_i$ is decomposed by taking the **Singular Value Decomposition (SVD)** of the matrix:

$$\left[\widehat{G_{yy}}(\mathrm{j}\omega_i)\right] = [U]_i [S]_i [U]_i^H \tag{3.19}$$

where the matrix $[U]_i$ is a unitary matrix holding the singular vector $\{u_{ij}\}$ and $[S]_i$ is a diagonal matrix holding the scalar singular values s_{ij}.

The singular values, a function of the varying frequency, are assumed as a modal indicator. Under some assumptions (white noise excitation, low damping and orthogonal mode shape for close modes) it can be shown that the singular value curves in the frequency domain belonging to the diagonal of $[S]_i$ are autospectral density functions of a (SDOF) system with the same frequency and damping as the structure vibration modes. Thus, the peaks of the singular value curve, in the frequency domain, allow the identification of the system frequencies, whereas the singular vectors at the peaks estimate the corresponding mode shape. The damping ratio is determined from the Inverse Fourier Transform of the

autospectral density function of the SDOF by applying the method of the logarithmic decrement [4].

More details about frequency-domain identification methods can be found in [16]. In the next section, instead, attention is focused on time-domain methods, used in several case studies presented in the present dissertation.

3.3.2 OMA in time domain

Time domain models are a powerful analytical tool for the description and interpretation of stochastic processes deriving from the observation of dynamic phenomenon. These models are initially developed in fields of system theory and control engineering. The main characteristics and basic fundamentals are described in [17,18].

In the last decades these models have been used by several researchers for dynamic identification of structural systems (bridge, buildings, etc.) subjected to environmental loads. Dynamic response acquired during experimental tests can be considered as discrete-time series and can be described in a statistical manner by stochastic processes.

Mathematical models are represented by differential equations with discrete-time variables, which coincide to differential equations corresponding to continuous-time systems. These models can be divided in two main groups: **input-output models** and **state-space models**. The former consider the observed variables (input variables and output variables). State-space models use auxiliary variables, called state-space variables.

In order to evaluate modal properties of the structures modal models have to be solved searching model coefficients.

Prediction Error method (PEM) allows the estimation of dynamic parameters by a "predictor function" that provides, knowing the time history up to time instant *t*, the best accuracy estimation of the time history up to time instant *t+1*. It is then possible to obtain the coefficients by iterative optimization non-linear procedure. The so-called "predictor error function" is defined by the difference between the output signal (e.g. measured acceleration of the structure) respect to the signal predicted by the model.

State-space models, that will be debated in the next paragraphs, can be conveniently solved by subspace algorithm. Dynamic identification by subspace methods [19] is usually based on manipulation of matrix using linear algebraic operations.

The name "subspace methods" reflects that the matrix containing the measured signal can be interpreted as a vectorial space where the columns of this matrix represent a base of vectors. These matrixes can be evaluated through the only knowledge of the output, without the a-priori knowledge of the matrix of the model [20].

The prediction of the signal, necessary for the determination of the system matrix, is associated with the development of the Kalman filter [21].

The last step of the identification process is the validation of the modal model.

3.4 Stochastic Subspace Identification

In the present work modal identification is carried out through Subspace methods. For this reason a deep argumentation of these techniques is reported, omitting the mathematical presentation of other procedures.

The model given by (3.12) is a deterministic model, that is to say the system is driven only by a deterministic input. However, stochastic components must be necessarily

included in order to describe actual measurement data (external random input as wind, traffic, earthquake, etc.). If stochastic components are included in the model, the following "**discrete-time combined deterministic-stochastic state-space model**" is obtained:

$$\begin{aligned} x_{k+1} &= Ax_k + Bu_k + w_k \\ y_k &= Cx_k + Du_k + v_k \end{aligned} \tag{3.20}$$

where w_k is the "process noise" due to disturbances and model inaccuracies, while v_k is the "measurement noise" due to sensor inaccuracy.

These vector signals are both unmeasurable: they are assumed to be zero mean Gaussian white noise processes. Due to the lack of information about the input u_k , it is implicitly modelled by the noise terms w_k and v_k, thus obtaining the following "discrete-time stochastic state-space model":

$$\begin{aligned} x_{k+1} &= Ax_k + w_k \\ y_k &= Cx_k + v_k \end{aligned} \tag{3.21}$$

The equation (3.21) can be interpreted as a model where the forcing function is white noise. In this case the terms $[B]$ and $[D]$ of the equations (3.20) can be included in the terms w_k and v_k obtaining the formulation (3.21).

The white noise assumption about w_k and v_k cannot be omitted for the proof of this class of identification methods [19]. If this assumption is violated, that is to say the input includes white noise and some additional dominant frequency components, these components will appear as poles of the state matrix $[A]$ and cannot be separated from the eigenfrequencies of the system.

Thus, when a stochastic state-space model is adopted, the objective is the determination of the order n of the unknown system and of a realization of the matrices $[A]$ and $[C]$ (up to within a similarity transformation) from a large number of measurements of the output y_k generated by the system itself. The state matrix $[A]$ transforms the current state of the system y_k in the next state y_{k+1}, while the product of the observation matrix [C] with the state vector provides the observable part of the dynamics of the system.

When dealing with discrete-time stochastic state-space models, where the input is implicitly modelled by disturbance, an alternative model, the so-called "**forward innovation model**" can be obtained by applying the steady-state Kalman filter to the stochastic state-space model (3.20). In order to describe this model, some concepts about Kalman filter are reported, together with definitions of "state prediction error" and "innovation".

3.4.1 The Kalman filter

The stochastic state-space model in can be expressed in an alternative form through the introduction of the so-called Kalman filter.

The process noise and the measurement noise w_k and v_k are both immeasurable and they are assumed to be zero mean, stationary white noise processes with covariance matrices given by:

$$E\left[\begin{Bmatrix} w_p \\ v_p \end{Bmatrix}\left\langle \{w_q\}^T \middle| \{v_q\}^T \right\rangle\right] = \begin{bmatrix} [Q^{ww}] & [S^{wv}] \\ [S^{wv}]^T & [R^{vv}] \end{bmatrix} \; p = q \qquad [0] \qquad p \neq q \tag{3.22}$$

where "p" and "q" are two arbitrary time instants. The estimation of the matrices $[Q^{ww}]$, $[R^{vv}]$ and $[S^{wv}]$ is also part of the identification process. The problem is defined in this way: the estimation of the state of the system at time "$k+r$" having the observations of the output "y" up to the instant "k".

For a given time instant t_{k+1} previous measurements $[y_k]$ are known:

$$\overline{y_k} = \left[y_k, y_{k-1}, y_{k-2}, \dots y_1\right] \tag{3.23}$$

The components $\overline{y_k}$ generate the so-called **past subspace**. The "**innovation**" e_{k+1} produced by the measure (k+1) respect to $\overline{y_k}$ is given by:

$$e_{k+1} = y_{k+1} - E(y_{k+1}|y_k) \tag{3.24}$$

The innovation cannot predict only by the knowledge of the signal up to the instant "k". The state predictor error v_{k+1} is defined as follows:

$$v_{k+1} = x_{k+1} - E[(x_{k+1}|\overline{x_k})] \tag{3.25}$$

It represents the part of x_k which cannot be predicted by the one-step ahead predictor of the state vector:

$$y_{k+1} = E[(y_{k+1}|\overline{y_k})] \tag{3.26}$$

which is defined as the conditional mean of x_k given all previous measurements.

The optimal state estimation can be obtained by the **Kalman filter**. The Kalman filter is standard in control theory. Only some basic concepts are presented here. More details and mathematical derivations are reported in [21].

Let us suppose that the state-space model matrices and the measurements y are known: the optimal (in the sense that the state prediction error is as small as possible) estimate $\widehat{x_k}$ for the state x_k can be obtained by applying the Kalman filter. In order to obtain the Kalman gain matrix, the state prediction error covariance matrix $[P_k]$ has to be obtained as a solution of the algebraic Ricatti equation [22]. Then, the Kalman gain matrix and the state estimate can be computed.

The non-steady-state Kalman filter state estimates $\widehat{x_k}$ are obtained by a recursive process. However, the estimates often reach a steady value very quickly: it is possible, therefore, to compute the constant value $[P]$ of the error covariance which satisfies the steady-state algebraic Ricatti equation and then the steady-state Kalman filter gains matrix $[K]$ (which is a constant matrix, too).

Theoretically, the Kalman filter is very attractive because of the closed form solution (given by the Ricatti equation) for its gain matrix: however, the Kalman filter requires information about the system matrices, including the covariances of the process and measurement noises. Even if the measurement noise can be quantified by a large number of repeated tests on the sensors, the process noise due to modelling errors and system

uncertainties is very difficult to quantify in practice. In practical applications, therefore, the Kalman sequence $\widehat{x_k}$ is estimated directly from experimental data without estimating the covariance of the process and measurement noises and solving the Ricatti equation [18].

Even if in system identification the Kalman filter is unknown, the stochastic state-space model (3.21) can be expressed in terms of the SteadyState Kalman filter and of the innovation, thus obtaining the following forward innovation model:

$$\begin{aligned} \widehat{x_{k+1}} &= Ax_k + [K]e_k \\ y_k &= Cx_k + e_k \end{aligned} \qquad 3.27$$

3.4.2 Covariance-Driven Stochastic Subspace Identification

The Covariance-driven Stochastic Subspace Identification (Cov-SSI) method addresses the problem of identifying a stochastic state-space model from output-only data.

A system of order "*n*" is observable if and only if the observability matrix is of rank "*n*". The solution of the realization problem consists in determining a minimal realization of order "*n*" of the state-space matrices from the measured data. In practical applications the actual order of the system is unknown and its determination is always affected by a certain degree of uncertainty due to noise effects. As a consequence, even if a minimal realization of a system of order *n* can be theoretically identified from the measured data and used to extract the modal parameters, the determination of the correct order of the system is usually a very complex task. A conservative approach to identify all the structural modes in the data consists in the overestimation of the order of the system. This causes the appearance of additional nonphysical poles next to the physical poles, and specific criteria and tools to sort the structural poles are needed (refer to **Sect. 3.5** for more details).

The Cov-SSI method can be classified as a time-domain, parametric, covariance-driven procedure for OMA. It starts from the computation of output correlations:

$$\left[\widehat{R_\iota}\right] = \frac{1}{N-i}\left[Y_{(1:N-i)}\right]\left[Y_{(1:N)}\right]^T \qquad 3.28$$

where $\left[Y_{(1:N-i)}\right]$ is obtained from the "*L x N*" data matrix $[Y]$ by removal of the last *"L"* samples, while $\left[Y_{(1:N)}\right]$ is obtained from $[Y]$ by removal of the first i samples; $\left[\widehat{R_\iota}\right]$ denotes the unbiased estimate of the correlation matrix at time lag "*I*" based on a finite number of data. The estimated correlations at different time lags are gathered into the following block Toeplitz matrix:

$$\left[T_{1/i}\right] = \begin{bmatrix} \left[\widehat{R_\iota}\right] & \left[\widehat{R_{\iota-1}}\right] & \dots & \left[\widehat{R_\iota}\right] \\ \left[\widehat{R_{\iota+1}}\right] & \left[\widehat{R_\iota}\right] & \dots & \left[\widehat{R_2}\right] \\ \vdots & \vdots & \ddots & \vdots \\ \left[\widehat{R_{2\iota-1}}\right] & \left[\widehat{R_{2\iota-2}}\right] & \dots & \left[\widehat{R_\iota}\right] \end{bmatrix} \qquad 3.29$$

Each correlation matrix has dimensions "*L x L"*; thus, the block Toeplitz matrix has dimensions "*Li x Li"*. For the identification of a system of order *"n"*, the number of block rows "*i*" has to fulfil the following condition:

$$l\,i\ \geq n \tag{3.30}$$

In practical applications the actual order of the system is obviously unknown. However, an estimate of the number of modes in the frequency range of interest can be obtained in a number of ways, for instance as the number of peaks in the trace of the PSD matrix or in the singular value plots given by the SVD of the PSD matrix (see **Sect 3.3.1**).

Assuming that the order of the system has been estimated and taking into account that the number of outputs *"L"* is a constant of the identification problem, a value for *"i"* larger than or equal to *"N / L"* can be set.

Applying the factorization property to the block Toeplitz matrix:

$$\left[T_{1/i}\right] = \begin{bmatrix} [C] \\ [C][A] \\ \vdots \\ [C][A]^{i-1} \end{bmatrix} \begin{bmatrix} [A]^{i-1}[G] \ldots [A][G] & [G] \end{bmatrix} = [O_i][\Gamma_i] \tag{3.31}$$

the **observability matrix**:

$$[O_i] = \begin{bmatrix} [C] \\ [C][A] \\ \vdots \\ [C][A]^{i-1} \end{bmatrix} \tag{3.32}$$

and the **reversed controllability matrix**:

$$[\Gamma_i] = \begin{bmatrix} [A]^{i-1}[G] \ldots [A][G] & [G] \end{bmatrix} \tag{3.33}$$

are obtained. $[O_i]$ and $[\Gamma_i]$ have dimensions *"li x n"* and *"n x li"*, respectively. If the condition of (3.30) is fulfilled and the system is observable and controllable, the rank of the block Toeplitz matrix equals *"n"*.

The SVD of the block Toeplitz matrix:

$$\left[T_{1/i}\right] = [U][\Sigma][V]^Y = \begin{bmatrix} [U_1] & [U_1] \end{bmatrix} \begin{bmatrix} [\Sigma_1] & [0] \\ [0] & [0] \end{bmatrix} \begin{bmatrix} [V_1]^T \\ [V_2]^T \end{bmatrix} \tag{3.34}$$

provides its rank, which equals the number of nonzero singular values. If the zero singular values and the corresponding singular vectors are omitted, (3.31) and (3.34) yield:

$$\left[T_{1/i}\right] = [O_i][\Gamma_i] = [U_1][\Sigma_1][V_1]^T \tag{3.35}$$

where the matrices $[U_1]$ and$[V_1]^T$ have dimensions *"li x n"* and *"n x li"*, respectively, and the *"n x n"* diagonal matrix $[\Sigma_1]$ holds the positive singular values. The matrices $[O_i]$ and $[\Gamma_i]$ can be computed by splitting the SVD in two parts as follows:

$$[O_i] = [U_1][\Sigma_1]^{1/2}[T] \tag{3.36}$$

$$[\Gamma_i] = [T]^{-1}[\Sigma_1]^{1/2}[V_1]^T \tag{3.37}$$

where $[T]$ is a nonsingular matrix.

From definitions (3.32-3.33) of the observability and controllability matrices, the output matrix $[C]$ and the next state-output covariance matrix $[G]$ can be obtained as the first *l* rows of $[O_i]$and the last *l* columns of $[\Gamma_i]$ respectively. In order to compute the state transition matrix [A], the shifted block Toeplitz matrix has to be computed:

$$\left[T_{2/i+1}\right] = \begin{bmatrix} [\widehat{R_{i+1}}] & [\widehat{R_i}] & \dots & [\widehat{R_2}] \\ [\widehat{R_{i+2}}] & [\widehat{R_{i+1}}] & \dots & [\widehat{R_3}] \\ \vdots & \vdots & \ddots & \vdots \\ [\widehat{R_{2i}}] & [\widehat{R_{2i-1}}] & \dots & [\widehat{R_{i+1}}] \end{bmatrix} = [O_i][A][\Gamma_i] \tag{3.38}$$

which can be decomposed as shown in equation (3.38). The state matrix [A] can be computed by introducing equations (3.36) and (3.37) into (3.38) and solving for [A]:

$$[A] = [O_i]^+\left[T_{2/i+1}\right][\Gamma_i]^+ = [S_i]^{-1/2}[U_i]^T\left[T_{2/i+1}\right][V_1][S_1]^{-1/2} \tag{3.39}$$

being [U] and [V] orthonormal matrices.

The identification problem is now theoretically solved. The modal parameters can be obtained from the two matrices $[A]$ and $[C]$. The eigenvalue decomposition of [A] yields:

$$A = \Psi\Lambda\Psi^{-1} \tag{3.40}$$

where $\Lambda = diag(\lambda_q)$ is a diagonal matrix containing the discrete-time complex eigenvalues and Ψ contains the eigenvectors as columns. The continuous time state equation is equivalent to the second-order matrix equation of motion, so they have the same eigenvalues and eigenvectors

$$A_c = \Psi_c\Lambda_c{\Psi_c}^{-1} \tag{3.41}$$

where $\Lambda_c = diag(\lambda_{c_q})$ is a diagonal matrix containing the continuous-time complex eigenvalues and Ψ contains the eigenvectors as columns. The eigenvalues of A_c occur in complex conjugated pairs and can be written as:

$$\lambda_{c_j}, {\lambda_{c_j}}^* = -\xi_q f_j \pm j f_j\sqrt{1-{\xi_j}^2} \tag{3.42}$$

Where ξ_j is the modal damping ratio of mode "j" and f_q is the eigenfrequenciy of mode "j" (rad/s). The eigenvalues λ_c can be computed as:

$$\lambda_{c_j} = \frac{\ln(\lambda_{dj})}{\Delta t} \tag{3.43}$$

where the subscript "$_d$" denotes discrete time. Natural frequencies are, then, obtained from the complex modules of the continuous-time poles as:

$$f_j = \frac{|\lambda_{cj}|}{2\pi} \tag{3.44}$$

while damping ratios are given by:

$$\xi_q = \frac{Re(\lambda_{cj})}{(\lambda_{cj})} \tag{3.45}$$

The mode shapes φ_j at the sensor locations are observed parts of the system eigenvectors Ψ and are obtained using the observation equation

$$\Phi = C\Psi \tag{3.46}$$

In conclusion the modal parameters ω_j, ξ_j, and φ_j can be extracted analytically from the identified system matrices $[A]$, $[C]$.

3.5 Post-Processing of Modal Parameter Estimates

3.5.1 Analysis of mode shapes

The first check has to be done in terms of **analysis of mode shapes**. Most of the OMA methods provide their results in the form of complex eigenvalues and complex eigenvectors.

For most structures of e.g. concrete and steel a proportional damping model is usual a good approximation. In such a case the mode shapes are real-values meaning that minimum and maximum values occur at the same time during a mode shape animation.

If mode shapes are complex it can be due to one or more of the above reasons: (i) non-proportional damping, (ii) bad measurements or poor modal parameter estimation, (iii) inconsistent data due to e.g. time variant conditions. In these cases the mode shape animation will show a "traveling wave" due to the fact that minimum and maximum values do not occur at the same time [23].

Another way to view this is to look at all the mode shape components in the complex plane. Such a diagram is called a **Complexity Plot** and is shown below for a certain mode (Fig. 3.3).

Each mode shape component is represented by a vector starting in 0,0 and the pointing out to the mode shape components real and imaginary value. If the component is real valued, it should point in a straight direction, so complexity is illustrated by the vertical component.

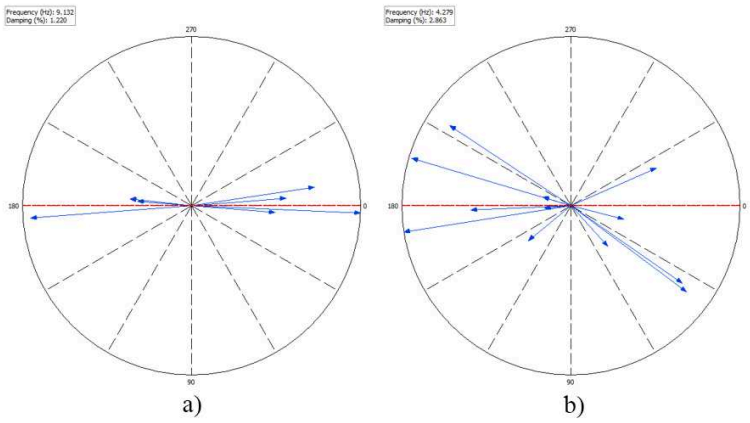

Figure 3.3 Complexity plot: (a) real/normal mode, (b) complex mode

It permits the evaluation of the degree of complexity by a simple visual inspection. If a structure is proportionally damped, the mode shape components for a certain mode lie on a straight line in the complex plane.

Whenever normal modes are expected from the modal test, the simplest approach to carry out the complex-to-real conversion consists in analyzing the phase of each mode shape component and setting it equal to 0° or 180° depending on its initial value. If the phase angle lies in the first or in the fourth quadrant it is set equal to 0°; it is set equal to 180° if it lies in the second or in the third quadrant. To be rigorous, this approach should be applied only in the case of nearly normal modes, when the phase angles differ no more than +-10° from 0° to 180°. However, it is frequently extended to all phase angles [13].

The experimentally identified mode shapes have to be graphically displayed, because the visual inspection of the estimated mode shapes represents the simplest method for a preliminary check of the modal identification results. Two approaches exist for the graphical display of mode shape estimates. The static display provides a picture of the mode shape, the dynamic display provides an animation of the mode shape.

Taking into account the measurement directions of the sensors installed on the structure and their positions, the deformed shape is obtained by assigning to each measured point in each measured direction a displacement proportional to the corresponding component of the mode shape vector. The sign of the mode shape component determines if the measured point is moving in-phase (+) or out-of-phase (-) with respect to the reference direction of the sensor.

One of the main drawbacks inherent in the visual inspection of the identified mode shapes is related to the fact that the identified model is incomplete, since measurements are carried out in a few points. The number of measurement points is typically much lower than the number of DOFs adopted, for instance, in numerical models. Since there are several unmeasured DOFs during tests, in the grid of points adopted to represent the geometry of the structure some of them will always be characterized by null modal displacements. This effect, caused by the finite number of measurement channels, has to be taken into account in the visual inspection of mode shapes. In some cases interpolation of modal displacements or consideration of some constraints (for instance, the presence of rigid diaphragms) can compensate the lack of information about some modal displacements in the experimental estimates.

3.5.2 Analysis of natural frequencies

Validation of modal identification results mainly relies on consistency checks obtained by **comparing experimental and numerical estimates** of the modal properties. This represents the primary tools to verify numerical models. A *verified model* is a model that includes all the necessary features to provide an acceptable representation of the actual dynamic behavior of the structure. A verified model can eventually undergo some adjustments to make its dynamic properties closer to the experimental values. The calibration of a numerical model based on experimental estimates of the modal properties is referred to as model updating. This is one of the main applications of modal testing.

Natural frequencies can be compared by a simple tabulation, quantifying the relative scatter, expressed in percent, as follows:

$$\Delta f_n = \frac{f_{2,n} - f_{1,n}}{f_{2,n}} \cdot 100 \qquad 3.47$$

where $f_{1,n}$ and $f_{2,n}$ are the two values of the natural frequency for the nth mode under comparison; $f_{1,n}$ and $f_{2,n}$ can be either experimental estimates, obtained from two different OMA methods, or represent the numerical and the experimental estimate of the experimental frequency of the nth mode, respectively.

An alternative approach to compare two sets of natural frequency estimates consists of plotting the natural frequencies in the second set against the natural frequencies of the first set in a Cartesian plane. The first set holds the reference natural frequency estimates while the second set holds the values of the natural frequencies that have to be compared with the corresponding estimates in the first dataset (Fig. 3.4). In the ideal case of very good correlation between the two sets of natural frequencies, the points lie very close to the line passing through the origin of the axes with 45° slope.

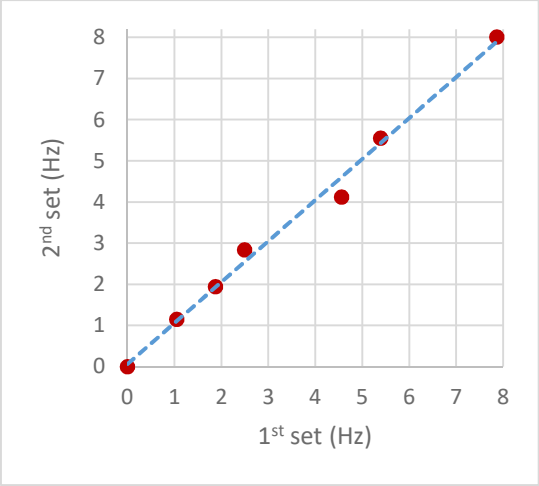

Figure 3.4 Comparison between two sets of natural frequency

3.5.3 Modal Assurance Criterion (MAC)

A more effective comparison of mode shapes, is based on numerical indexes. One of the most popular tools for the quantitative comparison of modal vectors is the Modal Assurance Criterion (MAC) [11]. The development of the MAC was modeled after the development of the ordinary coherence calculation associated with computation of the frequency response function [24].

Given the two mode shape vectors under comparison, for instance the experimentally estimated mode shape $\{\varphi_n^e\}$ and the numerically predicted mode shape $\{\varphi_n^a\}$ of the nth mode of the investigated structure, the MAC is computed as follows:

$$MAC(\{\varphi_n^a\},\{\varphi_n^e\}) = \frac{\left|\{\varphi_n^a\}^T\{\varphi_n^e\}\right|^2}{(\{\varphi_n^a\}^T\{\varphi_n^a\})(\{\varphi_n^e\}^T\{\varphi_n^e\})} \qquad 3.48$$

The MAC is often to used to pair modes shapes derived from analytical models with those obtained experimentally. It is bounded between 0 and 1, with 1 indicating fully consistent mode shapes. It can only indicate consistency and does not indicate validity or orthogonality. A value near 0 indicates that the modes are not consistent.

It is worth taking into account that it provides only a measure of consistency between the vectors but it does not ensure validity.

In practical applications, given N_m^e experimentally identified modes and N_m^a numerically predicted modes, the N_m^e x N_m^a a MAC matrix (Fig. 3.5) is computed. Assuming that $N_m^e = N_m^a$, if the numerical and experimental mode shape vectors are consistent the MAC matrix will show values close to 1 along its main diagonal, where the MAC is computed for mode shapes corresponding to the same mode, and close to 0 elsewhere, where the MAC is related to two different modes.

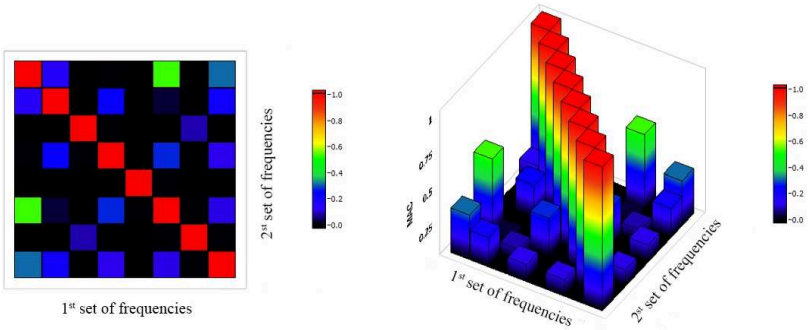

Figure 3.5 MAC: Comparison between two sets of natural frequency

When the MAC matrix is different from this ideal case additional investigation is needed. These anomalies can be the result of poor modeling, poor analysis of the experimental data, inappropriate choice of the DOFs included in the correlation or incorrect mode pairing.

3.5.4 Stabilization Diagrams for Parametric OMA Methods

An appropriate parameter setting in parametric OMA methods requires some prior knowledge about the order of the model to identify all modes in the analyzed frequency range. Unfortunately, due to noise and modeling inaccuracies, serious problems often happen in determining the correct model order. So, in practical applications a conservative approach is adopted based on the over specification of the order of the model, which is set large enough to ensure the identification of all physical modes.

In any case over modeling introduces spurious poles, which have to be separated from the physical poles. This makes the modal parameter estimation more complicated. Spurious modes can be:

- noise modes: they are represented, for instance, by poles of the excitation system and, as such, they are due to physical reasons;
- mathematical modes: they are created by the model in addition to the physical poles to ensure the mathematical description of the measured data, which are inevitably affected by slight imperfections (measurement noise, computational noise, modeling inaccuracies).

The separation of the physical poles from the spurious mathematical ones can take advantage of the construction of the so-called stabilization diagram (Fig. 3.6).

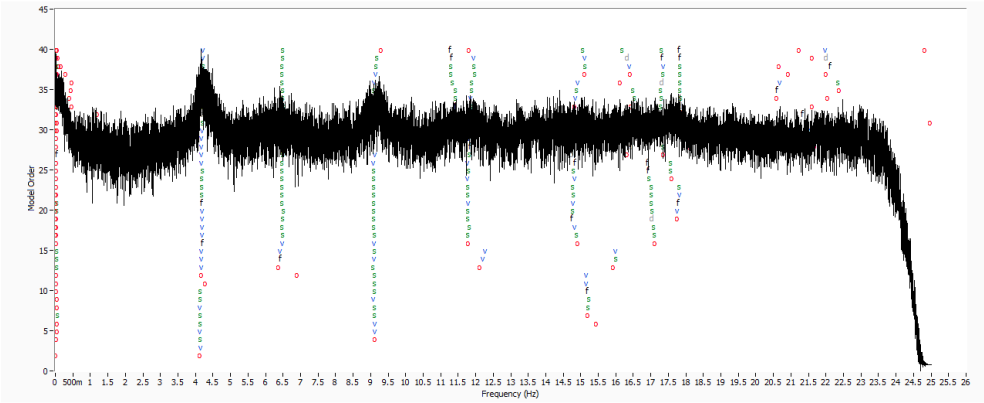

Figure 3.6 Stabilization diagram

It shows the alignments of stable poles, for increasing model orders. It also allows the determination of the “n” eigenvectors of dynamic matrix A which are representative of structural modes, and how many are instead purely numeric.

The points in red indicate the negative result of the stability test and the points in green indicate the positive results: because natural modes show the intrinsic characteristics of the structure, they are invariant to the process and the order of the NM [19]. Thus, it is possible to isolate the natural modes from the numerical ones by increasing the order of the model and checking the stability of the results.

The construction of the stabilization diagrams is based on the comparison of the poles associated to a given model order with those obtained from a one-order lower model. Only the poles that fulfill assigned user-defined stabilization criteria are labeled as stable. Typical stability requirements are expressed by the following inequalities:

$$\frac{|f(n)-f(n+1)|}{f(n)} < 0.01 \quad 3.49$$

$$\frac{|\xi(n)-\xi(n+1)|}{\xi(n)} < 0.05 \quad 3.50$$

$$[1 - MAC\ (\{\varphi(n)\}, \{\varphi(n+1)\})] < 0.02 \quad 3.51$$

In other words, (3.49) implies that the scatter between the estimates of the natural frequency at two subsequent model orders has to be lower than 1 % for a pole to be labeled as stable. Similar conditions on damping ratios and mode shapes are expressed by (3.50) and (3.51), respectively. If all the conditions expressed by the previous inequalities are satisfied, the pole is labeled as stable.

After the identification of the alignments of stable poles, eventual noise modes can be discarded according to physical criteria based on the expected damping ratio or the expected properties and aspect of the mode shapes.

Chapter 4
The measurement process

SHM is not just a single technique, but includes several functions, each of which must be designed carefully.
The main components in a modal analysis test are the structure under investigation, a number of motion transducers, a data acquisition device, and a data processing system for the extraction of the modal information from recorded data.
The first phase includes the choice of the instrumentation, data acquisition and signal processing (Fig.4.1).

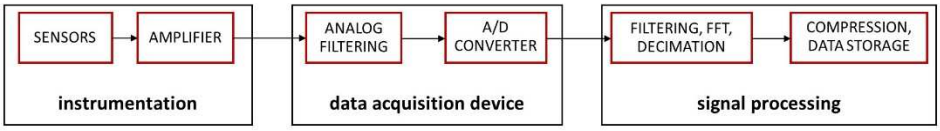

Figure 4.1 data acquisition system setup

High-quality measurements represent the first fundamental step for a successful modal identification. A proper selection and good knowledge of equipment and measurement instruments is just as important as theoretical knowledge of experimental modal analysis procedures.
The function of any sensor is the conversion of a physical quantity into an electrical one, typically voltage. Then, the electrical signal in the form of voltage is transferred to the data acquisition hardware for digitization.

4.1 Instrumentation

Instrumentation includes deciding on the quantities to be measured and the selection of the type of network (wired vs. wireless), the choice of the transducers and their positions.

The last decade has been characterized by substantial effort in the development of wireless sensor networks for structural testing and health monitoring (see **Chapter 7**). Even if a number of wireless sensing solutions are currently available, offering attractive advantages such as the reduction of costs and installation time associated to the use of cables, they have not fully replaced wired systems. Nowadays a wired solution is the best way for a continuous monitoring system because of the absence of problems related to power consumption.

The sensor type depends on the application. Typical sensors are accelerometers, strain gauges, fiber optics, and laser. The measured motion is typically very small at a low frequency. Therefore, the sensitivity of the sensor has to be high.

The number of sensors can change from one to several hundred because vibration measurements can be used to detect damage also remote from the sensor.

4.1.1 Data Acquisition Hardware

Data acquisition systems perform the conversion of analog signals originating from sensors into digital signals, which can be stored into a digital medium and analyzed by software.

A rough distinction can be made between dedicated solutions (Fig. 4.2 a)) and customizable solutions based on programmable hardware (Fig. 4.2 b)). For the first class of equipment, a basic knowledge about signal acquisition is sufficient to carry out the first tests. On the other hand, the solutions based on programmable hardware require more time and deeper theoretical knowledge. However, the main advantages with these solutions are the higher versatility.

a) b)

Figure 4.2 Dynamic data acquisition system (a) DaTa500 by DRC – Diagnostic Research Company, (b) programmable hardware by National Instruments

An **Analog-to-Digital Converter (ADC)** is a device that converts the continuous signal coming from the sensors into a sequence of digital numbers representing the amplitude of the signal. The conversion is based on the discretization of time (**sampling**) and signal amplitude (**quantization**).

The **resolution** of an ADC can be defined as the smallest step that can be detected.

The **noise level** is related to the number of bits occupied by noise when the input is zero. Only the last two bits are typically corrupted by noise in good quality 24-bit digitizers.

The **dynamic range** is defined as the ratio between the largest and the smallest value the ADC can acquire without significant distortion. It is usually expressed in dB.

The **sampling rate** is the number of samples acquired per second. The maximum sampling rate of the ADC defines the largest frequency range that can be investigated. For the majority of applications of OMA in civil engineering, a maximum sampling rate of 100 Hz or 200 Hz is satisfactory.

In the present dissertation both dedicated solutions and customizable solutions are used. A smart data acquisition system developed by DRC is employed to carry out dynamic investigation of civil structures using wired solutions (see **Chapter 5**). The main advantage of this equipment is the high flexibility thanks to the embedded energy cell. Moreover DaTa500 is able to acquire different physical quantities using several types of sensors.

A data acquisition system can also be easily developed starting from a National Instruments Compact DAQ device managed by a data acquisition software implemented in LabView environment. In the present case, the system for acquisition of acceleration data is developed through the NI 9234 modules, gathered into a CDAQ 9132 and linked via USB to a PC.

CDAQ 9132 is a stand-alone DAQ system for high-performance embedded measurements and logging. The controllers feature built-in powerful Intel multicore processors so that CompactDAQ can run acquisition and analysis software while logging data to onboard or removable SD memory. The main advantage of CompactDAQ is the possibility of operating completely stand-alone integrating a processor, DAQ hardware, and signal conditioning with software to reduce system costs and complexity and increase measurement accuracy.

The controllers can operate as stand-alone devices to expand the capabilities of the platform while taking advantage of the modularity and flexibility of the C Series platform and LabVIEW system design software. A controller system is composed of an embedded controller including a powerful Intel multicore processor to run an embedded OS and a hard disk drive with up to 32 GB of nonvolatile storage for data logging. The controllers offer module options with integrated signal conditioning for almost any sensor type as well as standard connectivity such as USB and Ethernet.

Data Acquisition system is assembled using **NI 9234 modules** (Fig.4.3). These are a 4-channel C Series dynamic signal acquisition module for making high-accuracy frequency measurements from Integrated Electronic Piezoelectric (IEPE) and non-IEPE sensors. NI 9234 delivers 102 dB of dynamic range and incorporates software-selectable AC/DC coupling and IEPE signal conditioning for accelerometers. The four input channels simultaneously digitize signals at rates up to 51.2 kHz per channel with built-in anti-aliasing filters that automatically adjust to sampling rate.

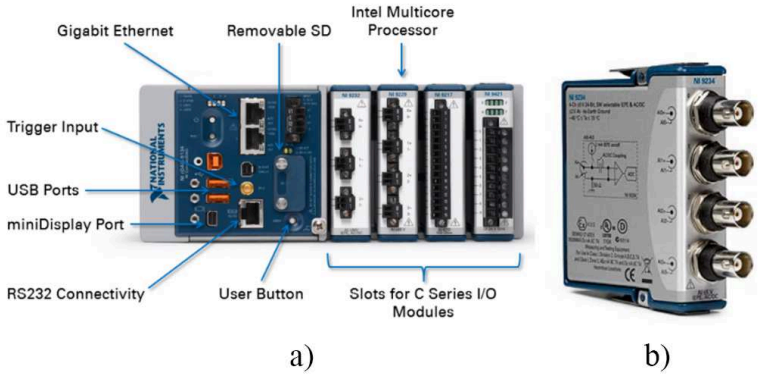

Figure 4.3 Customizable solutions by National Instruments: (a) CDAQ 9132 data acquisition, (b) NI 9234 modules b)

In this case, NI 9234 are connected to IEPE accelerometers as reported in the following section. The link between accelerometers and recorder has been made through a RG-58/U low impedance coaxial cable, to achieve the best accuracy.

4.1.2 Transducers

Different types of sensors are available to measure the dynamic response of civil structures. In this section attention is mainly focused on piezoelectric accelerometers, even if different types of sensors can also be adopted in output-only modal testing.

In **piezoelectric sensors** the conversion of the mechanical quantity into an electrical quantity is obtained by taking advantage of the piezoelectric property of some natural (quartz) or man-made (polycrystalline ceramics, such as barium titanate) materials [25]. As a consequence of piezoelectricity, when a force is applied to the crystal, negative and positive ions accumulate onto the opposite surfaces of the crystal. The amount of accumulated charge is directly proportional to the applied force. In piezoelectric accelerometers a mass is coupled to the crystal. When an input acceleration is applied at the base of the accelerometer, the inertia force associated to the mass causes a deformation of the crystal. The piezoelectric material generates an electric charge proportional to its deformation.

The charge collected by electrodes on the piezoelectric crystal is transmitted to a signal conditioner, which converts the electric charge into voltage. A remote signal conditioner characterizes chargemode sensors. On the contrary, a built-in signal conditioner characterizes the so-called **Integrated Electronics Piezo-Electric (IEPE) accelerometers**.

In the presence of a built-in signal conditioner, the signal cable carries also the required power supply. Therefore, the signal is high-pass filtered to remove the frequencies close to DC. Nowadays IEPE accelerometers are replacing charge mode sensors since they offer a number of advantages, such as simplified operation, lower cost, resolution virtually unaffected by cable type and length (long cables can be used without increase in noise, loss of resolution, or signal attenuation).

Because of the low amplitude of motion and the limited frequency range of the structure under test, high-sensitivity accelerometers are necessary. However, frequency band and sensitivity are not the only parameters to be taken into account.

Independently of the type of sensor, the output voltage signal is proportional to the measured physical quantity through a constant, which is the sensitivity of the sensor.

Sensitivity is usually given as the gain of the sensor (for example, 10 V/g) and it is related to the smallest signal that can be resolved. In fact, the sensitivity of a sensor is defined as the smallest absolute amount of change that can be detected by a measurement. However, the smallest detectable signal is also limited by the noise generated in the electronics. From a general point of view, a high gain should be preferred since an amplified signal minimizes the noise effects associated to the transmission over cables. Besides, it is important to verify that the maximum sensor output has a level fitting the recorder maximum input so that the sensor dynamic range is optimally used.

The **dynamic range DRs** of a sensor (often expressed in dB) is the ratio between the largest and the smallest signal it can measure:

$$DR_s = 10log\left(\frac{V_{max,s}}{V_{n,s}}\right)^2 \quad 4.1$$

In (4.1) $V_{max,s}$ and $V_{n,s}$ represent the maximum voltage signal and the noise floor of the sensor, respectively. A dynamic range in the order of 120–140 dB is also suitable since it fits well the dynamic range of the average 24 bit digitizers.

Sensor **resolution** represents the smallest incremental change of physical quantity that leads to a detectable change in the sensor output. It is usually expressed in absolute terms or as a percentage of the full-scale range. This provides the minimum and maximum values of the physical quantity that can be measured by the sensor.

An ideal sensor should behave linearly, but a certain deviation from **linearity** is always present. Such deviation should be as limited as possible and it is expressed by the percentage of nonlinearity. Accelerometers with good performance typically show a nonlinearity lower than 1 %.

It is worth noting that the final choice of the sensors is always the result of a number of factors such as: (i) the expected amplitude of the motion to be measured, (ii) the type of investigated structure (e.g. masonry, reinforced concrete, steel, etc.) and (iii) of course, the available budget.

In the first part of this work piezoelectric accelerometers are used because of their high performance in measuring low-amplitude ambient vibrations.

In particular **KS48C** and **KB12VD** accelerometers are used (Fig. 4.4a)). These sensors are often called seismic accelerometers because they are used to monitor construction activity, volcanoes and earthquakes. Both models use the IEPE technology previously described. Model KB12VD has an unusual design featuring air damping for a low resonance peak and friction coupling for overload protection (Fig. 4.4b)).

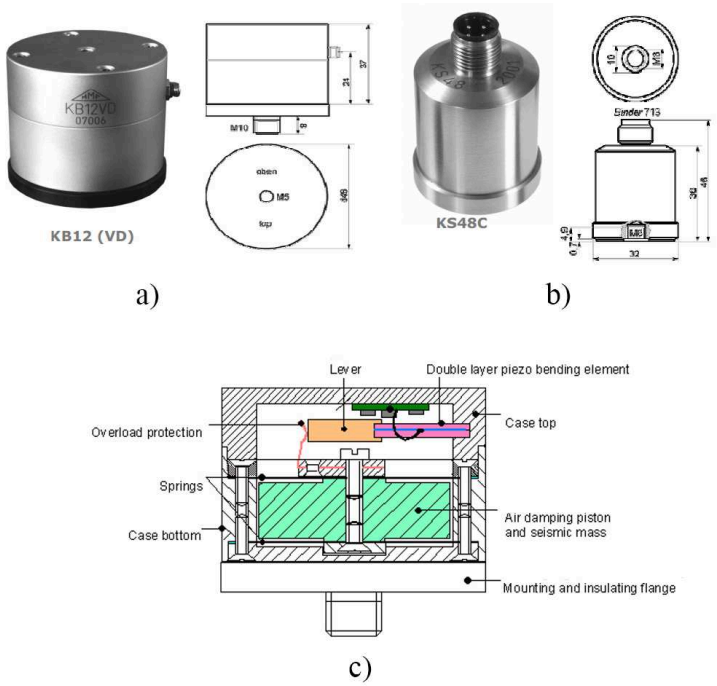

Figure 4.4 Piezoelectric sensors: (a, (b) KS48C and KB12VD accelerometers, (c) cross-section of KS48C sensor

4.2 Signal Processing

In this section some basic concepts related to signal theory are reported, focusing on data pre-processing. Several signal manipulations are necessary in order to achieve good acquisitions and suitable for their introduction into the dynamic identification software.

The definition of the value of the **sampling frequency** represents one of the most important settings in dynamic tests. It represents the number of samples acquired in one second. The sampling frequency cannot be set too low, because it determines the frequency range that can be investigated. Therefore, it has to be set depending on the maximum frequency of the structure under test.

If the sampling rate is f_s, the maximum frequency f_{max} that can be observed in a sampled signal is:

$$f_{max} = \frac{f_S}{2} \tag{4.2}$$

Assuming, for example, that the expected value of the maximum frequency is 50 Hz, a sampling frequency larger than 100 Hz is needed, so that the upper bound of the observable frequency range (the so-called **Nyquist frequency** f_N=fs/2) is higher than 50 Hz.

Figure 4.5 shows the effect of an inadequate selection of the sampling rate that causes an erroneous reconstruction of the waveform after digitization of the continuous signal with a high-frequency signal appearing as a low-frequency one.

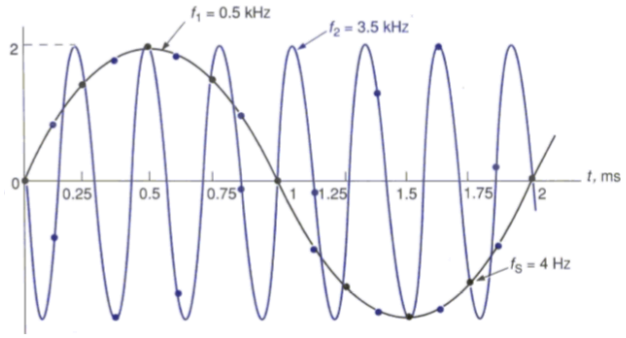

Figure 4.5 Aliasing. True signal (3.5kHz), Aliased signal (0.5kHz)

Thus, a typical problem of digital signal analysis caused by the discrete sampling of continuous signals is the so-called **aliasing**. Aliasing is the generation of a false (alias) frequency along with the correct one when doing frequency sampling. An analog **anti-aliasing filter** is therefore always required before the A/D converter because after the A/D converter, the aliasing cannot be corrected.

Filtering operations are often necessary to clean signals from unwanted frequency components. Digital filters are usually classified as low-pass, high-pass and band-pass, depending on the frequency range of the signal that the filter is intended to pass from the input to the output. In particular, a low-pass filter excludes all frequencies above the cut-off frequency of the filter, while a high-pass filter excludes the frequencies below the cut-

off frequency; a band-pass filter excludes all frequencies outside its frequency band, while a band-stop filter excludes the frequencies inside the filter band.

In the context of modal identification, high-pass filters are often used to remove frequencies close to DC, while low-pass filters are used to exclude high-frequency components in view of decimation. The acquired signals are often sampled at a higher frequency than needed for the analysis. **Decimation** (or down-sampling) is therefore used to resample the acquired signals to a lower sampling frequency. Assuming, for example, that data are acquired with a sampling frequency of 100hz, by applying a Decimation Factor of 2 the sampling frequency is reduced and the ultimate frequency is equal to 50Hz.

4.2.1 Data Acquisition Software

Several industrial software are currently available to carry out operational modal analysis according to a number of different methods.

Dewesoft is a powerful example of dedicated solutions for data acquisition software and data processing.

However, in order to build customizable solutions for measurement and data processing, a solution could be the adoption of appropriate data acquisition boards which can be controlled by LabView (www.ni.com/labview).

LabVIEW programs are called Virtual Instruments, or VIs, because their appearance and operation imitate physical instruments. LabVIEW contains a comprehensive set of tools for acquiring, analyzing, displaying, and storing data, as well as tools for code troubleshooting [26].

In LabVIEW it is necessary to build a user interface, or Front Panel with controls and indicators, which are the interactive input and output terminals of the VI, respectively.

Controls (e.g. knobs, push buttons, dials, and other input mechanisms) simulate instrument input mechanisms and supply data to the Block Diagram of the VI. Indicators (e.g. graphs, LEDs, and other output displays) simulate instrument output mechanisms and display data the Block Diagram acquires or generates.

The Block Diagram contains the code. Objects on the Block Diagram include terminals and nodes. Block Diagrams are built by connecting the objects with wires.

LabVIEW can be used also to communicate with hardware such as data acquisition, vision, and motion control devices. Hardware configuration is carried out through the Measurement and Automation eXplorer (MAX): here it is possible to test the hardware and configure it (Figure 4.6), before managing it through LabView.

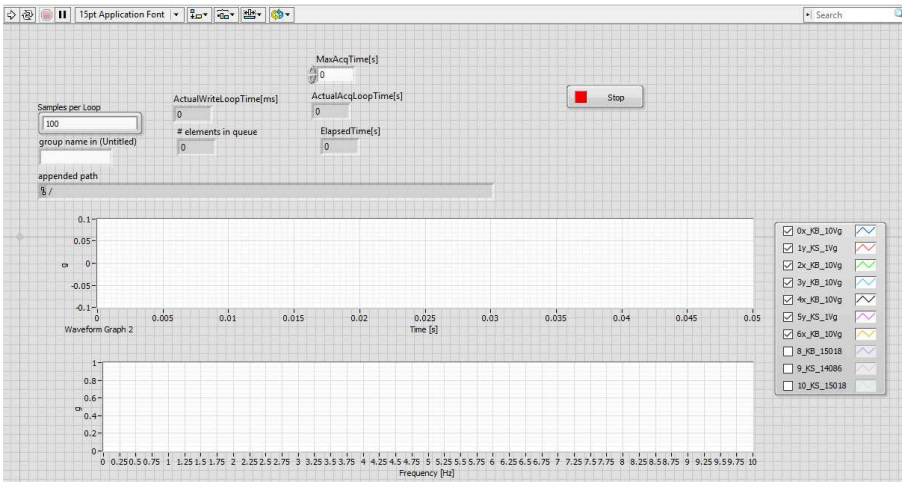

Figure 4.6 The Measurement and Automation eXplorer

The first main module of the implementation is data acquisition. When carrying out field measurements, it is important to carry out a quick processing: thus, a data acquisition module, able to manage the measurement hardware and to store data during field tests, has been developed.

In Figure 4.6 the user interface of the data acquisition management software is shown: when the "Run" button is pressed, communication with measurement hardware is started. The first chart on the top shows the recorded accelerations for the channels selected. Here it is possible to select the sampling rate and the duration of the acquisition.

The second chart shows the FFT of each channel. In this way it is possible to check the frequency of the signal in "real-time".

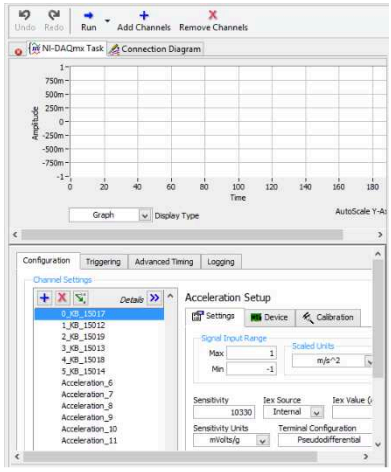

Figure 4.7 Front panel, channel management

Fig.4.7 shows the front panel of the channel management where it is possible to select the characteristics of each channel connected to the respective sensor (sensitivity, units, etc.).

After having verified that all sensors are properly working and that meaningful spectra can be obtained, it is possible to store data into one or several files.

Moreover, data acquisition is programmable in different ways. First, one can select the duration of acquisitions. Second, data collection can be triggered by a specific event, e.g. when a measured parameter exceeds a threshold (e.g. continuous monitoring). Third, acquisitions can be automatically set up in different periods using specific algorithms (e.g. periodic monitoring).

The second main module of the implementation is data pre-treatment. In the first state, the "Remove mean" VI is loaded: since the DC component of the signal has no physical meaning in civil engineering applications (accelerometers are mounted on structures characterized by a null net acceleration, so the DC component of the signal is only due to sensor circuitry), it has to be removed.

The second state is based on computation of the Fast Fourier Transform (FFT) of each channel, since it can be useful to detect eventual non-linearities and, above all, spurious harmonic components.

When all checks are done, the ultimate step before the modal identification is decimation procedure. This is done to reduce the sampling rate of the acquired data.

Then time histories can be processed according to the SSI algorithms as reported in (Sect. 3.4).

Chapter 5
Damage Detection

5.1 Introduction

The primary issues in civil and mechanical engineering is the detection of structural damages. Throughout its service life, a civil structure can be subjected to random seismic loading. These events may have a deep impact on building safety. Prediction of the remaining life of the building examined and the health conditions are the ultimate step in the SHM process (Fig.5.1).

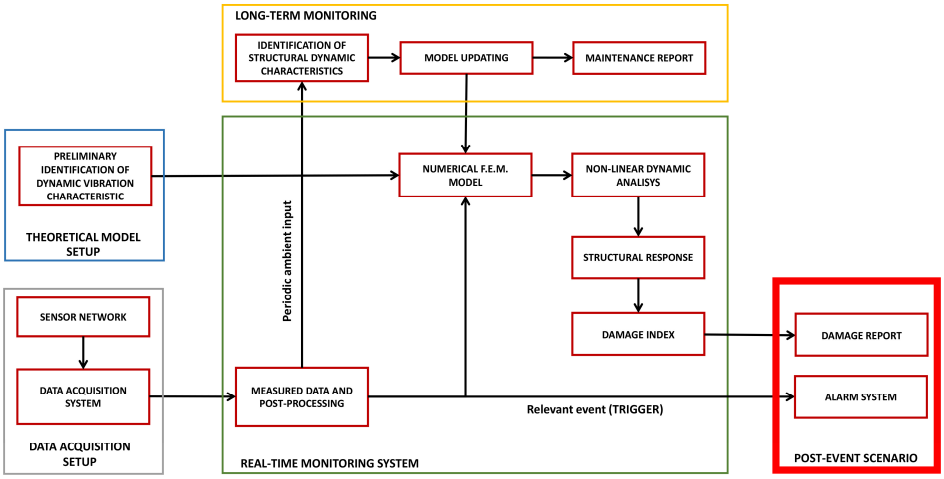

Figure 5.1 SHM process: from acquisition to damage detection

In recent years, the development of structural design criteria for new structures and the renewed importance of the assessment of seismic vulnerability of existing under-designed buildings have broadened the objectives of seismic design. While safety against collapse is still the main goal, performance in terms of functionality and economy have assumed a central role in the design criteria. Hence, a great effort has been made to improve the current earthquake-resistant design methods in order not only to avoid collapse under a destructive earthquake, but also to limit the damage under moderate earthquakes. Furthermore, the new design philosophy is tending to multi-level probabilistic structural performance criteria, replacing completely the simple force strength approach [27].

Seismic design is based on the following main criteria:

- preventing a non-structural damage in case of low-intensity seismic events;
- preventing a structural damage in case of medium-intensity seismic events;
- avoiding structural collapse in case of high-intensity earthquakes.

The implementation of all these new concepts requires the definition of quantitative **damage indices** and measures.

In the last twenty years numerous efforts have been made to estimate the damage level following a seismic event, using damage indices and calibrating them with available experimental data.

The seismic damage indices are used in the field of (i) vulnerability assessment, (ii) postearthquake damage assessment, (iii) decision regarding retrofitting of structures and (iv) performance evaluation of the structure. In all such applications, the threshold values of seismic damage indices play a very important role. The threshold values of the damage index can be determined by comparing different damage levels of the analytical model with the corresponding damage states. These values also have great importance when taking decisions related to repair and retrofitting of the building. Hence, quantification of the relationship between damage index, which quantifies the damage using analytical models, and the damage states, which provide categorization of observed seismic damage is a crucial task.

In this section, after a brief introduction of damage index definition and classification, a new method for damage localization and quantification is proposed, through a numerical approach.

5.2 Definition of Damage Index

In order to assess the structural damage it is necessary to know the available deformation capacity of the structure. The degree of structural damage can be estimated through **Damage Index DI**, comparing specific structural response parameters demanded by the earthquake with available structural deformation capacity:

$$DI = D/C \tag{5.1}$$

where *D* is the maximum inelastic response quantity (e.g. displacement, curvature, etc.) during a ground motion and *C* is capacity of the structure. Damage index is a normalized quantity, whose numeric value is, by definition, between 0 and 1. Value of *DI = 0* denotes the non-damaged structure, i.e. linear elastic behavior of the structure during earthquake, while *DI = 1* denotes the failure of the structure, i.e. local or general collapse of the structure.

The crucial aspect is the correlation between the analytically obtained damage indices with observed damage states. There have been several attempts to reach this goal worldwide, but this is still an open issue.

The dependence of damage degree of the structure from damage index was initiated by Park and Ang [28]. On the basis of data on damage in RC buildings that were moderately or severely damaged during several earthquakes in USA and Japan, they defined the relation between degree of damage and damage index (Table 5.1).

Degree of Damage	Damage Index	State of Structure
Minor	0.0 - 0.2	Serviceable
Moderate	0.2 - 0.5	Repairable

Degree of Damage	Damage Index	State of Structure
Severe	0.5 - 0.1	Irreparable
Collapse	> 1.0	Loss of storey or buildings

Table 5.1 Interpretation of damage index

For the values of damage index *DI < 0,2* the structure is exposed to minor damage, which is accompanied by visible cracks in structural elements and partition walls of the building. For this degree of damage there is no delay in the functioning of the facility, and rehabilitation of structures is relatively easy to implement. Damage index between 0,2 and 0,5 corresponds to a moderate degree of damage, which is accompanied with the appearance of reinforcement yielding in critical regions of some structural elements, including spalling of the concrete cover, as well as the formation of larger cracks in plastic hinge zones. The value of damage index *DI = 0,5* is usually considered as the boundary between moderate and severe degrees of damage, i.e. the boundary between the damage that can be repaired and the damage that is irreparable or the cost of their repair is economically unacceptable. Severe damage (*DI > 0,5*) at the critical sections of structural elements presents the appearance of concrete crushing and local buckling of longitudinal bars in plastic hinge zones. The failure of the structure corresponds to the value of damage index $DI \geqslant 1$. It is usually accompanied by loss of shear and/or axial load bearing capacity of some structural elements, resulting in partial or complete collapse of the building.

In 1989 Bracci [29] proposed another classification that takes into account the possibility of repairing a building: undamaged building, minor damaged building, repairable building, collapsed building.

As reported in [27] several authors have tried to correlate the analytically obtained damage indices with observed damage states.

Many of them still suffer from some limitations. First, representing the health state of an entire structure with a damage index is a difficult task. Second, many of these indices take into account a damage state greater than 1. This means that the capacity of the structure would be underestimated in relation to the demand of external actions.

5.2.1 Damage Indices: Classification

The problem of classifying seismically induced damage indices was approached by [30–32] and others. The main classification of damage indices can generally be done as follows:

- **Local damage indices**, refer to a structural member (e.g. column, beam, etc.);
- **Global damage indices**, take into account the whole structure by combining local damage indices. They are calculated by weighting the local indices or by comparing the modal properties of the structure before and after the seismic action;
- **Individual damage indices**, refer to a subset of the structure or structural portion.

Each of them can also be classified into two main damage index families;

- **non-cumulative damage indices,** consider damage as function of a physical quantity (e.g. displacement, curvature, etc.) respect to the maximum capacity offered by the structure;
- **cumulative damage indices,** consider damage as a function of accumulated plastic deformation and can incorporate a term referring to the seismically absorbed hysteretic energy.

The first **Local non-cumulative DI's** were proposed by Newmark and Rosenblueth [33], using the ductility factor as a mean to assess damage. The factor can be expressed either as a function of curvature φ , rotation ϑ or displacement d, using the following relations (5.2):

$$\mu_r(\varphi) = \frac{\varphi_m}{\varphi_y},\ \mu_r(\vartheta) = \frac{\vartheta_m}{\vartheta_y},\ \mu_r(d) = \frac{d_m}{d_y} \qquad 5.2$$

where *m* denotes the maximum value and *y* the yielding value. The choice of kinematic or cyclic ductility as a damage measure is equivalent to assuming that the collapse of the structural model is expected for maximum plastic displacement, independent of the number of plastic cycles and the amount of dissipated energy.

Other similar approaches consider the elastic stiffness and curvature of members.

Local Cumulative DI's consider damage accumulation and are expressed in terms of hysteretic cycles of the considered element. These can be formulated in terms of Displacement, Force, Hysteretic energy or as a combination of them.

A classical example is given by Banon and Veneziano [34] where N_{cr} will denote the normalized cumulative rotation damage index, φ_{im} is the maximum rotation in cycle *i*.

$$N_{cr} = \frac{\sum_{i=1}^{n}|\varphi_{im}-\varphi|}{\varphi_u} \qquad 5.3$$

Using the same formulation Cumulative Indices can be expressed in terms of Force or Hysteretic Energy.

Global damage indices take into account the whole structure and its characteristics and provide information about the global damage state as a function of the distribution and severity of local damage.

A classical example is formulated by Roufaiel and Meyer [35]. Using the structures capacity curve they developed a strain-based global damage index that is defined as:

$$I_{Dglobal} = GDB\,\frac{d_m-d_y}{d_u-d_y} \qquad 5.4$$

where d_y is the yielding displacement, d_u ultimate displacement, d_m maximum displacement, GDP global parameter defining the damage state.

5.2.2 Review of the most commonly used damage indices

There are several definitions of the damage indices, and it is common to all of them that they compare the response parameters demanded by the earthquake with structural capacity [36]. Structural capacity refers to an ultimate value of the response parameter, which is usually defined in the sense of its maximum value under monotonically increasing

lateral deformation. For example, a deformation δ_u under which an abrupt loss of the strength occurs, and which represents a fraction of the ultimate deformation capacity of the system under monotonically increasing deformation, has been used as the available deformation capacity during the earthquake motion (Fig. 5.2).

Structural damage indices usually consider a measure of the deformation demands in the structure. While some consider the maximum deformation demand, others take into account the cumulative plastic deformation demands.

Damage index based on plastic deformation under monotonically increasing lateral deformation was proposed by Powell and Allahabadi:

$$DI_\mu = \frac{\delta - \delta_y}{\delta_u - \delta_y} = \frac{\mu - 1}{\mu_u - 1} \qquad 5.5$$

where δ is the maximum inelastic displacement during an earthquake, δ_y is the yelding displacement and δ_u the ultimate displacement, i.e. the capacity, both computed with a preliminary nonlinear static (pushover) analysis. This index is representative of the conditions of the entire structure and belong to the category of Global Damage Index, according to the classification reported in [37].

In equation (5.5), μ is the maximum ductility demand during an earthquake ($\mu = \delta/\delta_y$), while μ_u is the monotonic ductility capacity, defined as $\mu_u = \delta_u/\delta_y$.

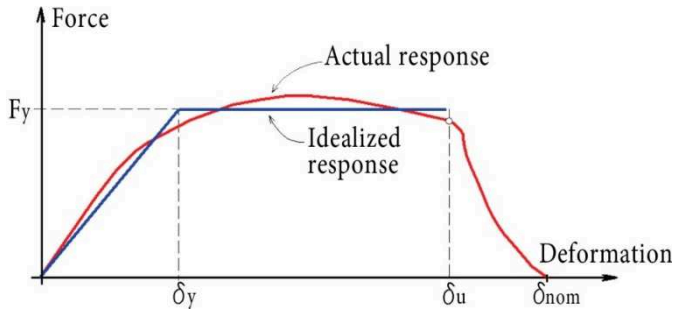

Figure 5.2 Force-displacement relationship under monotonically increasing deformation

Damage index DI_μ is based on displacement ductility, i.e. on the maximum inelastic deformation. It gives an accurate value of damage due to static unidirectional load (Fig. 5.2), but displacement ductility itself does not reveal information on the repeated cycles of inelastic deformation and energy dissipation demand during an earthquake.

Following a seismic event a number of the repeated cycles of inelastic deformations occur, so the other structural response parameters are also used for estimation of the structural damage. Considering that the hysteretic energy includes cumulative effects of inelastic response and is associated with the structural damage, Mahin and Bertero defined normalized hysteretic energy ductility μ_h:

$$\mu_h = 1 + \frac{E_h}{F_y u_y} \qquad 5.6$$

where E_h, F_y and u_y are hysteretic energy, yield strength of the structure and yield displacement, respectively.

Numerical value of hysteretic ductility μ_h is equal to the displacement ductility of an elastic-perfectly-plastic (EPP) system under a monotonically increasing lateral deformation that dissipates the same hysteretic energy as the actual system. For the EPP system the damage index, which depends of the hysteretic energy [5], can be defined:

$$DI_h = \frac{E_h}{F_y(\delta_u - \delta_y)} \tag{5.7}$$

For a general force-displacement relationship, this damage index can be presented in the following form:

$$DI_h = \frac{E_h}{E_{hu}} \tag{5.8}$$

where E_{hu} is hysteretic energy capacity of the system under monotonically increasing lateral deformation.

A widely used damage index is the Park and Ang index [38], which is defined as the linear combination of the maximum displacement and the dissipated energy:

$$DI_{PA} = \left(\frac{\mu - 1}{\mu_u - 1}\right) + \beta \frac{E_h}{F_y(\delta_u - \delta_y)} \tag{5.9}$$

where parameter β depends on the value of the shear and axial forces and the total amount of longitudinal and confining reinforcement using a regression curve experimentally obtained. However, parameter β is difficult to determine experimentally, and the methodology is not well stated [39].

Another approach, based on damage accumulation due to cyclic loading, can be modeled by the general deformation cumulative index defined as the plastic fatigue index [40]:

$$DI_f = \sum_{i=1}^{n} \left(\frac{\mu - 1}{\mu_u - 1}\right)^b \tag{5.10}$$

where *n* is the number of hysteretic cycles. The value assumed by this damage index is defined regarding the constant *b*, which depends on the structural material, on the type and number of different plastic displacements. The DI_f index is difficult to determine due to its dependence on the aleatory parameter *b*.

Starting from these formulations, several researchers developed others damage indices. Many of these are geared toward damage accumulation in terms of hysteretic energy.

In this way the concept of "number of equivalent cycle" n_{eq} has been introduced, and is given by [41]:

$$n_{eq} = \frac{E_h}{F_y \cdot \Delta\delta_{max}} \tag{5.11}$$

here $\Delta\delta_{max}$ is the maximum value of plastic deformation, E_h is the hysteretic energy dissipated, F_y is the yelding force. It is referred to an elastic perfectly plastic behavior.

A value of $n_{eq} = 1$ state the presence of a unique cycle, typical of impulsive earthquake. Higher values of n_{eq} indicate the presence of several hysteretic cycles, typical of long-lasting seismic events.

This group of indices are very attractive and the research initiatives makes them an open task for future developments. Despite their appeal, these indices are difficult to determine in the monitoring system of civil structures.

Against this background, in the next section a damage detection application is proposed through a numerical approach.

5.3 Damage detection in a civil structure subjected to an earthquake

5.3.1 Research motivation

The present research describes a numerical approach for damage detection of a precast building.

Seismic risk mitigation is a relevant issue in European regions, such as Italy, characterized by the presence of a large stock of existing vulnerable industrial buildings.

Through a case study, the work proposes an integrated novel approach for the diagnosis of structures after a seismic event. The suggested monitoring system is based on recording the accelerations of a real structure during an earthquake and on their introduction as input into a Numerical Model (NM), suitably tuned, to outline a possible post-earthquake scenario.

The leading idea of this approach is to provide an estimation of the health and remaining life of monitored structures and to detect and quantify the damage, some of the crucial issues of SHM. The technique is applied to a real structure, an industrial building liable to some seismic vulnerabilities.

It is worth noting that, when the present work was developed, the structure had not yet been subjected to an earthquake. Recent seismic events of September 2016 struck the Italian regions of Umbria-Marche. The investigated building did not suffer any damage, even though the epicenter was quite close. Unfortunately, the monitoring system was not in operation and data acquisition is not available. For this reason, the present research is based on numerical simulations using different FE models.

In addition, the present work has been developed before the execution of the Ambient Vibration Survey (AVS) (see Chapter 6) so it is referred to numerical simulation and theoretical assumptions. Future developments will be focused on the application of the presented approach using the updated Numerical Model (NM).

Recent seismic events in Italy (e.g. Emilia Romagna earthquake, 2012) have clearly shown the high seismic vulnerability of existing precast (industrial) buildings that often reveal an inadequate safety level against seismic actions [42,43]. These events produce structural damages and, in the worst case, lead to loss of life. Therefore, an integrated structural monitoring system for existing buildings is very useful for determining the effects of an earthquake, in particular for precast concrete structures.

SHM techniques are used, among others, to predict the residual life of the structure before it reaches its collapse [2,44]. In fact, following the evolution of structural damage

over time it is crucial to understand if the damage mechanism has stopped and if the structure still has an adequate resistance.

These techniques belong to the field of Nondestructive Damage Detection (NDD), where much effort has been devoted to develop not only local but also global methods able to assess the health condition of the whole structure [45] and are referred to as "Global Damage Detection Method" (GDDM).

Usually, building safety assessment after a natural disaster, such as an earthquake, is currently evaluated manually by certified inspectors who identify visible damage on the structural elements. This process has been proven to be time-consuming [46], costly, as well as subjective due to the reliance on the opinion and judgment of the inspector [47] and can delay response and recovery [48].

Building assessment practices are a significant factor when concerning loss of life as well as the impact on the community and economy [49]. It has been established that economic losses and the overall impact of earthquakes could be significantly reduced by critical and timely information provisions in the response after the disaster [50].

Consequently, this research is focused on a cost-effective and automated procedure aimed to evaluate the damage level and health conditions of monitored structures.

It should be considered that following a seismic event only the final effect of deformations on a structure is visible. Moreover, it is difficult to understand what happens to a structure during an earthquake, resulting in limited knowledge of the structural response.

In this work a novel approach is presented – previously introduced in a preliminary manner and in a different kind of structure in [51–53] with which to perform the diagnosis of a structure.

The method is based on recording floor accelerations of a real structure during a seismic action, and on their introduction as nodal accelerations in a refined Numerical Model (NM) of the structure, strongly nonlinear, endowed with an elastic plastic (softening) constitutive law. The model is then able to detect the existence, the position and the amount of damage induced in the structure by the earthquake, providing a possible post-earthquake scenario.

The system, through the evaluation of the structural response, provides information that can be used in the process for assessing the practicability of the building. For example, in the case of a low-intensity earthquake that does not produce visible damage, the proposed monitoring system is a powerful support tool for the immediate resumption of production activities with clear economic and business advantages, especially for industrial buildings. On the other hand, when a high-intensity seismic event occurs, the present monitoring system can not only warn people inside the building during the earthquake but also become a design tool for structural rehabilitation.

Another principal purpose of this work is quantification of the damage through the evaluation of damage indices. The ductility damage index will be used to evaluate the structural capacity in the plastic field. Considering that this index is defined regarding displacement, it seems to be the most suitable for precast structures. Using this approach, a comparison between two configurations of the system (initial and damaged) can establish location and severity of damages according to Rytter's classification [54].

It is necessary to estimate the yield and ultimate displacement to calculate the ductility damage index. Thus, a nonlinear static analysis is preliminarily performed to extract the capacity curve of the considered structure. However, it should be noticed that deformable storeys often characterize precast structures with very slender columns. Therefore, for these particular constructions, the capacity curve strictly depends on the choice of the

analysis control node. Because of these considerations, it was decided not to assume a priori a given control node, but to identify it through a procedure, called "Global Control Pushover Analysis" (GCPA), as described in the next sections.

A Finite Element Method (FEM) model simulates the response of the structure under a given seismic input. In this first part, the non-linear analysis is performed with the Seismostruct© software, using as input both artificial (generated with Simqke-GR [55]) and real recorded accelerograms. Certainly, in practical SHM applications, this part is absent since accelerometers directly measure true accelerations on some key points of the structure.

From this NM, the "pseudo-measured" accelerations of the points where the accelerometers are installed are stored, using them as input for the SHM procedure. Also, the SHM requires an NM of the structure (to convert the measured accelerations into, e.g., damage to the structure). To make the whole process is more precise and realistic, in this part, a different software (MidasGen©[56]) is used for the numerical simulation. This phase constitutes the core of the proposed SHM approach.

To obtain reliable results, it is necessary that both software agree in describing the mechanical behavior of the structure. Tuning the two models is done regarding displacement, velocity and acceleration obtained from linear and nonlinear dynamic analyses.

In the final part a comparison is performed between the displacements resulting from a nonlinear dynamic analysis having pseudo-measured accelerations as input, and the displacement thresholds given by the capacity curves of the structure. The process permits to calculate the damage indices, which represent the main result of this paper.

A global damage index will be proposed, evaluated according to the thresholds established from the GCPA results. This index is representative of the health of the entire structure, and it is used for emergency conditions when the plastic regime is activated (e.g. building evacuation).

In the following sections the main results of the research are reported, for details see [57].

5.3.2 Description of the structure

The industrial building is situated in a small Italian town 80km from Ancona, the main city of Marche region. This area was subjected to the Umbria-Marche earthquake (which in the epicenter zone registered a magnitude of 6.3) that struck central Italy in 1997. The structure has a simple and geometrically regular structural scheme, which is typical for r.c. precast industrial architecture (Fig. 5.3).

Figure 5.3 External view of the building.

Despite this, it is characterized by a non-uniform distribution of the storey masses because the building has two floors, while the central part is double-height. The plan covers an area of about 4.000 m2. It is a rectangle of 80 m in the longitudinal direction and 50 m in the transversal one (Fig. 5.4), and is characterized by rectangular nets of columns of 10 m x 10 m and 10 m x 15 m.

All elements are precast, except for some in-situ cast concrete substructures. The structure has reinforced (precast) concrete columns, while beams and other horizontal elements are made of pre-stressed concrete. The building also has concrete bearing walls and a reinforced concrete lift, which constitutes a significant rigidity core. The first-floor height is 3.84m while the second-floor is equal to 4.57m; the NM is realized assuming fixed base at the finished ground floor (z = 0 m), the first level at z = 3.84 m and the roof at z = 8.41 m.

The maximum height of the columns, measured from foundations, is about 8.41 m, with a square cross-section of 0.6 m x 0.6 m (Fig. 5.5a). There are two main types of beam: the perimetric ones have an L cross-section (Fig. 5.5c), while the others have a T cross-section (Fig. 5.5b). A beam with a double-T cross-section connects the top of the double-height central columns (Fig. 5.5d).

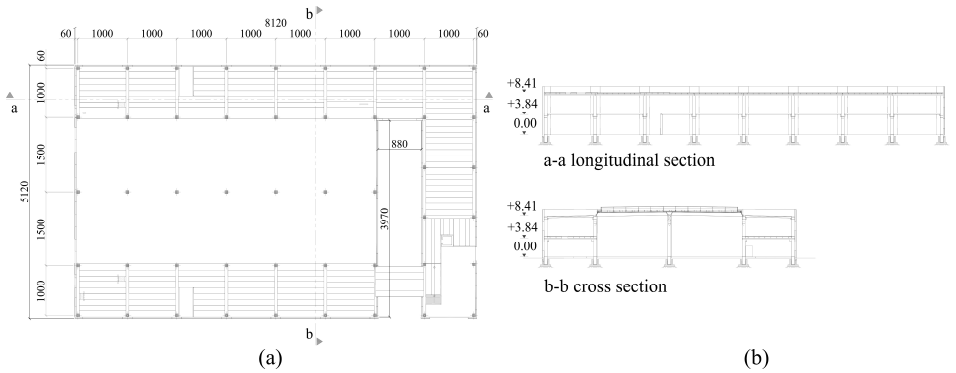

Figure 5.4 (a) Plan view and (b) vertical sections of the building

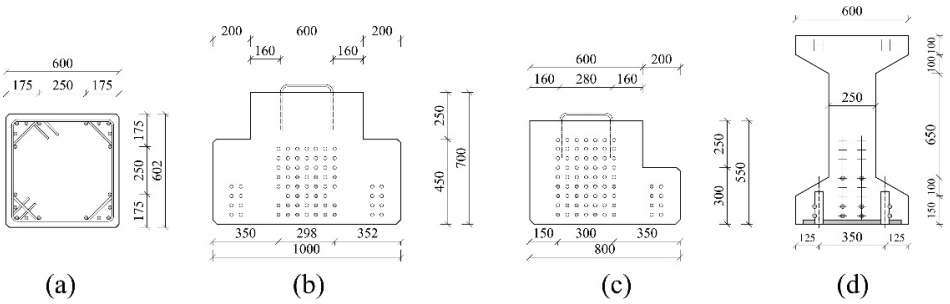

Figure 5.5 Main dimensions of the cross-section elements: (a) columns, (b) (c) beams, (d) double T beams.

The foundations consist of plinths linked by a reinforced concrete slab, and at the ground level, there is a reinforced industrial floor: these characteristics permit one not only to consider the columns fixed at their base but also to neglect any effect related to seismic input asynchrony at the base of different columns.

All components (beams, columns and roof elements) are joined (to each other) with double-sided dowel pin connections (evaluated with CNR 10025/84 [58] and CNR 10025/98) with end anchors. The relative slip between the main elements is thus nil [59], and the possible concrete spalling rupture (see also Fib n. 43 [60]) is always controlled by the transversal reinforcement of the considered elements.

Table 5.2 reports the mechanical parameters used in the NM of the structure. The accuracy level used to set all the associated parameters (materials, the dimension of elements, rebar, stirrups, connections and mechanical properties) is high enough to consider the NM extremely reliable both in the linear and nonlinear field.

F_{ym} = mean value of the yielding strength; E_m = Young Modulus of the concrete

	f_c (Mpa)	E_m (Mpa)	f_{ym} bars/stirrups (Mpa)
Columns	40	35220	450
Beams	45	36283	450

Table 5.2. Mechanical characteristics of the main elements (see Fig. 5.5)

5.3.3 FEM model calibration with linear and nonlinear analysis

The examined industrial building is a precast structure: typically, the connections among the elements should be modeled as cylindrical or spherical hinges depending on the constraint degree offered by the connections. Due to the recent construction and the use of double-sided dowel pin connections [61] it is plausible to consider the cylindrical constraints where only the torsional moment of the beams is restrained.

All columns are modeled as one-dimensional finite elements fixed at the ground level (z=0 m). Despite the presence of a concrete slab on three sides of the building, it is reasonable to consider a structural configuration with deformable storeys due to the large distance between columns (10 m).

The presence of the panels was considered regarding concentrated loads and masses applied to the columns.

The masses are uniformly distributed along the elements as well as the loads.

In Table 5.3 the results of the eigenvalues analysis are shown; the two NMs provide very similar periods, participant masses and modal shapes (Fig. 5.6), confirming that they match satisfactorily (at least in the linear regime) and can be used for the current purposes.

In the simulated monitoring system, it is necessary to perform a nonlinear dynamic analysis and then to acquire data from the SeismoStruct© model, which is considered the "real structure", and introduce them as input in the MidasGen© model to obtain the post-event damage scenario.

MODE (n°)	**Frequency (%)**		**Error (%)**	**Particip. Mass X-dir. (%)**		**Particip. Mass Y-dir. (%)**	
	MIDAS	SEISMO		MIDAS	SEISMO	MIDAS	SEISMO
1	**0.938**	**0.947**	0.95%	0.000	0.000	**9.378**	**9.473**
2	**0.968**	**0.974**	0.63%	0.004	0.013	**33.568**	**32.758**
3	**1.002**	**1.006**	0.46%	**55.070**	**53.342**	0.526	0.598
4	**1.051**	**1.039**	1.08%	0.000	0.979	1.198	0.761
5	**1.156**	**1.177**	1.83%	0.000	0.024	0.737	11.048
6	**1.185**	**1.209**	2.03%	0.000	0.000	15.419	0.783
7	**1.279**	**1.248**	2.42%	0.100	0.055	**5.726**	**7.351**
8	**1.354**	**1.275**	6.15%	0.001	0.000	1.194	2.388
9	**1.365**	**1.323**	3.14%	0.693	0.846	0.021	0.381

Table 5.3 Modal parameters of the structure (in bold the participation masses of the main modes)

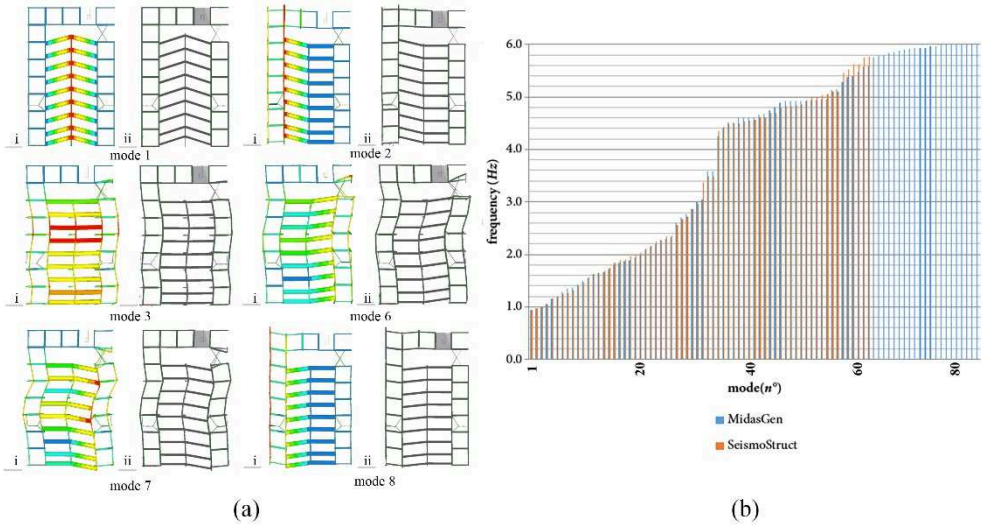

Figure 5.6 (a) Modal shapes with Seismostruct© (i) and MidasGen© (ii) (b) Frequency comparison between the two models.

The fiber model approach [62,63] is used in both software to have a realistic description of the post-elastic behavior of the reinforced concrete structure. In a fiber model, the axial force and the bending moments of the section are calculated by summing up the stress of each fiber. The elements are transversely and longitudinally discretized in a considerable number of fibers using a force-based element formulation [64]. Each fiber is then associated with a specific constitutive law defining the hysteretic behavior of each material.

The literature proposes many examples, based on experimental tests, for the behavior of concrete subjected to cyclic loads [65][66]. The Kent and Park model [67] is used, which is refined to take into account the confinement contribution of the stirrups and which does not consider the low traction resistance of concrete (Fig. 5.7 a). For the nonlinear behavior of steel, the Menegotto and Pinto model as modified by [68] including the hardening effect, is used (Fig. 5.7 b).

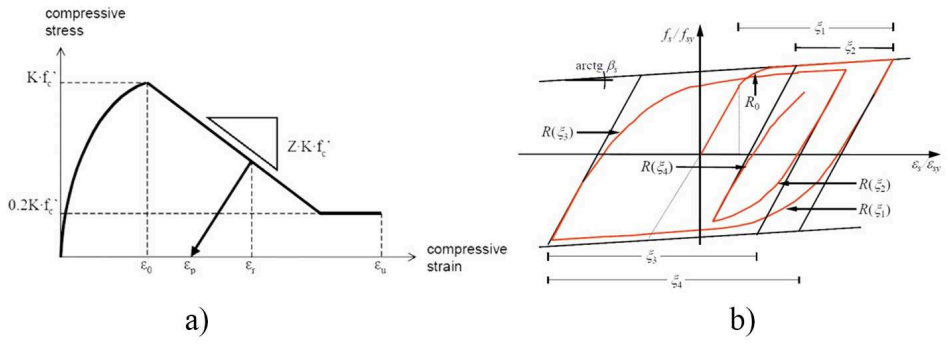

Figure 5.7 Constitutive laws of materials: (a) Kent & Park model for concrete, (b) Menegotto & Pinto model for steel

For the Kent & Park model formulation the following parameters have to be defined:

- f_c': compressive strength. In this case the inelastic properties are assigned to the columns (C40/50) which correspond to $f_c' = 40\ MPa$;
- ε_{c0}: strain value corresponding to maximum strength, set at 2‰;
- ε_{cu}: maximum strain, $\varepsilon_{cu} > \varepsilon_{c1} = 0{,}8/Z + \varepsilon_{c0}$;
- K: strenght increment for concrete confinement, given by:

$$K = 1 + \frac{\rho_s f_{yh}}{f_{c'}} \tag{5.12}$$

  Where ρ_s is the ratio between stirrups and concrete volume, and f_{yh} is the yielding strength of the stirrups
- Z: slope of softening curve, given by:

$$Z = \frac{0{,}5}{\frac{3+0{,}29 f_c'}{145 f_c' + 1000} + 0{,}75\rho_s\sqrt{\frac{h'}{s_h}} - 0{,}002K} \tag{5.13}$$

Where h' is the maximum side of the concrete core and s_h is the interaxle of the stirrups.

In the following table the parameters used for the formulation of Kent & Park model are reported:

f_c'	f_{yh}	ρ_s	K	h'	s_h	Z	ε_{c0}	ε_{c1}	ε_{cu}
(MPa)	(MPa)	(%)	(-)	(cm)	(cm)	(-)	(-)	(-)	(-)
40	450	0.015	1.17	48	12	212	0.002	0.006	0.007

Table 5.4 Kent and Park parameters

For steel elements Menegotto & Pinto model is defined through the following formulation:

$$\overline{f_s} = \beta_s \overline{\varepsilon_s} + \frac{(1-\beta_s)\overline{\varepsilon_s}}{\left(1+|\overline{\varepsilon_s}|^R\right)^{1/R}} \tag{5.14}$$

where:

- $\overline{f_s} = f_s/f_{sy}$ e $\overline{\varepsilon_s} = \varepsilon_s/\varepsilon_{sy}$ for the first load curve;
- $\overline{f_s} = (f_s - f_{si})/(f_{sy} - f_{si})$ e $\overline{\varepsilon_s} = (\varepsilon_s - \varepsilon_{si})/(\varepsilon_{sy} - \varepsilon_{si})$ for the load curves following the first inversion.

f_{sy} and ε_{sy} are the tension and deformation corresponding to the first load curve, respectively (Fig. 5.7b). f_{si} e ε_{si} are the coordinates corresponding to the most recent point of load inversion.

Others parameters are proposed by Menegotto and Pinto and are summarized in Tab. 5.5.

E_s	f_{sy}	β_s(b)	R_0	a_1	a_2	γ_s
(MPa)	(MPa)	(-)	(-)	(-)	(-)	(KN/m^3)
$2{,}0\cdot10^5$	450	0,0052	20	18,5	0,15	78

Table 5.5 Menegotto and Pinto parameters

Each time-history is obtained using Newmark's integration algorithm [69] present in both software. The accuracy of Newmark's method depends on the period of excitation; in the subsequent analyses, each step of integration ($\Delta t = 0.01$ sec) satisfies the relation

$\Delta t \leq 0.318\, T_n$, where T_n (0.162 sec) is the period of the vibration mode that allows to reach 85% of the participating mass [23].

The dissipation in both NMs is introduced by the Rayleigh approach, where the dissipation matrix [C] is assumed as a linear combination of the mass [M] and the stiffness matrix [K]:

$$[C] = \alpha_0[M] + \alpha_1[K] \quad . \tag{5.15}$$

The coefficients α_0 e α_1 are calculated, using the same damping ratio $\xi_0 = 0.05$ for r.c. structures and considering the range of frequency of interest $\omega_i\ e\ \omega_j$ as follows:

$$\alpha_0 = \xi_0 \frac{2\omega_i\omega_j}{\omega_i+\omega_j}\ [\text{sec}^{-1}] \qquad \alpha_1 = \xi_0 \frac{2}{\omega_i+\omega_j}\ [\text{sec}] \tag{5.16}$$

The number of modes that altogether excite 85% of participation mass is 87. Thus, the frequency related to the 1st and the 87th mode, respectively equal to 0.938 and 6.110 (cycles/sec), have to be substituted in (5.16), obtaining the values of $\alpha_0 = 0.5111$ and $\alpha_1 = 0.00225$. All the damping values corresponding to the frequency range $\omega_i\ e\ \omega_j$ have been calculated, obtaining the follows graphs (Fig. 5.8b):

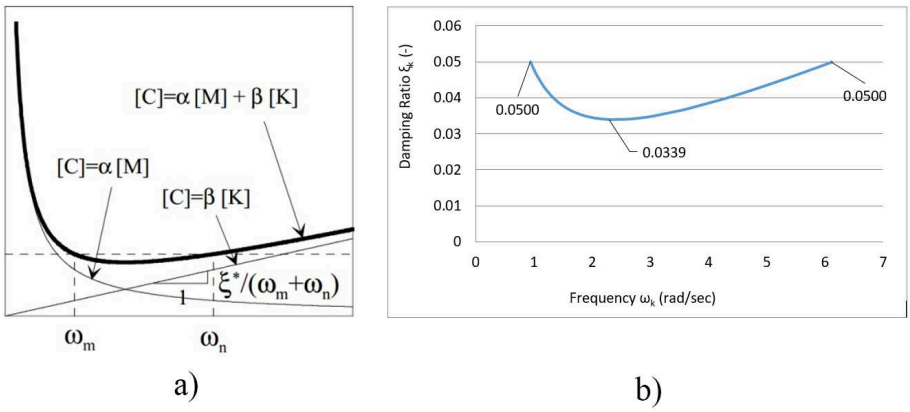

Figure 5.8 Rayleigh dissipation approach: (a) general formulation, (b) Rayleigh curve obtained with numerical parameters

The graph (Fig.5.8b) shows the damping ratio corresponding to the frequency range of interest: the minimum value is 3.39% that corresponds to the 28th mode (2.40Hz). Several research works concerning the dynamic identification of civil r.c. structures have shown that the value of damping coefficient obtained from AVS often ranges between 1Hz – 3Hz [70][4]. For this reason, the proposed dissipation approach can be considered applicable, according to the experimental results.

To have realistic accelerations to reintroduce as input into the damage identification process, 25 seconds spectrum-compatible time-histories are generated (Fig. 5.9) through the Simqke_GR software [55] and used as ground acceleration at the base of the columns.

As already mentioned, this step is necessary because real acquisitions are not available, and the ground excitation with an artificial input has to be simulated.

Ground acceleration is also used to check the agreement of the two software in the post-elastic regime.

The considered industrial building belongs to “Class II” in the Italian seismic code [71] This implies that the Limit State of Collapse (SLC in Italian) is associated with a recurrence period (TR) of 475 years, which corresponds to an expected peak ground acceleration (PGA) equal to 0.312g. The other parameters that characterize the elastic response spectrum are (soil type T1 and category of subsoil C are considered): S = 1.5; TB = 0.169 s; TC = 0.509 s; TD = 2.494 s. The frequency content of the seismic signal using the Fast Fourier Transform algorithm (FFT) with a frequency resolution of 0.05Hz is also reported (Fig.5.9).

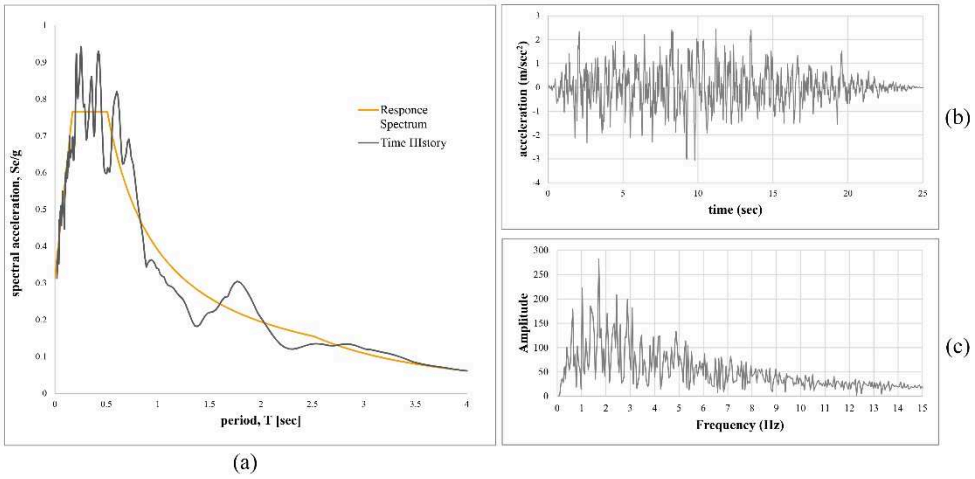

Figure 5.9 (a) The reference response spectrum for T_R (SLC) = 475 years and the spectra corresponding to the considered ground accelerations (TH), damping ξ=5%. (b) Time history accelerations. (c) FFT

A comparison in terms of displacement, velocity and acceleration time histories (output) obtained by the two models subjected to the same ground acceleration (input), is reported in Fig. 5.10 and shows an excellent agreement. For brevity only results in the X and Y directions for two nodes situated in different structural portions are presented (similar results are obtained for the other nodes).

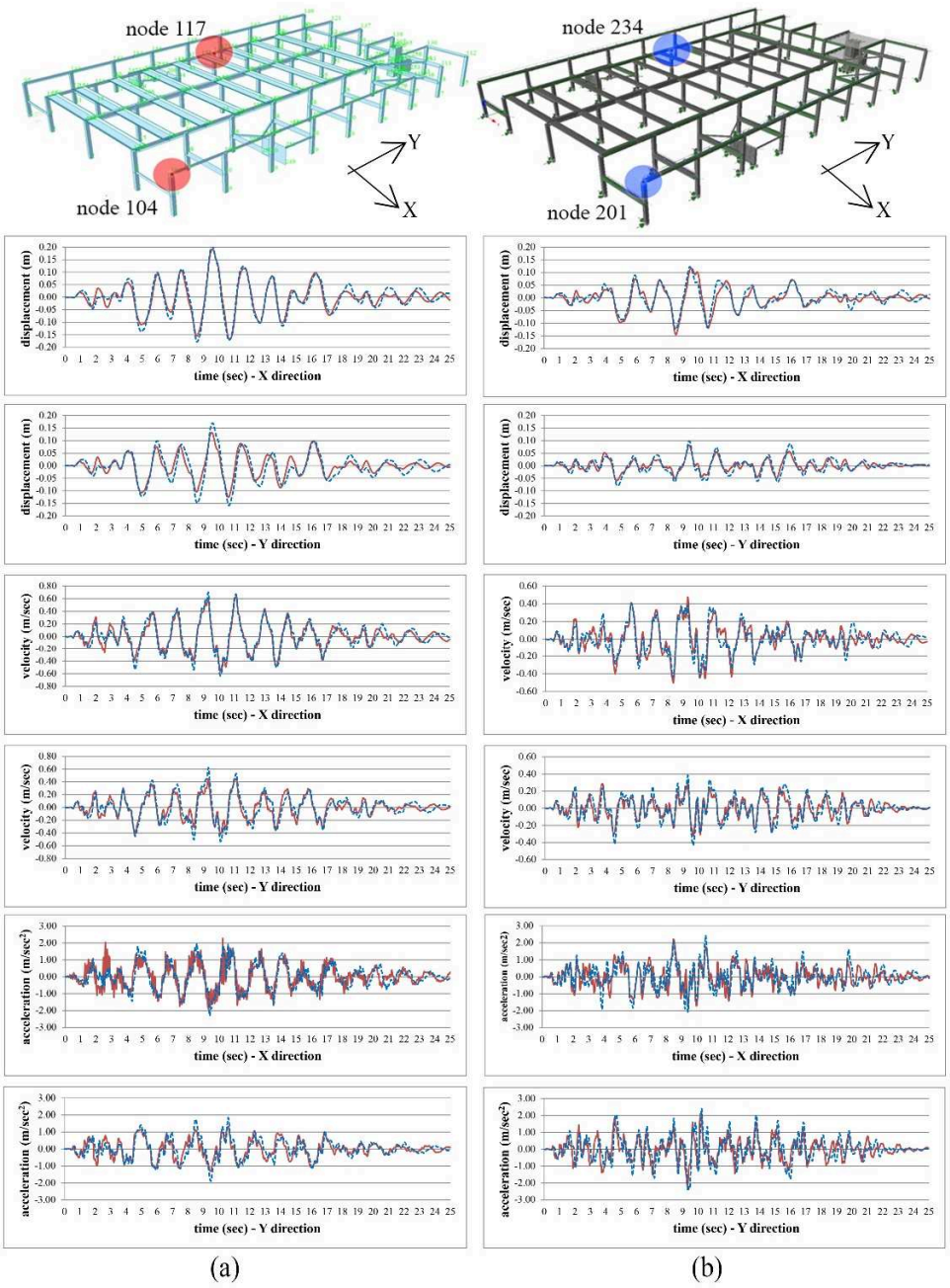

Figure 5.10 Comparison between the two software: displacement [m], velocity [m/sec], acceleration [m/sec^2] (red line – Seismo, blue line – Midas): (a) node 234 (Midas) and 117 (Seismo); (b) node 201 (Midas) and 104 (Seismo)

5.3.4 SHM implementation and damage indices

Accelerations are derived from the SeismoStruct© software and then reintroduced as input into the MidasGen© software to simulate the process of the proposed monitoring system.

Due to storey deformability, not all the nodes at the same level have the same acceleration. However, structural parts having similar nodal acceleration can be identified. In fact, instead of taking a different acceleration for each node, different columns with similar behavior were grouped, checking this similarity by comparing each nodal time-history response. Candidate columns have been selected by two different criteria, that involve time and frequency domains. First, the time values corresponding to the most significant acceleration peaks of each selected node can differ no more than 0.2sec (synchronization criterion). Second, the difference between each main frequency peaks in the Fourier transform of the selected time histories must be less than 0.1Hz (frequency content criterion). Both criteria have to be simultaneously satisfied.

Each group will be associated with the same acceleration (the maximum obtained by the nonlinear dynamic analysis conducted by Seismostruct©): this allows to consider just a few acceleration time histories, considerably reducing the computational time. This approach seems to represent quite well a real monitoring system, where in SHM applications the structures are usually equipped with a reduced number of sensors compared to the number of structural nodes. It would be too costly and difficult to use as many accelerometers as the nodes of the structure. Fig. 5.11 highlights the portions of the structure with similar behavior; this is done for the first and the second level.

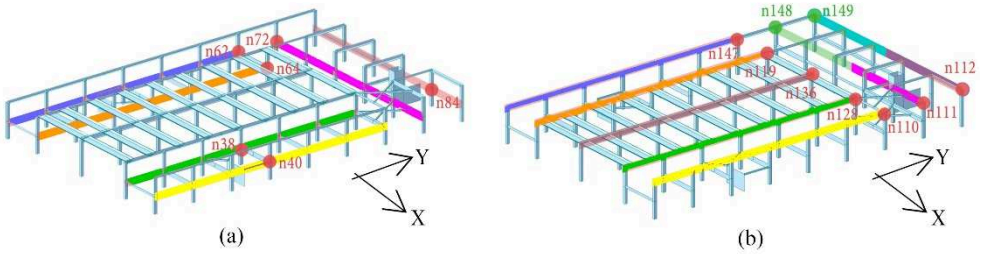

Figure 5.11 Groups of columns with uniform behavior and nodes with maximum acceleration response for (a) the first level, and (b) the second level.

At this stage, the nonlinear dynamic analysis in MidasGen© can be performed to detect the amount of structural damage and to calculate the damage indices, as subsequently discussed.

Damage indices and localization of the damage

One of the goals of this work is to compute a specific damage index that can be implemented within a system of real-time SHM and can be used to quantify the damage state at each time step and the possible incipient collapse [32].

As said, in the first instance, the damage can be classified as “local” when it refers to a single member, as “intermediate” if it concerns a portion of the overall structure or as “global” if it regards the whole structure.

In this work the ductility damage index DI_μ proposed by Powell and Allahabadi [72] is used, as reported in previously sections.

This index is representative of the conditions of the entire structure and belongs to the category of Global Damage Index, according to the classification reported in the previous section.

The $\boldsymbol{DI_\mu}$ does not consider damage accumulation [73], but depends on displacements beyond the elastic threshold, one of the most representative parameters to keep under control in these precast structures. Moreover, the presence of double-sided dowel pin connections voids the relative slip between columns and beams. For this reason, the specific vulnerability of the case study is due to the appearance of plastic hinges at the column bases.

It is worth noting that if the displacement remains below the elastic threshold the damage index is equal to zero and the structure is undamaged.

To evaluate a damage index, a pushover analysis must be preliminarily performed: it is usually achieved with a master node coincident with the center of mass of the last floor that is representative of the structural behavior [74].

In this case, however, the classic approach would be incorrect considering that the capacity curve is strictly dependent on the choice of the node, because of the in-plane deformability of the flat floors. For these reasons a "Global Control Pushover Analysis" (GCPA) is proposed, monitoring which node first reaches the target displacement, set at 0.30 m, under monotonic loading. In this way, it is possible to detect which portion of the structure reaches collapse first, and then to perform a pushover analysis monitoring the selected nodes in each direction.

The pushover analyses were performed not only with a diffused plasticity formulation (fiber approach) of the model, but also with a lumped one. This permitted to compare the two different nonlinear models, and to understand if the output response was approximately the same.

The capacity curves obtained from the two analyses (fibers and lumped hinges) were comparable, having very similar shear and displacement values at yielding. On the other hand, the ultimate shear and the ultimate displacement obtained with lumped plasticity are lower than the values provided by the fiber approach. As a result, it was decided to opt for the lumped approach because it allows to stay on the safe side. Furthermore, the concentrated plasticity captures the softening behavior of the capacity curve more clearly.

In the lumped plasticity approach the nonlinearity has been assigned only to the bottom of the columns, with elastoplastic curves for bending moments in agreement with the nonlinear constitutive law suggested by Eurocode 8 [75]. Shear failures have been taken into account by introducing plastic hinges with limited ductility behavior [76].

The pushover analyses highlighted which part of the structure reaches the target displacement first in both directions (Fig. 5.12 a-b). The pushover analyses agree with the modal analyses, which suggest the same regions as the most vulnerable. It is also worth noticing that the reference capacity curve of the grouped columns corresponds to the column with the highest acceleration values in that group.

For brevity, only the comparison between the PushMass curves obtained with lumped and diffused plasticity approach is reported (Fig. 5.12 c).

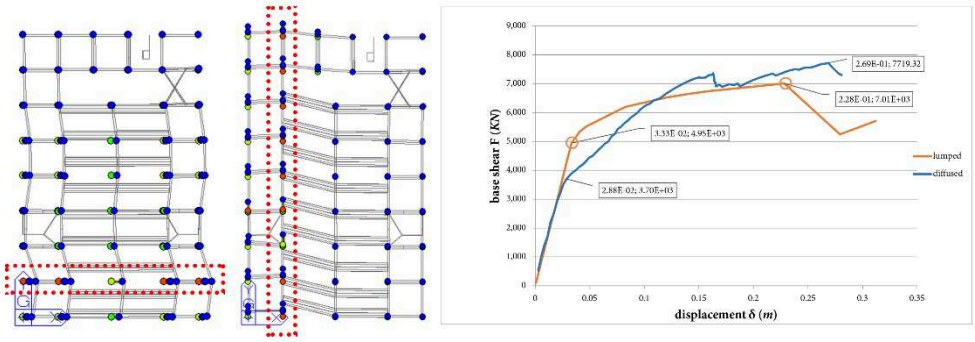

Figure 5.12 Pushover global control analysis. (a) X direction: δ_y = 0.033m, δ_u = 0.228m, T_b = 7010 kN, (b) Y direction: δ_y = 0.035m, δ_u = 0.232m, T_b = 6480 kN, (c) comparison between pushover analysis conducted with lumped and diffused approach (x-direction)

Figure 5.12 also shows what part of the structure is expected to be the most damaged. The approach can facilitate structural inspections in the post-earthquake scenario, focusing the possible weak elements. In fact, the proposed method can be used as a safe and non-invasive instrument to assess the structural conditions following an earthquake, in particular where the damage may not be noticeable. Furthermore, it is also useful in the subsequent repair of the structure, which can be based on the level of harm reached.

From the computed capacity curves the yield and the ultimate displacement (the latter corresponding to the simultaneous collapse of the plastic hinges referred to a specific group of columns for each direction as shown in Fig. 5.12), needed in Eq. 5.5, are easily identifiable.

It is important to stress the fact that performing a GCPA is a convenient way to obtain a representative capacity curve able to describe the global behavior of the structure; this is also one of the crucial aspects of the seismic assessment of existing precast concrete buildings with deformable storeys.

Concluding the section, it is important to state that a unique damage index is considered only to have a synthetic measure of the overall damage level of the structure, which can be useful for immediate decisions related to evacuation or not of the building. However, thanks to the numerical simulations with "real" nodal accelerations in the FEM model, it is possible to determine the (estimated) damage level in each cross-section of the structure, a fact that can be useful for the retrofitting design.

Quantification of damage

Using the values of the yield and the ultimate displacements obtained in the previous section, the damage index DI_μ is computed.

Displacement time histories in two different nodes belonging to the structural portions identified by the GCPA are reported in Fig. 5.13. These represent the structural response regarding displacement of the most vulnerable part of the structure.

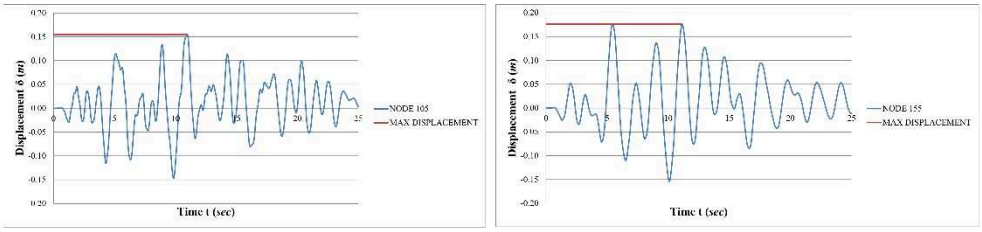

Figure 5.13 Displacements obtained from nonlinear time history analysis. (a) X-direction: δ_{max} = 0.155m; (b) Y-direction: δ_{max} = 0.176m.

The two maximum displacements, highlighted in Fig. 5.13, are δmax = 0.155m (X direction) and δmax = 0.176m (Y direction). In turn, they give the maximum damage indices, DIμ max = 0.626 and DIμ max = 0.714, respectively, in X and Y directions.

Because of the considered earthquake, the structure reaches a relatively high level of damage, so that the structure must be evacuated and certainly becomes unusable. On the other hand, the damage index is still sufficiently far from its maximum value 1, so that collapse is not expected to occur.

Another noticeable result of the proposed approach concerns the possibility of tracking the development of damage level at each time step. In fact, the combination between the updating of the model allowed by SHM techniques and the damage model built with the nonlinear static analysis permits to know how damage evolves in time, as shown in Figure 5.14. In both directions, the damage level experiences suddenly increment in correspondence of the maximum displacement time histories.

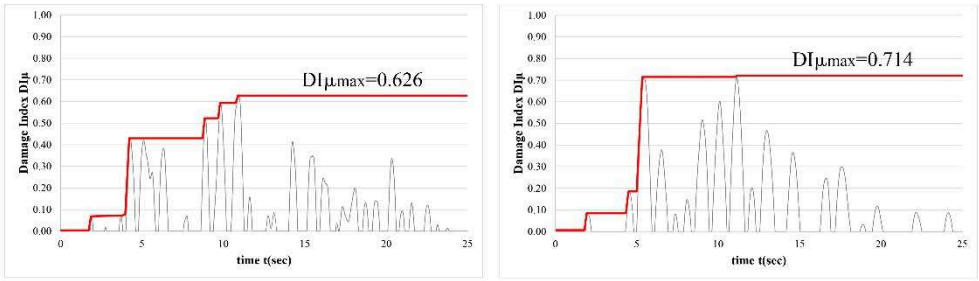

Figure 5.14 Evolution of damage indices during the seismic event. (a) x-direction: DIμ max = 0.626. (b) y-direction: DIμ max = 0.714.

Another consideration can be drawn from Fig. 5.14. There is a difference between the two principal directions. In the X-direction (Fig. 5.14a) the damage index rises slower than in the Y-direction, having some intermediate steps before reaching its peak. In the Y-direction (Fig. 14b), instead, the damage index goes from zero to its maximum value in a few steps that present a significant amplitude. The latter is clearly the most dangerous from a practical point of view.

Damage scenarios using real earthquakes

Using the proposed procedure, the process is applied using real recorded earthquakes, different in terms of intensity, shape and frequency content.

The following two ground accelerations reported in Fig. 5.15, are considered [77]. The Umbria-Marche earthquake (1997) involved the central part of Italy, which caused the loss of a significant number of cultural heritage buildings. It was an earthquake of medium intensity, characterized by a PGA of 1.69 m/sec2.

The L'Aquila earthquake (2009) was a destructive event marked by a magnitude of 6.3 and a PGA of 6.44 m/sec2. This earthquake destroyed the city center of L'Aquila and caused much damage to historical constructions.

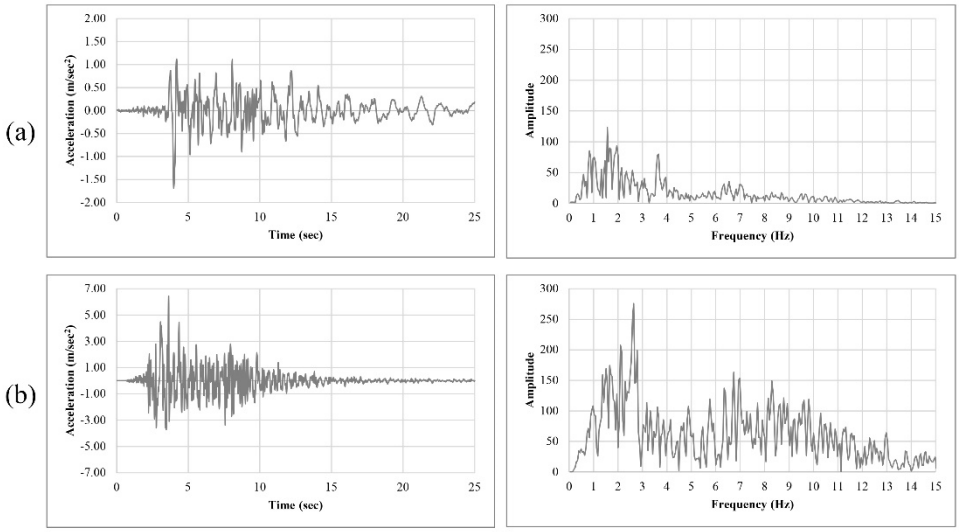

Figure 5.15 Time histories and FFT of registered accelerograms: (a) Umbria-Marche (1997), PGA 1.69 m/sec^2; (b) L'Aquila (2005) PGA 6.44 m/sec^2

The two maximum displacements obtained from the Umbria-Marche earthquake are δmax = 0.101 m in the X-direction (Fig. 5.16a) and δmax = 0.093 m in the Y-direction (Fig. 5.16b). These correspond to the maximum damage indices, DIμ max = 0.346 and DIμ max = 0.296, respectively, in X and Y directions.

The response of the structure subjected to the L'Aquila earthquake, is different; the maximum nodal displacements are δmax = 0.117 m (X-direction) (Fig. 5.16c) and δmax = 0.114 m (Y-direction) (Fig.5.16d). In turn, they give the maximum damage indices, DIμ max = 0.433 and DIμ max = 0.403, respectively, in X and Y directions.

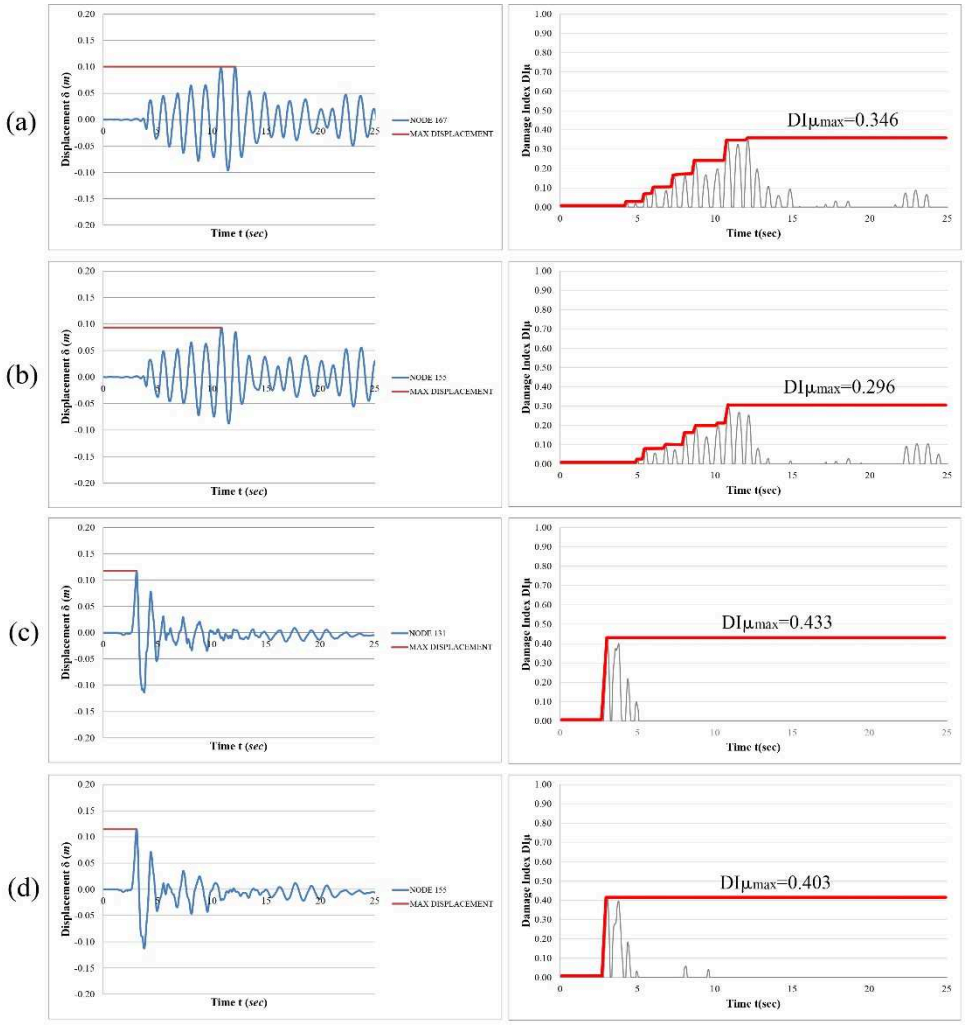

Figure 5.16 Maximum displacement and damage indices obtained with real time history: (a) Umbria-Marche: *X*-direction δ_{max} = 0.101; DIμ max = 0.346, (b) Umbria-Marche: *Y*-direction δ_{max} = 0.093; DIμ max = 0.296, (c) L'Aquila: *X*-direction δ_{max} = 0.117; DIμ max = 0.433, (d) L'Aquila: *Y*-direction δ_{max} = 0.114; DIμ max = 0.403

Based on the previous results, the following considerations can be drawn. A medium intensity characterizes the Umbria-Marche earthquake, but it presents quite a long cyclic behavior with similar values of peak accelerations over time. This entails mild time increment of the damage index, especially for the X-direction (Fig. 5.16a). In the Y-direction (Fig. 5.16b) a similar qualitative behavior can be seen, with a slightly lower final value of the damage index.

Differently, the L'Aquila earthquake shows an impulsive behavior characterized by acceleration values in the first part of the time history, much higher than ones in the second part. Maximum displacement occurs suddenly and almost at the beginning of the seismic event. This trend is noticeable for both the principal directions (Fig. 5.16c-d).

Another important comment can be made examining the seismic signals in the frequency domain. The main frequency content of the L'Aquila earthquake is included between 2.09Hz and 2.78Hz (Fig.5.15b): these values are sufficiently far from the principal periods of the investigated structure. Despite the higher value of PGA the structural response is not very high for this deformable building.

On the other hand, the frequency content of the (simulated) Maiolati earthquake involves a frequency content between 1.02Hz and 1.70Hz: these frequencies essentially correspond to the natural modes of the structure associated with the significant participation masses. For this reason, this accelerogram provides higher values of damage indexes also because the corresponding ground motion is able to mainly influence the dynamic behavior of the building, amplifying the structural response.

5.3.5 Final remarks

In this Chapter, a new approach to implementing an SHM system of an ordinary building has been proposed to outline a possible post-earthquake scenario and to evaluate damage indices. The case study is an industrial building that can be susceptible to damage during a seismic event due to some horizontal and vertical irregularities.

The excellent convergence reached between two commercial software allowed an SHM simulated process. In fact, it was possible to extract nodal accelerations from the Seismostruct© model as if they were measured from accelerometers installed on the real structure. Consequently, these acquired data became the input for the MidasGen© model, which was analyzed with the aim of outlining a possible post-event damage scenario.

For the structural diagnosis, a damage model is implemented using a ductility damage index; the latter is based on the displacements beyond the elastic threshold, one of the most important parameters to keep under control in precast structures.

The most relevant information resulting from the proposed procedure is the location and magnitude of the damage. In this way, it is possible to obtain an important instrument for the choice of evacuation routes in emergency conditions. Moreover, this approach is a powerful NDD tool for the evaluation of post-seismic structural conditions, which is one of the fundamental aspects not only related to the safety of the occupants but also concerning an economic point of view.

Further developments of this work are reported in **Chapter 6**, where an ambient vibration survey is performed to detect the main modal parameters of the structures and to calibrate a more reliable model for the nonlinear analysis. Other advances in SHM are focused on the use of wireless sensor networks (WSN), which are less expensive and more flexible than the wired ones (see **Chapter 7**).

Chapter 6
SHM Applications

6.1 Introduction

The rapid urbanization of the last decades has significantly increased heritage buildings of European countries. The most recent seismic events have clearly shown the high seismic vulnerability of the Italian existing RC buildings, which often provide an inadequate safety level against seismic actions [76].

Many of these constructions present several typical seismic vulnerabilities. For these reasons, structural interventions are absolutely necessary for ensuring an adequate level of seismic protection. Effective measures have to be taken in order to protect constructions at risk and to mitigate losses due to seismic events.

From the structural engineering perspective, this objective can be reached by increasing the knowledge of structural behavior, in particular with respect to dynamic loads.

As stated in the previous paragraphs, seismic analyses for structural interventions are frequently performed using simplified numerical models that try to best reproduce the real dynamic behavior of the building. Often these models are not sufficiently refined and do not adequately represent the real structure.

Due to the many uncertainties about construction systems - material properties, modelling techniques, analysis methods and successive past interventions - the evaluation of structural behavior is a difficult task [78]. These uncertainties can be the cause of completely wrong results.

SHM techniques solve these aspects providing valuable knowledge of the dynamic behavior of monitored structures, of their response to service environmental loadings, and of rise and distribution of the deterioration conditions [7] (see **Chapter 2**).

OMA concerns the possibility of describing structural dynamics at small vibration amplitudes in real operating conditions with unknown excitation inputs (e.g., wind force) [4] (see **Chapter 3**). The importance of this issue comes from the fact that for the identification of large civil structures, applying known excitation forces is costly, if not infeasible [5,6]. Moreover, output only algorithms are the best option for an online monitoring system, which can monitor vibrations of a structure constantly, without the application of a measurable input to the system.

In the following sections the results of two different SHM applications are shown. The first one consists of an Ambient Vibration Survey (AVS) performed in the precast structure previously analyzed (**Section 5.3**). The main objective is the extraction of the dynamic parameters in order to understand the real structural behavior and for further seismic analysis.

The second one consists of a one-year monitoring of a school r.c. building, with the aim of tracking the dynamic evolution during the retrofitting works.

6.2 Dynamic Identification of a precast industrial building

6.2.1 Research motivations

Interest in industrial buildings arises from the need of its service utilization, assuring a sufficient level of safety with respect to both vertical loads and earthquake actions, especially after the seismic event that struck the Emilia Romagna region (Italy).

When, in particular, seismic performances are considered, a number of aspects have to be taken into account. The presence of degraded materials are cause of reduction of local and global stiffness and strength. Moreover secondary elements (e.g. infill panels, sub-structures, etc.) play an important role in structural behavior.

In this case study, attention is focused on the precast structure previously introduced (**Section 5.3**). After many numerical simulations in order to propose a method for damage quantification and localization [57], it was necessary to investigate the real structural dynamic of the building. This was done through a rapid onsite dynamic testing. The work demonstrates the enhancement in comprehension of the structural behavior obtained by means of a 2-day testing campaign conducted on the industrial building.

As mentioned in Chapter 5, this data collection was subsequently available to the damage detection numerical approach.

The on-site testing was carried out with a network of 10 accelerometers opportunely located to identify the dynamic characteristics of the structure by means of ambient noise-induced vibration. Stochastic Subspace Identification (SSI) output-only procedures were used to identify the main modal parameters of the structure. Modal characteristics were used to update a finite element model representing small amplitude vibrations of the damaged structures.

6.2.2 Ambient Vibration Survey

The rapid testing measurement was carried out in two days, with the aim of furnishing sufficient information to update an FE numerical model that would be used to support design choices for the on-line monitoring [57].

Several acquisitions were stored in order to compare different identification procedures, as listed below (Tab 6.1):

number of acquisition	data	Time	duration of acquisition
1	17/12/2015	1.34 PM	60min
2	17/12/2015	5:02 PM	45min
3	17/12/2015	6.14 PM	25min
4	17/12/2015	6.53 PM	45min
5	17/12/2015	8.06 PM	45min
6	18/12/2015	5.35 AM	60min
7	18/12/2015	8.40 AM	60min
8	18/12/2015	11:18 AM	60min
9	18/12/2015	12.33 PM	60min

Table 6.1 number and duration of performed AVS's

The dynamic response of the structure was measured by ten accelerometers placed as reported in figure 6.1. Sensor placement has taken into account the results of the previous numerical modeling.

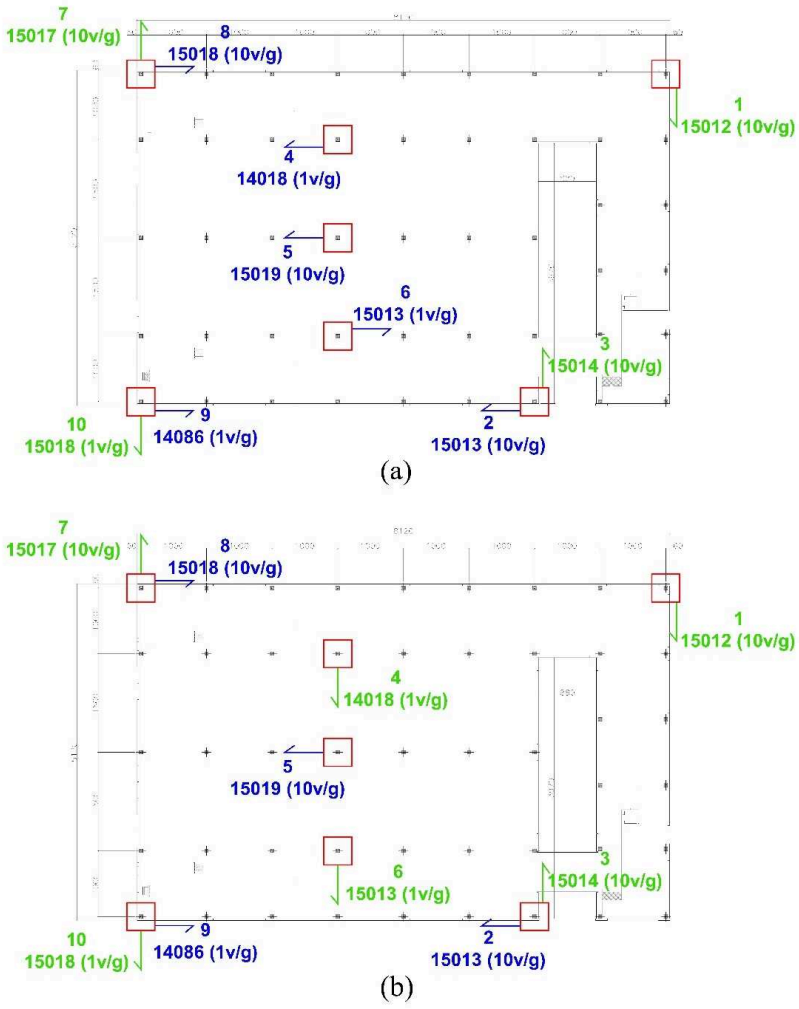

Figure 6.1 sensors placement, (a) AVS performed the 17/12/2015, (b) AVS performed the 18/12/2015

Two similar configurations are adopted, moving only two sensors during the second day of measurements, in order to capture the ODS of both directions (Fig. 6.1 a)-b)).

Each acquisition was performed with a sampling rate of 2.048Hz, using the instrumentation described in **Chapter 4**. In particular (Fig. 6.2):

- 4 seismic accelerometers KS48C, sensitivity 1000mV/g;

- 6 seismic accelerometers KB12VD, sensitivity 10000mV/g;
- Acquisition system composed by CompactDAQ-9132 and 4 acquisition module NI 9234.

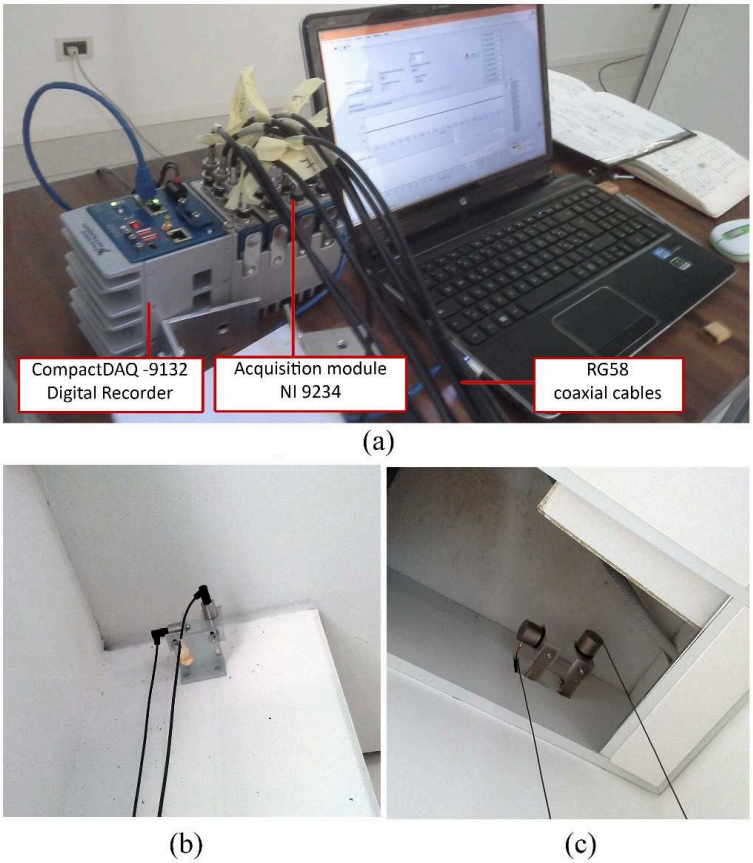

Figure 6.2 Instrumentation used for each AVS: (a) CompactDAQ-9132 and NI 9234 module, (b) KS48C piezoelectric sensor 1V/g, (c) KB12VD piezoelectric sensor 10V/g

The collected measurements were originally sampled at 2.048Hz. They were decimated by a factor of 20 before processing in order to have data of 102,40 Sample per Second (SPS). A further decimation was applied by a factor of 2, obtaining the ultimate data of 51,20 SPS.

The record duration varies between 45 minutes and one hour: it should be long enough to eliminate the influence of possible non-stochastic excitations that may occur during the test [13].

Since the DC component of the signal has no physical meaning in civil engineering applications (accelerometers are mounted on structures characterized by a null net acceleration, so the DC component of the signal is only due to sensor circuitry), it has to be removed by applying a high-pass filter (0.20Hz).

According to the procedure described in **Chapter 3** the dynamic parameters are extracted from the collected data through the Cov-SSI.

Estimation of structural modes is performed through “stabilization diagrams” that show the alignments of stable poles, for increasing model orders.

The procedure was repeated for each acquisition, obtaining substantially the same results. The candidate time history is number 2 (see Tab.6.1).

By increasing model order the following stabilization diagram is obtained (Fig. 6.3 a)) and the related frequencies and damping ratio are estimated (Tab.6.2).

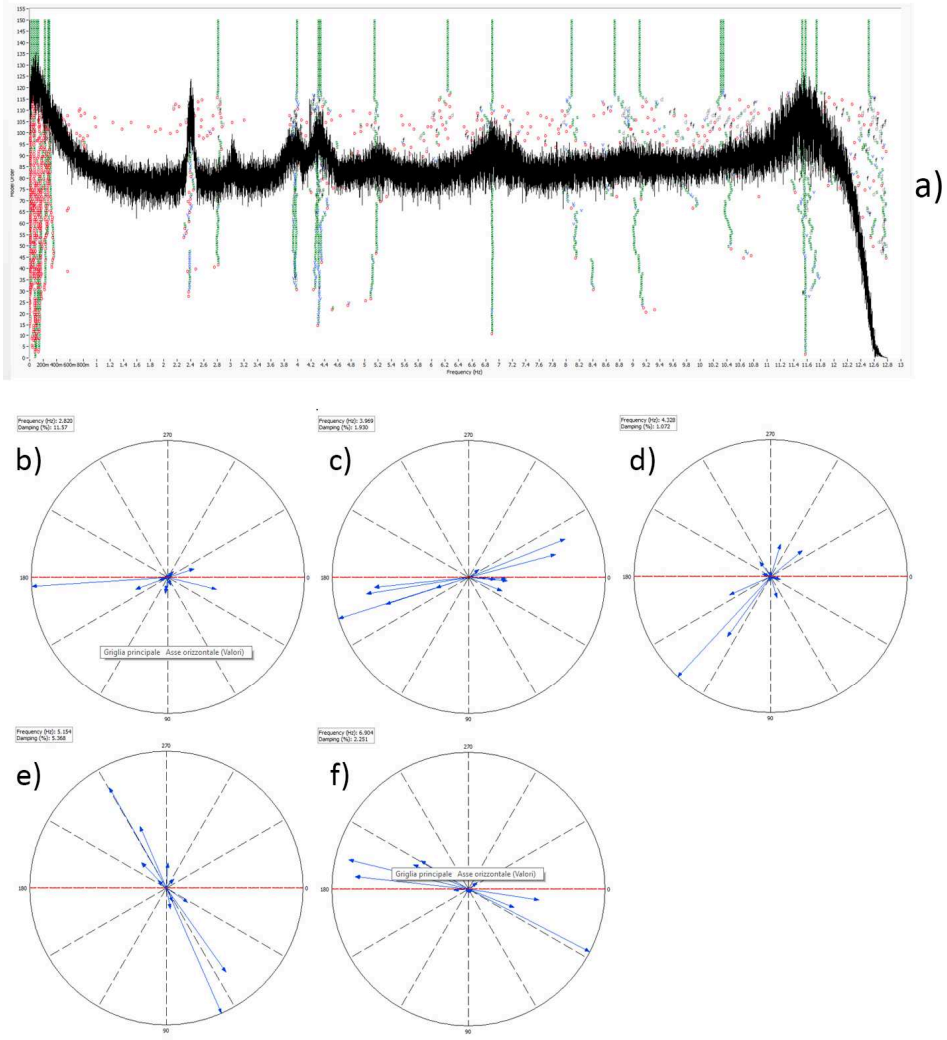

Figure 6.3 (a) stabilization diagram and (b), (c), (d), (e), (f) complexity plots of the firsts five modes identified

mode number	Mode type	natural frequency (Hz)	damping ratio (%)
1	**Translational Y**	**2.820**	**6.57**
2	**Transl X/torsional**	**3.969**	**1.93**
3	**Translational Y**	**4.328**	**1.072**
4	**Torsional**	**5.154**	**5.368**
5	**Translational X**	**6.904**	**2.251**
6	Local	8.074	5.334
7	Local	9.12	4.805
8	Local	10.35	0.1399
9	Local	11.56	1.649

Table 6.2 Results of dynamic identification: frequencies and damping ratios

Compared to the preliminary F.E. model, frequencies values and mode shapes obtained by the experimental investigation are rather different. The structure has a greater stiffness and, apart from the first mode, the ODS's present few similarities. This confirms the relevance of these non-destructive controls, able to reach a structural level of knowledge, otherwise unobtainable.

The preliminary F.E. model was affected by several simplifications. The next section the F.E. model refinement is shown, in order to obtain a model which reproduces as close as possible the experimental values of the modal properties of the structure.

6.2.3 Updating of F.E. Model

The dynamic response of the structure was characterized numerically by the implementation of FE model of the structure and carrying out modal analyses through the MidasGen© software [56].

The geometric and structural model of the building represents in detail, under different modelling assumptions, the geometric and mechanic characteristics of the structural elements and the mass distribution on plain and along height.

The results of AVS have shown that the dynamic behavior of the structure is considerably more rigid with respect to preliminary models.

As the structure was built a few years ago there are some uncertainties about material properties and construction techniques. For these reasons, the increasing of stiffness can be caused by the following possible factors:

- The presence of infill panels that, although independent from the bearing structure, can influence the dynamic behavior;
- The behavior of the floor can be more rigid respect to the initial suppositions;
- Friction connection effects between structural elements (e.g. beam-column).

The preliminary numerical model is then refined by introducing several structural aspects. First, infill panels are modelled using 2D plate elements, employing a modulus of elasticity equal to 3.00 e^{+07} kN/m^2. [79]. Panels are modelled using a thickness value of 0.30m. These elements are external to the columns, and they are supported at the

foundation by an independent concrete beam. They are connected to the columns with steel supports. In order to simulate the interaction with the structure, this connection is modelled by a rigid link, as shown in Figure 6.4.

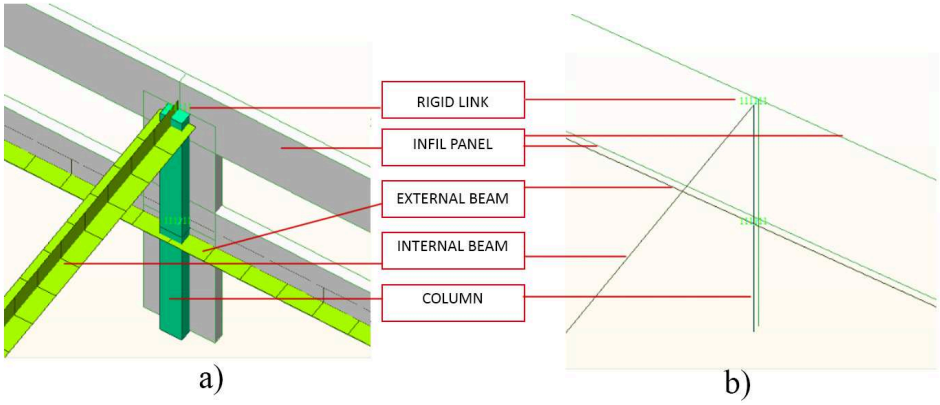

Figure 6.4 Particular of rigid modelled in F.E. model: (a) hidden view and (b) wireframe view

Concrete slabs of the storeys (first floor and cover floor) are modelled with Young Modulus equal to 3.00 e^{+07}a kN/m^2 and thickness is settled at 0.08m. Masses are uniformly distributed on the beams.

The third model refinement involves the mutual connection between the double T beam and the roof elements. Roof-to-beam connections are very large, and these elements are equipped with dowel pins. For this reason it is reasonable to consider a plastic behavior of the connections, despite the first modeling. This aspect is considered by introducing a rotational spring in the longitudinal direction (Y-Direction of F.E. model). The final value of moment is fixed at 1.50 e^{+06} kNm/rad, obtained with iterative numerical simulations. This was possible because first mode involves only the central part of the structure and the bending moment is the update parameter taken into account.

The updating procedure is done by compare-alter-check based iterative solutions like those preliminarily reported by Isidori et al. [78,51].

The NM was developed assuming a linear behavior for all materials because we are interested in knowing only the dynamic behavior.

R.c. beams and columns are modelled using general beam elements, with the same mechanical properties of the preliminary model (**Chapter 5**).

Experimental mode shapes are achieved with the parameter extractor. At each estimated frequency the correspondent ODS is obtained, checking the goodness of the identification process through the Complexity Plots [80] (see Fig. 6.3).

The results of the identification procedure compared with the refined model are reported in Fig.6.5 and Tab.6.3.

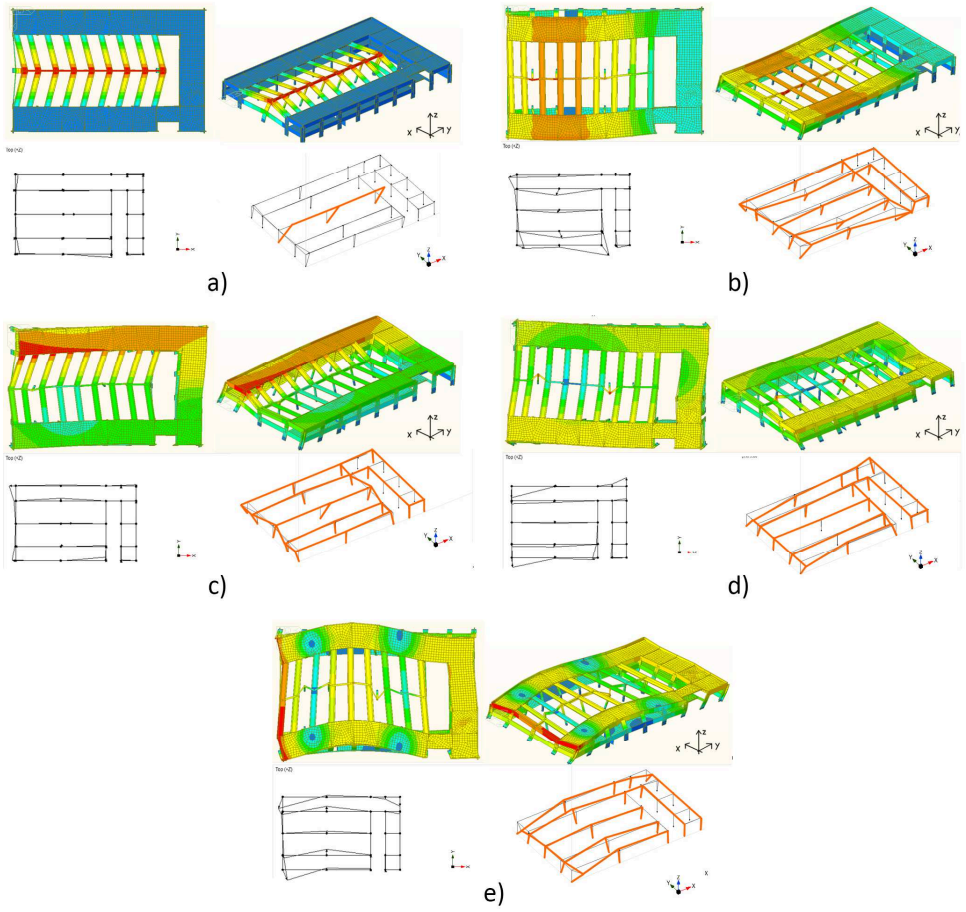

Figure 6.5 Comparison between FE model updated and ODS of AVS: (a) mode1, (b) mode2, (c) mode3, (d) mode5, (e) mode8

Mode No	AVS Freq.	FEM Freq.	TRAN-X		TRAN-Y		ROTN-Z	
	Hz	Hz	MASS(%)	SUM(%)	MASS(%)	SUM(%)	MASS(%)	SUM(%)
1	**2,820**	**2,763**	0,00	0,00	**21,42**	21,42	0,00	0,00
2	**3,969**	**3,494**	**62,45**	62,45	0,00	21,42	**11,37**	11,37
3	**4,328**	**4,824**	0,48	62,93	**51,04**	72,46	0,25	11,61
4	-	5,205	2,52	65,45	16,35	88,82	4,53	16,15
5	**5,154**	**5,724**	**5,71**	71,16	2,40	91,22	**66,33**	82,48
6	-	6,587	1,71	72,87	0,01	91,23	1,84	84,32
7	-	6,637	0,18	73,06	0,01	91,24	1,77	86,10
8	**6,904**	**7,141**	**13,73**	86,79	0,25	91,49	1,02	87,12

Table 6.3 Comparison between analytical and experimental values of natural frequencies (in bold the calibrated frequencies and the significant participation masses)

The participating mass ratio of a mode is a very important parameter, since it provides a measure of how important a mode is for computing the response of the modelled structure to the acceleration loads in each of the three global directions defined into the model. In this case the considered modes are characterized by a total participating mass ratio higher than 85%. As a result, the considered modes are well representative of the dynamic behavior of the structure.

The two sets of frequencies are in good agreement, as reported in the following correlation graph (Fig. 6.6).

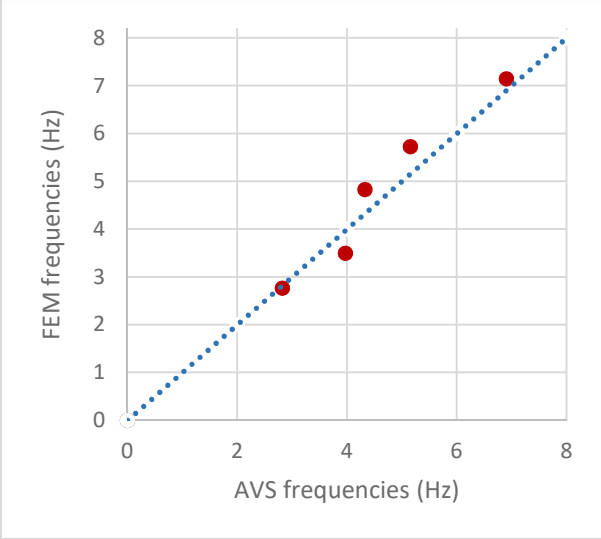

Figure 6.6 Frequency correlation between AVS and FEM

Based on the previous results, the following considerations can be drawn.

The first mode (2.82Hz) involves the central part of the industrial building. It is independent from the other modes and excites only the masses referred to the double T beam, the central frame and roof elements. The main update parameter is the rotational spring placed in roof elements-double T connection, opportunely calibrated.

The second mode (3.96Hz) it totally translational in X-Direction. In fact X-Direction, in global terms, is reasonably more flexible than Y-Direction because of the geometry of the concrete slab (the long side is Y-Direction). Qualitatively it corresponds, limited to mode shape, to the 3rd mode on the preliminary NM (see Tab.5.3).

The third mode (4.32Hz) involves the Y-Direction, in particular the lateral portions of the building. The part colored in red (see Fig.6.5 c) is more flexible, because of the presence of the reinforced concrete lift, which constitutes a significant rigidity core. Mode shape of this mode corresponds to the 2nd mode of preliminary NM (Tab.5.3).

The consecutive experimental mode (5.15Hz) corresponds to the 5th mode of the NM. It is a completely torsional mode. Real and theoretical ODS shapes are in very good agreement.

Finally, the last significant mode (6.90Hz) corresponds to the 8th mode of the NM. It excites an important modal mass in X-Direction.

Other experimental and numerical modes are fundamentally local modes, and are not significant for the identification process and model refinement.

Comparison, in terms of mode shapes, between the preliminarily NM and the update NM, is shown in Fig. 6.7.

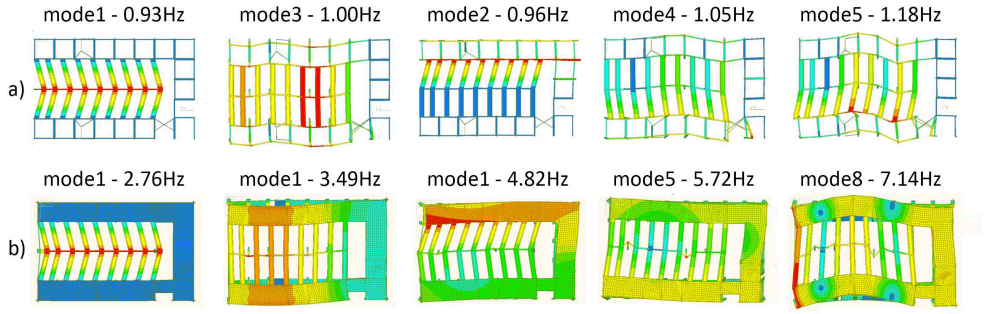

Figure 6.7 Comparison between the corresponding modes of preliminarily NM (a) and the updated NM (b)

Mode shapes are qualitatively in good agreement, but natural frequencies are rather different due to some omitted aspects of preliminarily NM (e.g. infill panel, rigid diaphragm, nodal friction, etc.).

This underlines the importance of AVS process, allowing a deep knowledge of dynamic behavior of structure under investigation.

It is worth highlighting the relevance of the presented case study for several aspects. First, literature is not provided by AVS carried out in precast industrial building. For this reason this data collection is an important contribution on structural behavior of this kind of buildings. Second, the high dimension of the structure makes it necessary to use a large amount of coaxial cables (800m). Despite the length of cables, acquired data are not affected by high noise level.

This refined model will be the starting point for the continuous monitoring of the industrial building, using the procedure described in [57]. The principal aim is to ensure adequate seismic protection both for the occupants and for the health of the structure.

6.3 One-year monitoring of a reinforced concrete school building

6.3.1 Research motivations

In the following sections, a number of ambient vibration tests carried out on a r.c. structure will be described and the main results will be discussed. Most of the datasets obtained from these ambient vibration tests can be used for an effective evaluation of seismic risk of the considered structure.

European countries, especially in the 70's, have suffered a rapid urban and demographic growth. In particular Italian regions were characterized by hasty overbuilding: the rate of land consumption in the 50's was 2.9%, today is 7.3%.

A large stock of these buildings are aged, built with low standards of construction and maintenance and were often designed without considering seismic concepts. Old existing RC framed buildings are today characterized by poor quality concrete, inefficient construction details and a lack of the fundamental principle of the capacity design [61].

For these reasons retrofitting interventions are often necessary in order to provide an adequate safety level and to improve the structural performances.

These aspects motivated the present work in understanding the dynamic behavior of a r.c. school building during and following the retrofitting works. Through repeated Ambient Vibration Surveys (AVS) the dynamic evolution of the investigated structure at different structural configurations is shown. The main objective is the extraction of structural dynamic parameters (such as natural frequencies, damping ratios and mode shapes) before, during and after the retrofit phase. The measurements are performed with high sensitive piezoelectric sensors and data acquisition system, able to record ambient vibrations with very low amplitude range.

Thus, ambient vibration tests have been carried out to effectively complement the structural assessment with the information about the dynamic properties. AVS provided reference values of the modal parameters useful for the calibration of the numerical models. The refined models could be referred to as representative of the dynamic behavior of the structure in each current state.

One of the most representative results of the present work is the possibility to quantify the variation of the building performances at each structural configuration.

For each dynamic identification a numerical model, suitably tuned, has been developed. It allows the enhancing of structural aspects of the monitored building, understanding and quantifying the structural changes during the works. Moreover, Numerical Models (NM) permit the clear localization of boundary conditions that deeply influence the structural modal behavior, justifying some anomalies observed during the identification process.

The procedure allows to experimentally evaluate the contribution of infill panels in the structural response. Furthermore, it has been possible to validate the increasing of building performance following the structural intervention.

This relevant data collection can be extremely helpful in calibrating other similar retrofitting interventions and provides useful guidelines that can assist in the planning of SHM applications.

6.3.2 Ugo Foscolo school building

The considered school building is called “Ugo Foscolo” (Fig.6.8a) and is situated in Ostra Vetere, a small Italian town 60km from Ancona, the main city of Marche region. This area was subjected to the 1997 Umbria-Marche earthquake (which in the epicenter zone registered a magnitude of 6.3) and to the recent seismic event that struck the same regions in October 2016 with a magnitude of 6.5.

The structure has a simple and geometrically regular structural scheme. The plan covers an area of about 500 m2 and it is composed by a rectangle of 41 m in the longitudinal direction and 12 m in the transversal one (Fig.6.8b). The height of the building is 15m, distributed in three in-situ cast concrete storeys and one roof floor. The first-floor height is 5.26m, the second-floor is 3.90m while the third-floor is 3.98 (Fig.6.8c).

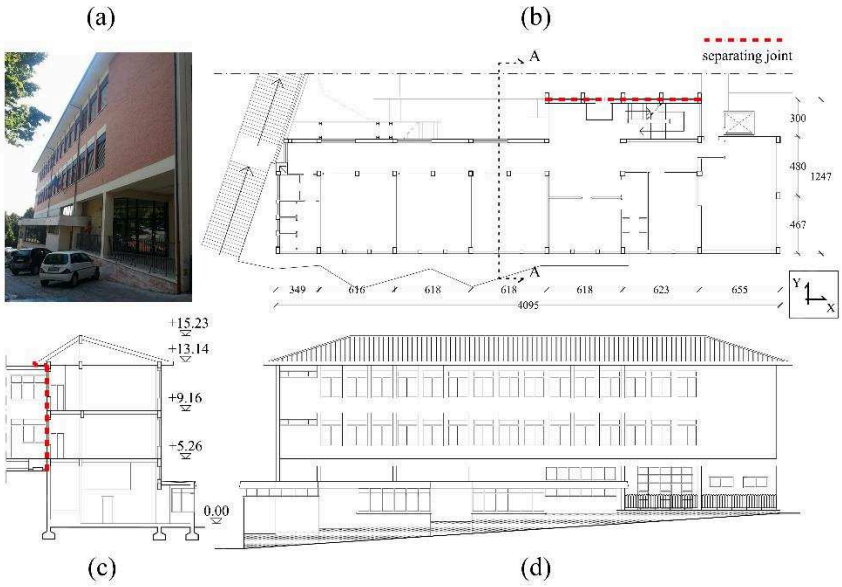

Figure 6.8 (a) External views of the Ugo Foscolo School building, (b) Plan View of floor type, (c) transversal section and (d) perspective drawing of the main façade

The columns have regular square cross sections (30x50cm), except for some columns composed by a cross section of 40x40cm in the central part of the plan. The external beams, located at the building perimeter, have a uniform rectangular cross section of about 30x50cm at the beam-to-column connection, while the internal beams have a rectangular cross section of 25x60cm and 40x60cm.

The foundations consist of plinths linked by concrete curbs: this aspect permits not only to consider the columns fixed at their base but also to neglect any effect related to seismic input asynchrony at the base of different columns. Because of the declivity of the ground-level, the foundation level is variable (Fig.6.8d).

Figure 6.8b shows, with a red dashed line, the structural joint separating Ugo Foscolo School from the adjoining gym, in correspondence of the r.c. stairs. This joint, as described in the next paragraphs, plays an important role in the dynamic behavior of the building during the works.

The examined building belongs to Italian building stock, of which RC buildings currently represent the greatest portion, mostly built after World War II when building stock increased exponentially. This structure presents typical and specific vulnerabilities (e.g. methods of construction, quality of materials, etc.) as reported in [76]. These vulnerabilities often affect similar constructions, and are as follows:

- The stairs are placed in an eccentric position and emphasize the irregular stiffness distribution provided by the position in plan of the infill panels. These features may result in global torsional effects and brittle collapse, in particular as soft-storey mechanism;
- Frames are present in one direction, the longer one (longitudinal), identifying a strong direction, whilst in the orthogonal direction the frames are present on the external

sides only. Due to this characteristic, the transversal direction can be considered as the weak direction;
- Slabs cannot be considered as rigid because solid concrete plates do not have the minimum thickness (40 mm), the necessary reinforcements to assure a rigid behavior as required by the Italian Standards and they are made of poor quality concrete. Consequently, this feature can be considered as an additional typical vulnerability of the examined building typology;
- the distribution of stirrups within structural elements is poor and ineffective, particularly within column-beam nodes, where they are completely absent.

For these reasons a deep structural intervention was carried out.

With regard to the properties of the materials, a large investigation with destructive (coring and sampling of the bars) and non-destructive (SonReb) testing was performed.

The mechanical characteristics of existing concrete was estimated through a combination of destructive and non-destructive tests. Some cores were extracted and the compressive strength was evaluated by tests. Some cores were extracted and the compressive strength was evaluated by tests, obtaining a mean value of the Young Modulus equal to 2.70e+07 kN/m2. A relevant uncertainty affects the experimental evaluation of the mechanical properties of concrete, including the elastic modulus. This is in agreement with similar investigations reported in the literature [81].

Based on the collected data and information about geometry of the structure and mechanical properties of concrete, a preliminary linear elastic model of the Ugo Foscolo School was set.

Because of its vulnerabilities, the structure was subjected to retrofitting works. The main features of the structural intervention are listed below:
- original column cross-sections were increased. External columns increased from 30x50cm to 55x75cm, while internal ones increased from 40x40cm to 55x55cm (Fig. 6.8c);
- during the enlargement of column cross-sections, additional longitudinal steel bars were introduced. This was done for each column (Fig. 6.8c);
- The distribution of stirrups was made effective, particularly in column-beam nodes, using a spacing of 15cm in the central part and 5cm in the nodes.
- Each beam was equipped with Fiber Reinforced Polymers (FRP), opportunely fixed to the elements through epoxy resin and FRP connectors in order to avoid the delamination (Fig.6.8b).

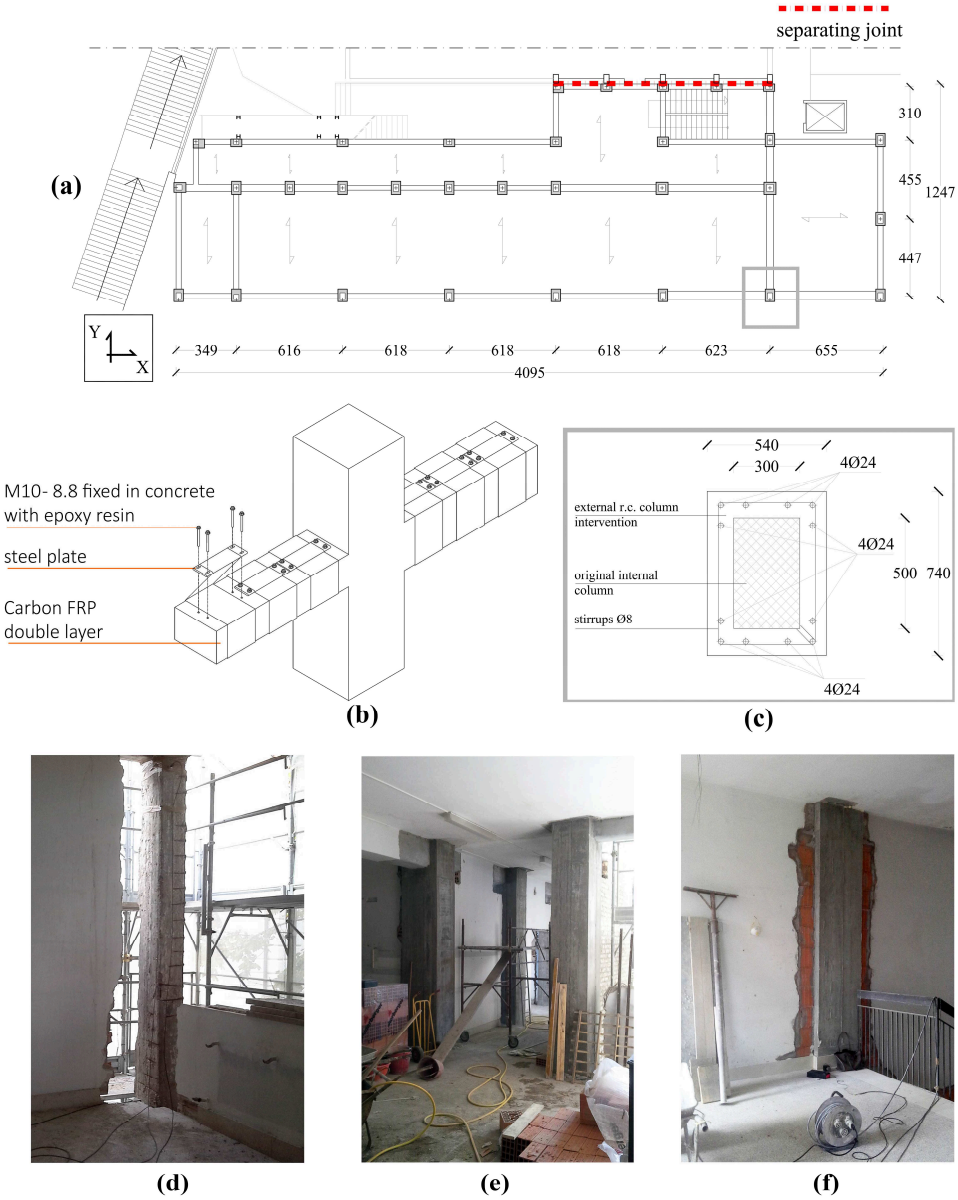

Figure 6.9 (a) Structural plan view, (b) structural drawing of CFRP in column-beam nodes, (c) executive drawing of a column intervention, (d) October 2015, original column type and disconnection of infill panels, (e) January 2016, significant enlargement of original columns, (f) April 2016, end of retrofit phase

In Figure 6.9 d-e-f some images of the retrofitting works are reported. It is worth pointing that during the works infill panels were only disconnected from the structure and they have never been removed, so the global mass was unchanged.

Because of the uncertainties affecting structural scheme and material properties, dynamic tests in operational conditions and model refinement were needed, with the aim

of obtaining useful information about the structural behavior and to reduce modeling uncertainties [70].

6.3.3 Long-term Ambient vibration tests

Many methods have been presented in the literature for the dynamic identification or damage identification based on vibration signatures [16,19]; these methods enable engineers to track the real behavior of the structure and calibrate the NMs to use in further assessments [61].

The present measurement campaign belongs to periodic SHM: several AVS's are performed in four time steps during the retrofitting works. This provided the opportunity to measure the changing characteristics of the building as the construction progressed. Each structural monitoring corresponds to a particular configuration, as listed below:

- AVS n.1: 17th March, 2015. The sensors were installed before the beginning of the works;
- AVS n.2: 15th October, 2015. In this stage all the connections between r.c. elements and infill panels were removed, so there was no interaction between them;
- AVS n.3: 26th January, 2016. In this structural configuration all the cross sections of the columns are enlarged in order to increase the structural performance. Here as well the interaction between external walls and r.c. elements is not considered;
- AVS n.4: 22nd April, 2016. The accelerometers were placed at the end of the retrofitting works.

The method used in the presented application works is in time domain and it is based on a state space description of the dynamic problem [19] using the Covariance Stochastic Subspace Identification (Cov-SSI) algorithm.

The ambient vibration response of the school was measured at each floor of the building keeping the sensors substantially in the same position at each AVS. Each level was instrumented at least in two corners. At each corner two high sensitive accelerometers, measuring in two orthogonal directions, were placed. Other couples of accelerometers were put in different positions at various levels.

The accelerometers were fixed directly in contact with the concrete slab (Fig.3) and parallel to the main directions of the building, in order to get both translational and torsional modes of the structure.

The wired sensor network described in Chapter 4 was used, composed of two types of piezoelectric sensors (Integrated Electronic Piezoeletric - IEPE):

- KS48C-MMF with voltage sensitivity of 1V/g and measurement range of ±6g;
- KB12VD-MMF with voltage sensitivity if 10V/g and measurement range of ±0.6g.

M28 and M32 signal conditioners with frequency range of 0.1 to 100kHz and selectable gain were also used at each record. Some images of the instrumentation used for AVS are reported in Fig.6.10.

Figure 6. 10 Instrumentation used for each AVS: (a) Digital Recorder DaTa500, RG58 cables, Signal conditioners, (b) KB12VD piezoelectric sensor 10V/g, (c) KS48C piezoelectric sensor 1V/g

The collected measurements were originally sampled at 1000Hz. They were decimated by a factor of 10 before processing in order to have the ultimate data of 100 Sample per Second (SPS). Data were resampled at 50Hz [82].

The record duration varied between forty minutes and one hour: it should be long enough to eliminate the influence of possible non-stochastic excitations that may occur during the test [13]. The described procedure was used for each AVS.

A modal parameter extractor developed in Labview® ambient carried out data processing. It is able to perform analyses in time domain according to the Cov-SSI procedure mentioned before.

6.3.4 Estimation of the structural dynamic parameters

This section reports the dynamic parameters extracted from the analysis of the collected data through the abovementioned Cov-SSI. The measured data acquired during the testing campaigns were opportunely selected to perform a parametric identification of a modal model for the tested building.

Estimation of structural modes is done through “stabilization diagrams” that show the alignments of stable poles, for increasing model orders.

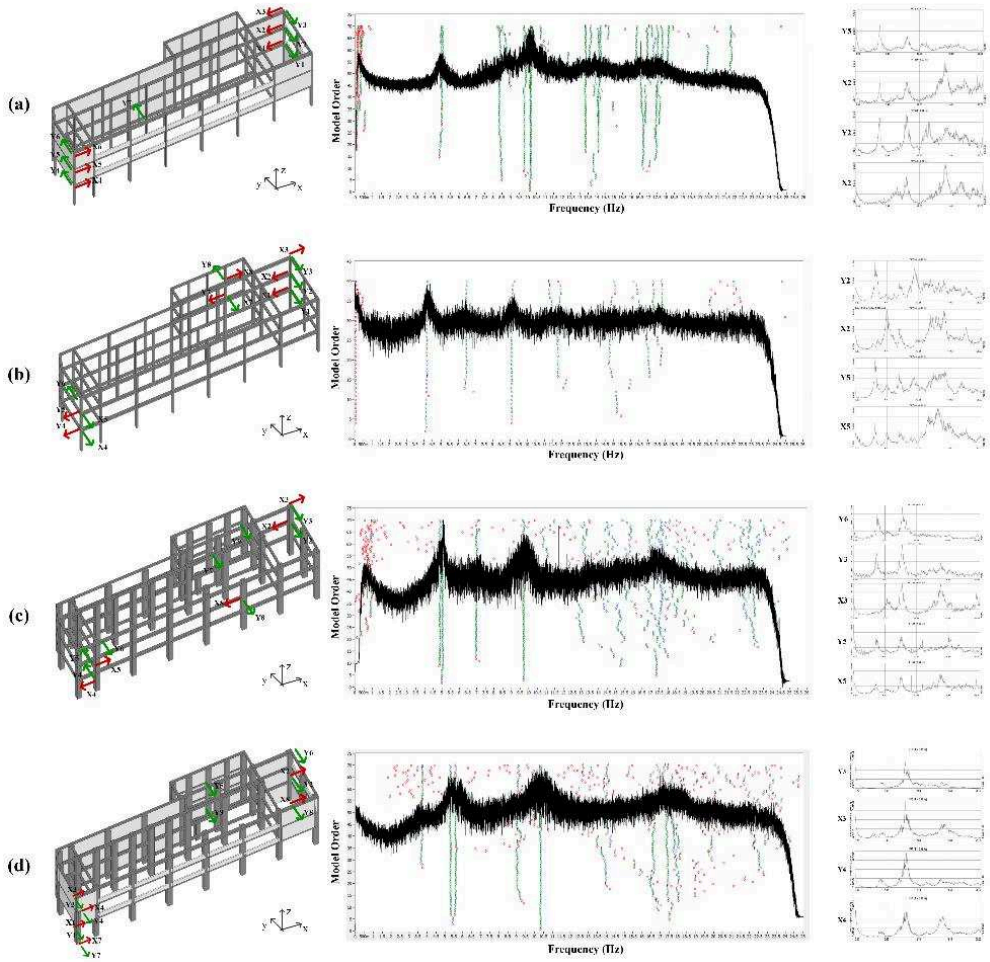

Figure 6.11 identification process of each Ambient Vibration Surveys: location of the sensors, stabilization diagrams and FFT of the most significant time histories. (a) AVS1, (b) AVS2, (c) AVS3, (d) AVS4

The stability of a pole is defined in terms of frequencies, damping and modal shapes, as reported in Section 3.5.4.

After this step, consistency checks made the discrimination between structural modes and spurious frequencies. Candidate modes were selected according to a traditional (manual) identification process based on user experience and according to specific method best practice [83]. Frequency associated with damping ratio higher than 10% was scattered. Complexity of mode shapes were also monitored, selecting only the frequencies associated with slightly complex components.

Measurements were performed during the works, so they are often affected by external noise caused by construction machinery. The assumption of stochastic excitations could sometimes be violated. For this reason, during the identification process, each time history was appropriately cleaned by non-stochastic inputs, clipping only the segment

without spurious excitations. This aspect, in some cases, does not allow the identification of higher local modes, obtaining clears stable poles only for the principal natural frequencies up to about 10Hz. Nevertheless, the repeated AVS permitted the validation of the results by the comparison and observation of natural frequencies and relative Operational Deflection Shapes (ODS).

Fig.6.11 shows the identification in four steps of AVS. At each step sensor placement, estimated frequencies and the most representative FFT of corresponding sensors are shown. Parameters extracted are reported in Tab.6.4.

AVS1			
Mode number	**Type**	**Natural Frequency (Hz)**	**Damping Ratio (%)**
1	Torsional Z	5.038	3.768
2	Translational X	8.42	8.246
3	Translational Y	10.17	3.023
AVS2			
Mode number	**Type**	**Natural Frequency (Hz)**	**Damping Ratio (%)**
1	Torsional Z	4.196	1.655
2	Translational X	6.507	8.389
3	Translational Y	9.132	1.22
AVS3			
Mode number	**Type**	**Natural Frequency (Hz)**	**Damping Ratio (%)**
1	Translational Y	4.878	2.662
2	Torsional Z	5.048	1.700
3	Translational X	6.967	7.533
4	Translational Y	9.722	2.437
AVS4			
Mode number	**Type**	**Natural Frequency (Hz)**	**Damping Ratio (%)**
1	Translational Y	5.321	3.72
2	Torsional Z	5.59	5.699
3	Translational X	9.043	9.92
4	Translational Y	10.35	4.051

Table 6.4 Dynamic parameters identified with Cov-SSI technique

Based on the previous results (Tab.6.4), the modifications of structural behaviour during the retrofitting works can be ascertained. Structural masses were invariant during the works, so the frequency shifting mainly correspond to the stiffness variation. The dynamic behavior of AVS1 and AVS2 is qualitatively the same. The first three modes involve the same directions (torsional and translational), exhibiting a noticeable decrease of global stiffness

(about 20% for the 1st mode, 29% for the 2nd mode, 11% for the 3rd mode, see Fig.6.11a-b). These values correspond to the quantification of the infill panel effects in the structural performances of the whole building, which clearly are not negligible, as commonly – and erroneously – assumed by designers.

AVS3 shows the appearance of a new translational Y mode, which is now the first. Two very close peaks are evident in the stabilization diagram (Fig.6.11c); the first one corresponds to the 1st translational mode, while the consecutive 2nd and 3rd modes correspond to the first two poles estimated in AVS1 and AVS2. As explained in the next paragraph, the appearance of this first mode is caused by the intervention in the structural joint, that deeply influence the dynamic of the building. Beside this, 2nd, 3rd and 4th modes are subjected to an important increase of stiffness (about 20% for the 2nd mode, 7% for the 3rd mode, 6% for the 4th mode) due to the enlargement of the cross-section of the columns.

In the last AVS4 the same four principal modes can be identified. The addition of infill walls plays a further increment of natural frequencies, keeping the mode order unchanged. In this last step increment is about 9% for the 1st mode, 11% for the 2nd mode, 30% for the 3rd mode, 6% for the 4th mode. The last stabilization diagram (fig.4d) shows that the firsts two modes are now well separated.

The dynamic evolution of the structure is graphically represented in Fig.6.12.

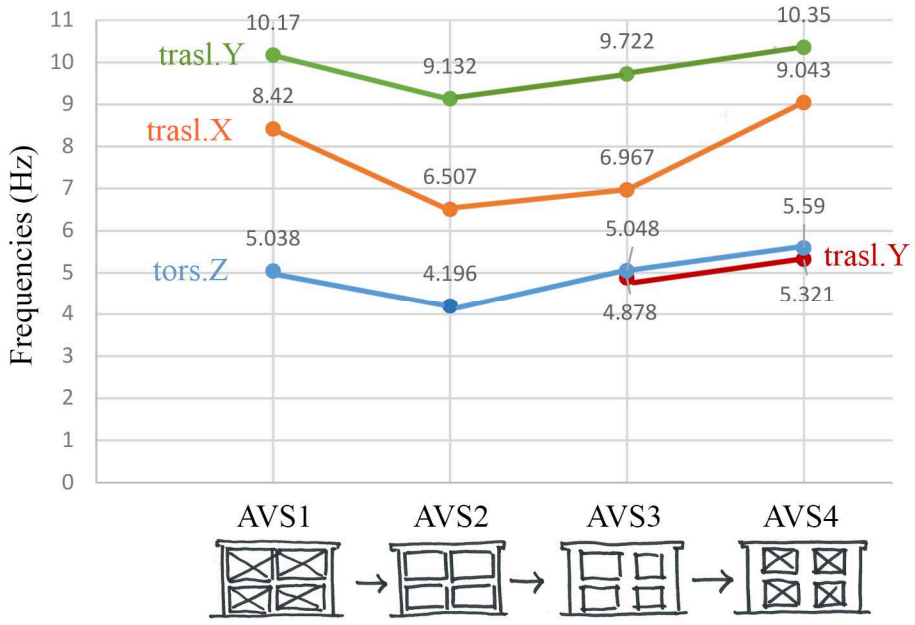

Figure 6.12 Tracking of natural frequencies at each AVS

6.3.5 F.E. model updating

FE models are commonly implemented to predict the response of a civil structure to the environmental and to other types of loads (for instance dynamic loads like wind and earthquakes). These models, even if well formulated, from the points of view of both

geometrical and mechanical aspects, show a series of uncertainties that affect the structural behavior, such as material properties, soil–structure interaction, and rigidity of nodes [84]. In order to reduce these uncertainties and understand structural dynamics, several numerical models are updated following the dynamic identification process previously shown.

Four different numerical 3D FE models of the structure were built using the commercial code MIDAS GEN [56], where geometry is based on the results of the geometric and structural surveys.

The NM was developed assuming a linear behavior for all materials because we are interested in knowing only the dynamic behavior.

R.c. beams and columns are modelled using general beam elements, with weight density equal to 25kN/m^3 and an averaged Modulus of elasticity equal to 2.708e+07 kN/m^2. This is done in AVS1 and AVS2 before the beginning of the retrofit phase. In AVS3 and AVS4 the Young Modulus of the enlarged columns is incremented to 3.407e+07 kN/m^2.

Infill panels and floors are modelled using 2D plate elements, with mechanical properties taken from statistical studies. The first ones have a Modulus of elasticity of 1.50e+06 kN/m^2. External walls are modelled using a thickness value of 0.30m while internal ones are 0.20m. Concrete slabs of the storeys are modelled with Young Modulus equal to 2.20e+07 kN/m^2 and thickness set at 0.08m.

Permanent loads are defined according to the structural surveys and destructive and non-destructive tests carried out.

Experimental mode shapes are achieved with the parameter extractor. At each estimated frequency the correspondent ODS is obtained, checking the goodness of the identification process through the Complexity Plots [80].

In the following paragraphs, for each AVS, the comparison between experimental and numerical mode shapes is reported.

First Numerical Model

Regular structural RC framed buildings are characterized by the firsts two transversal modes (X and Y directions) and a third torsional mode [6,85].

In the present case, the canonical mode shapes are inverted and the torsional one appears as first: this highlight the strong irregularity of the building. Tuning of NM helps in the understanding of this anomaly.

This apparent discrepancy is attributed to the absence of a clear structural separation (see Fig. 6.9a) with the adjacent building in correspondence to the RC staircase. In fact, following repeated model updating, the only variables that strongly influence the structural dynamic of the building are the boundary conditions localized in this area.

Thus, the conclusion is that unlike the planning previsions, the seismic structural separation was not completely efficient: during the years, several past interventions make the two structures not completely disconnected. This connection influences the entire rigidity of the building. For this reason, great attention has been paid during the intervention in this area.

In order to consider this aspect several linear springs are inserted in FE model in correspondence of the structural joint (Fig. 6.9a), obtaining a good convergence of numerical and experimental frequencies and mode shapes, as reported in Fig.6.13 and Tab.6.5.

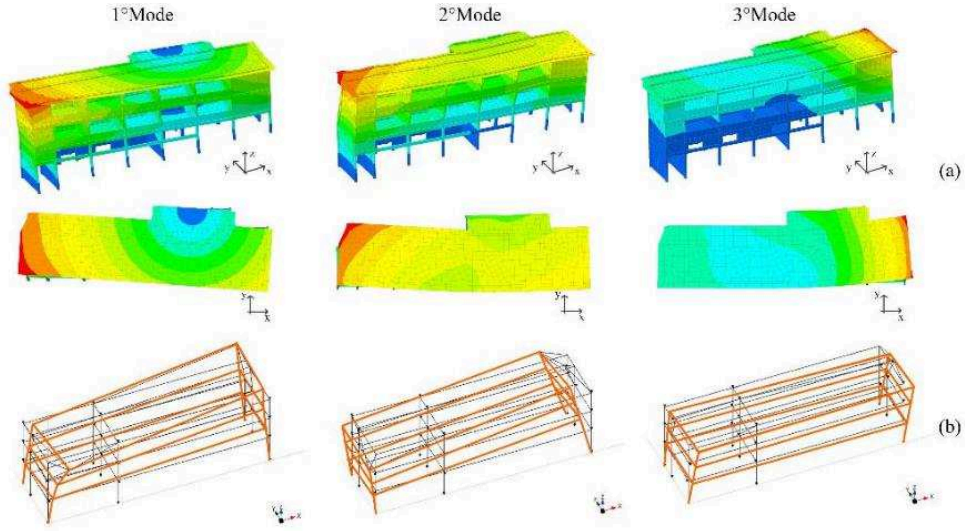

Figure 6.13 (a) Comparison between FE model updated and (b) ODS of AVS1

Mode	AVS1 Frequency	FEM Frequency	TRAN-X		TRAN-Y		ROTN-Z	
No	(Hz)	(Hz)	Mass(%)	Sum(%)	Mass(%)	Sum(%)	Mass(%)	Sum(%)
1	**5.04**	**5.31**	14.23	14.23	13.35	13.35	**57.03**	57.03
2	**8.42**	**8.14**	**50.88**	65.11	19.77	33.11	3.01	60.04
3	**10.17**	**10.17**	11.99	77.10	**35.57**	68.68	20.48	80.52

Table 6.5 Comparison between analytical and experimental values of natural frequencies (in bold the calibrated frequencies respect to the AVS1 and the significant participation masses)

It is worth remarking that, without the addition of these boundary conditions, the first NM would be not be translational in Y direction. Thanks to this procedure it was possible to identify the real operational conditions of the building, quite different from the expected one, and thus it was possible to have a clear picture of the effective behaviour of the structure, which is necessary in the vulnerability assessment and which was otherwise impossible to obtain.

Participant masses obtained by FE model confirm a good agreement with NM (Tab.6.5) and a considerable excited mass is associated to the first three modes.

Second Numerical Model

In this structural configuration, infill panels are completely disconnected to the r.c. frames, in order to allow the insertion of the enlarged columns that characterized the structural intervention.

The identification process detected the same experimental mode shapes previously obtained (Fig.6.14), where the torsional one still appear as first. This indicates that the structure is still affected by the presence of a structural connection with the other building.

At this stage the NM was conveniently modified, removing the connections offered by infill walls. The loads of this last are considered applying uniform linear loads to the beams.

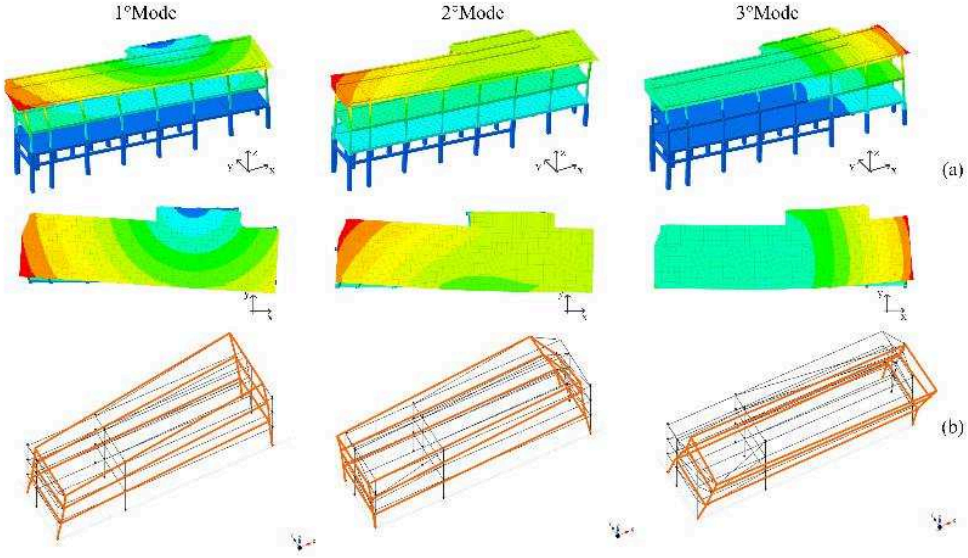

Figure 6.14 (a) Comparison between FE model updated and (b) ODS of AVS2

Mode	AVS2 Frequency	FEM Frequency	TRAN-X		TRAN-Y		ROTN-Z	
No	(Hz)	(Hz)	Mass(%)	Sum(%)	Mass(%)	Sum(%)	Mass(%)	Sum(%)
1	**4.20**	**4.52**	15.38	15.38	5.33	5.33	**32.12**	32.12
2	**6.51**	**6.49**	**46.15**	61.53	5.64	10.97	5.19	37.31
3	**9.132**	**9.61**	1.84	63.37	**31.94**	42.90	21.22	58.53

Table 6.6 Comparison between analytical and experimental values of natural frequencies (in bold the calibrated frequencies respect to the AVS2 and the significant participation masses)

Table 6.6 shows the good agreement in terms of frequencies and the correspondent participation masses validating the obtained convergence. As said, the absence of infill panels is responsible for a stiffness reduction of about 20%.

Third Numerical Model

The first two very close frequencies correspond two completely different mode shapes. In the first one all the eigenvectors are in phase and move in Y direction. In the second one the sensors fixed at each corner are out-of-phase, which corresponds to a torsional mode shape.

The appearance of this different first mode is in accordance to the classical dynamic of this structure type. The updating of the Third NM consists in removing the elastic springs used in the previous NMs, in increasing columns cross sections and in increasing the Young Modulus of the concrete. By modifying these boundary conditions in the structural joint the theoretical mode shapes are again in agreement with the experimental ones, as shown in Fig.6.15.

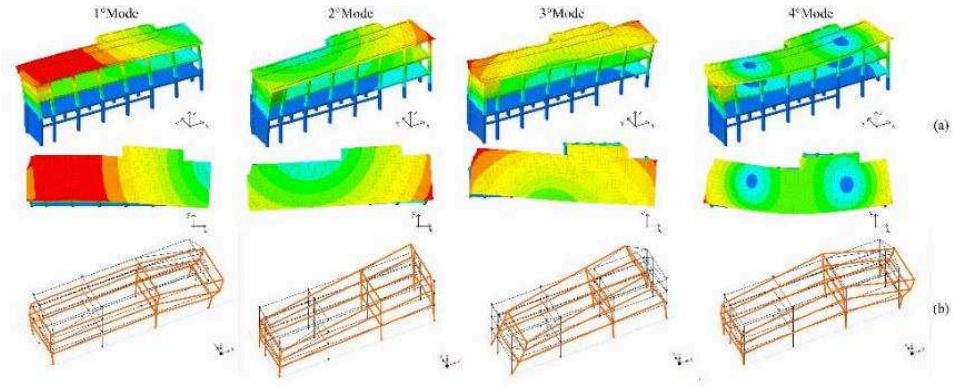

Figure 6.15 (a) Comparison between FE model updated and (b) ODS of AVS3

Mode	AVS3 Frequency	FEM Frequency	TRAN-X		TRAN-Y		ROTN-Z	
No	(Hz)	(Hz)	Mass(%)	Sum(%)	Mass(%)	Sum(%)	Mass(%)	Sum(%)
1	**4.88**	**5.03**	3.08	3.08	**51.15**	51.15	6.49	6.49
2	**5.04**	**5.44**	21.34	24.42	12.17	63.32	**38.53**	45.02
3	**8.42**	**7.37**	**42.08**	66.50	0.09	63.42	23.37	68.40
4	**9.72**	**10.58**	0.86	67.37	1.21	64.63	0.03	68.44

Table 6.7 Comparison between analytical and experimental values of natural frequencies (in bold the calibrated frequencies respect to the AVS3 and the significant participation masses)

The alteration of the structural joint characteristics was confirmed by the structural surveys. In December 2015 the joint was cleaned, eliminating all the parts that kept the two structures connected.

This is a proof of the fact that the stiff joint (strongly) influenced the dynamical behavior of the structure in the previous conditions. Moreover, it confirms the utility of dynamics identification to understand the structural behavior of building, well above the “sole” determination of the dynamical properties.

Tab.6.7 reports the comparison between AVS3 and the update NM. The retrofit intervention increases global structural stiffness by about 20%.

Fourth Numerical Model

The last AVS is performed in the ultimate structural configuration, at the end of the retrofit phase. All the column cross-sections are incremented and infill walls are completely connected to the structural frame.

The fourth dynamic identification process shows that the mode shapes are qualitatively the same. Mode1 and Mode2 are well separated compared to AVS3 (Fig.6.16).

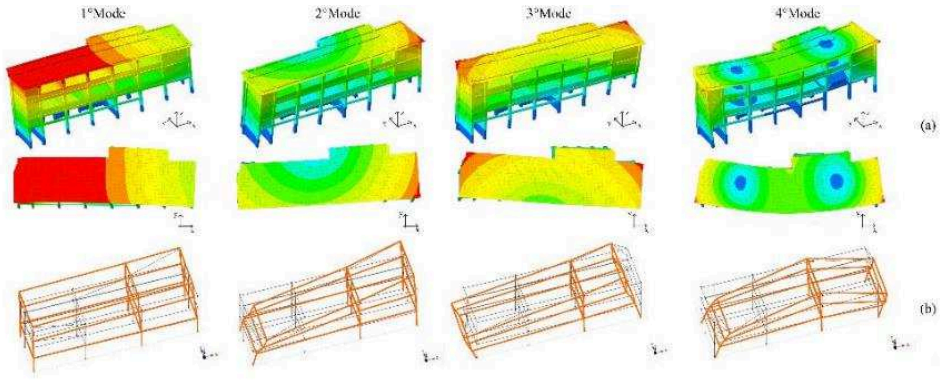

Figure 6.16 (a) Comparison between FE model updated and (b) ODS of AVS4

Mode	AVS4 Frequency	FEM Frequency	TRAN-X		TRAN-Y		ROTN-Z	
No	(Hz)	(Hz)	Mass(%)	Sum(%)	Mass(%)	Sum(%)	Mass(%)	Sum(%)
1	**5.321**	**5.24**	1.96	1.96	**79.01**	79.01	2.47	2.47
2	**5.59**	**5.61**	24.39	**26.35**	4.89	83.90	**56.21**	58.67
3	**9.043**	**8.79**	**56.42**	82.77	0.07	83.97	26.30	84.98
4	**10.35**	**10.81**	0.76	83.53	**6.39**	84.41	0.43	85.40

Table 6.8 Comparison between analytical and experimental values of natural frequencies (in bold the calibrated frequencies respect to the AVS4 and the significant participation masses)

As observed in the previous models infill panels influence the global structural stiffness but they do not modify qualitatively the aspect of ODSs.

Table 6.8 reports the comparison of the estimated frequencies and the respective participating masses. As the comparison between AVS1 and AVS2 shows, infill panel effects are responsible of a stiffness increment of about 10%.

6.3.6 Final remarks

The identification methodology was implemented to track structural changes of the Ugo Foscolo School during its retrofit. Several comments and remarks can be drawn.

- The simple method presented is a fine tool for a character-ization of in-situ natural frequencies of buildings. It shows great advantages in terms of effectiveness, accuracy and cost.
- The periodic AVS's exhibit the effectiveness of the retrofitting works. The increase of the natural frequencies of the building before and after the retrofit phase is extremely evident, underling the efficiency of the retrofit project.
- Knowledge of the experimental frequencies is of great importance to calibrate analytical models (checking the value of elasticity modulus of various materials, checking the influence of infill walls and of other always forgotten elements such as stairways, short columns, or characteristics such as depth of columns and beams, boundary conditions, etc.).
- The influence of infill walls is clearly detailed from in-situ measurement for the low amplitude ambient measurements. It confirms that analytical modelling can reach results very close to the measured ones if infills and other elements are modelled.

This work attempts to highlight the relevance of SHM techniques, able to reproduce the real dynamic behavior of the structure in its current state. Structural analyses should start the computations with a linear structure showing their initial fundamental frequencies, which are the ones measured at in-situ testing for low amplitudes.

Destructive and non-destructive controls are not sufficient to understand the dynamic properties of the building. Any structural intervention should be supported by ambient vibration surveys, able to reproduce the real operating conditions of the investigated structure.

In conclusion, this relevant experimental study shows that these identification techniques are extremely capable of being used in online structural health monitoring applications. The data set collected during this study is a useful contribution to the database of dynamic characteristics of engineering structures.

Chapter 7
Ambient Vibration Survey using Wireless Sensor Network

7.1 Introduction

Smart buildings equipped with several sensors, able to assess the safety of the building or indicate the need of maintenance actions, are becoming almost familiar not only in academic fields.

The development of low cost and low energy measuring devices, the new generation of acquisition systems, and the increasing availability of software for advanced computational analysis, makes it possible to extend smart structures from big infrastructures like bridges, dams and skyscrapers to historical heritage and public or residential buildings [86].

The damage level estimation for ordinary buildings affected by an earthquake is fundamental both from the safety and the economic point of view. SHM systems often require a large number of accelerometers, so the cost of each sensor and the architecture of the acquisition system become determining elements when evaluating the feasibility of this kind of studies.

The flexibility of the monitoring system is fundamental, especially in case of existing buildings, where the use of a considerable quantity of cable could compromise normal use, could affect the quality of acquired signal and finally be too expensive. For these reasons the adoption of Wireless Sensor Networks (WSN) able to manage several accelerometers nodes is desirable.

WSN have several critical aspects to be solved: most important are the synchronism and the high determinism in data sampling required in this kind of applications, and the possible loss of data during the wireless transmission.

Under such a background, this Chapter shows the preliminary results obtained with a wireless sensor system for structural health monitoring of civil structures placed in seismic zones.

The first six prototypes of sensors have been assembled and tested in collaboration with the Loccioni Group, in order to assess floor noise, performance and the synchronization method.

The preliminary tests were carried out in laboratory, with experience based on previous experiments [51,87].

In the final part of the Chapter the results of a one-day AVS using WSN is shown. The case study is a masonry building situated in Castelfidardo (Ancona, Italy). The identification procedure is performed and the structural parameters extracted, with the aim of obtaining an accurate numerical model that simulates the dynamic behavior of the whole structure.

7.2 Development of a Wireless Sensor Network

When monitoring large structures where several accelerometers are required, the cost of each sensor becomes a determining element in the system choice. Seismic

accelerometers based on piezoelectric or piezoresistive technology are largely employed in civil structural monitoring, but in recent years the possibility of using capacitive MEMS (Micro Electro-Mechanical Systems) accelerometers as an alternative to expensive conventional accelerometers has been the subject of several studies.

Of course a WSN always requires a power source that makes it not completely fit for continuous monitoring. Wireless solutions are instead almost always appropriate for periodic AVS.

Due to their cheap cost and their always increasing performances, MEMS based transducers are very interesting as they can significantly extend the range of applications of embedded sensors when compared to conventional sensors. These devices integrate mechanical sensing elements and electronic circuits for control and signal processing in a single component. Thanks to the evolution of silicon semiconductor processing technologies, it is now possible to create micro-sensors for the detection of mechanical quantities like pressure, vibration, acceleration, etc. that include signal conditioning and data samplers that can easily communicate with data acquisition and storage systems.

MEMS made for analog quantity measurements have analog sensing devices in the integrated version, which have the same problems as traditional analog systems when performing signal processing: amplification, filtering, conversion current-voltage, etc. . In fact, while for digital systems miniaturization does not pose many problems in the treatment of discrete signals, for analog systems in microelectronics scale there is a considerable decrease in the signal to noise ratio. Furthermore, the production process (assembly of components and assembly) can lead to degradation of the performance of the MEMS device, for example for thermal stress on the electronic components for signal conditioning. In order to solve these problems the electronic miniaturization has made it possible to integrate within the same package various components, making the device a “smart” micro device. Integrated signal conditioning hardware is used to amplify, filter, and linearize the output signal, since it is necessary to correct the distortions induced by the instrument. The reliability of the measurement is guaranteed by the introduction of suitable anti-aliasing filters, and through the possibility of adjusting the measuring range, in order to reduce the quantization error to obtain a better accuracy of A/D converters.

MEMS devices are the best choice for WSN implementation because of the low energy consumption and the limited costs.

7.2.1 Wireless sensor design

The SHM system has been conceived as a network of “nodes”, each one equipped with 2 accelerometers mounted along orthogonal directions, communicating via wireless with a master station, battery powered and synchronized through a GPS module. Figure 7.1 shows a diagram of node hardware architecture.

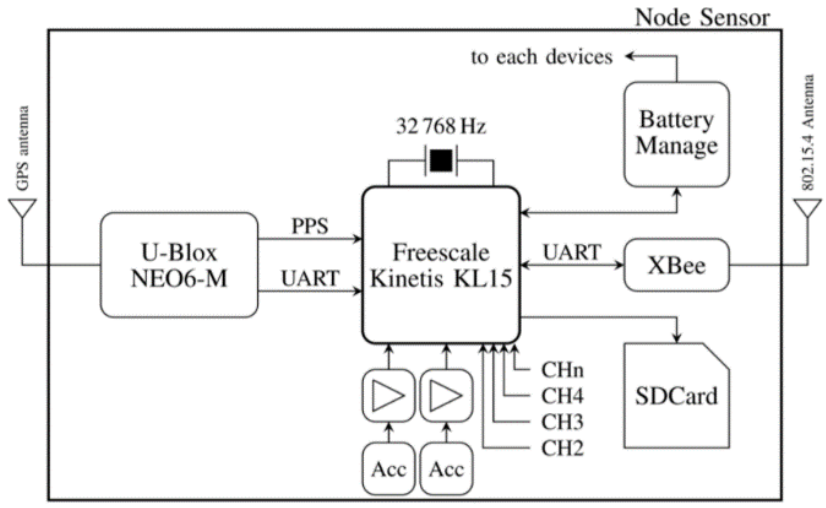

Figure 7.1 Single node hardware architecture.

All the hardware has been arranged in three stacked boards as reported in [88]. The lower board contains accelerometer connections and analogic electronics for signal filtering and amplification, the middle one the microcontroller and the SD card, the upper one GPS and wireless communication (Figure 7.2).

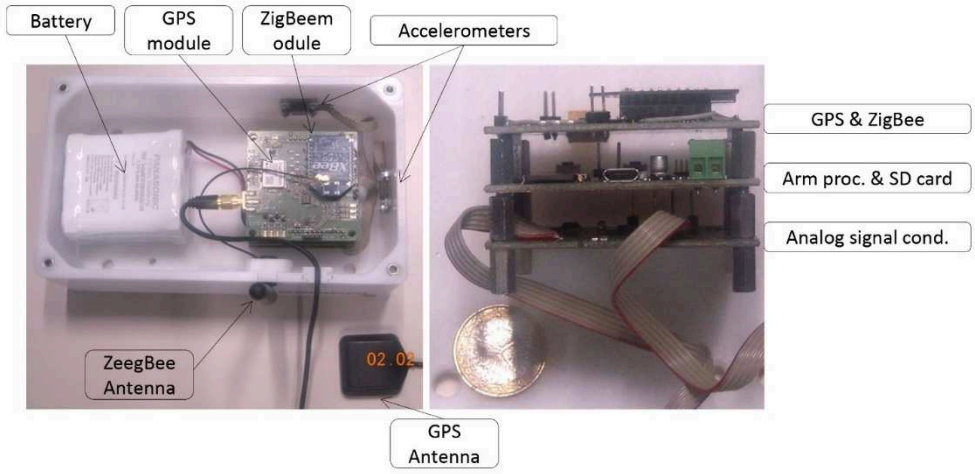

Figure 7.2 Nodes components arranged in their case (left), the 3 boards stacked in "tower" configuration (right).

The heart of the sensor is a Freescale Kinetis KL15 low power microcontroller, with high precision 16-bit Analog to Digital Converter (ADC). The acquisition of the data is synchronized among nodes using the signal 1PPS (1 pulse per second) generated by GPS receivers. For wireless communication and data transfer, a low power ZigBee protocol was chosen. These devices allow the transfer of data via radio frequency using a serial communication standard, known as "transparent mode". In this way each node can

communicate with the other, so for our application it was necessary to implement a custom structured and stable protocol for the communication with master controller.

Each node is equipped with two capacitive MEMS accelerometers MS9002 with ±2g full scale range. The signals from the accelerometers are acquired at a sampling frequency of 1 kHz and stored in the 4GB SD card of each node.

The battery pack consists of 6 rechargeable lithium-ion batteries connected in series in two groups. The assembled sensor is shown in Fig.7.3.

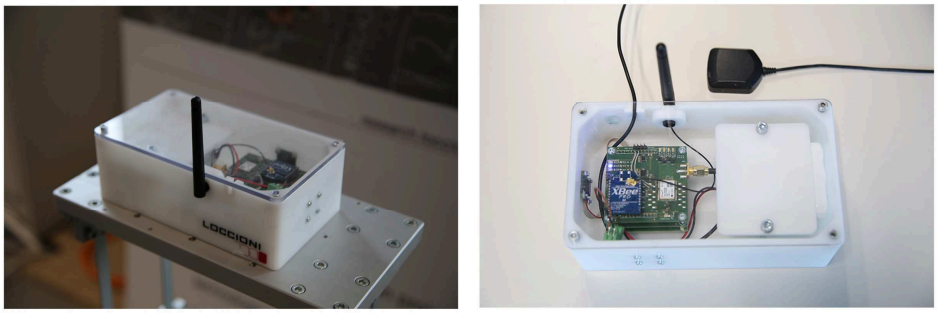

Figure 7.3 Sensor design

The developed WSN system is composed of 6 wireless measurement nodes and one master node connected to a laptop, as shown in the scheme of Figure 7.4. Before each measurement campaign it is necessary to set the start and the duration of acquisition, and then, when all nodes are connected and synchronized by pulse per second signal generated by GPS module, they can begin to record data autonomously.

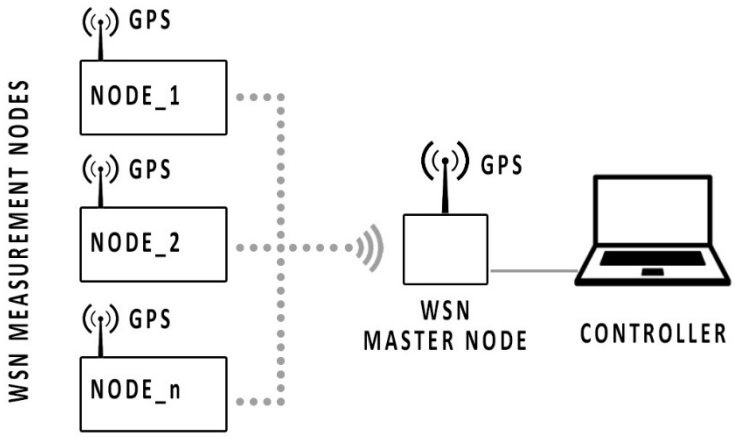

Figure 7.4 General architecture of wireless sensor network.

The sensors were assembled and tested in the laboratory before applying them on real case studies, in order to evaluate their performance and suitability to be used in a SHM system. The architecture of the first prototypes is designed to solve two critical aspects of the wireless networks:

- the synchronization at the level of the individual sample;
- the loss of data during wireless transmission.

Node synchronization tests were performed by removing accelerometers from the nodes and acquiring with two nodes the same signal produced by a signal generator. To precisely evaluate the phase shift between the two sensors, very low frequency sine and square waves were used.

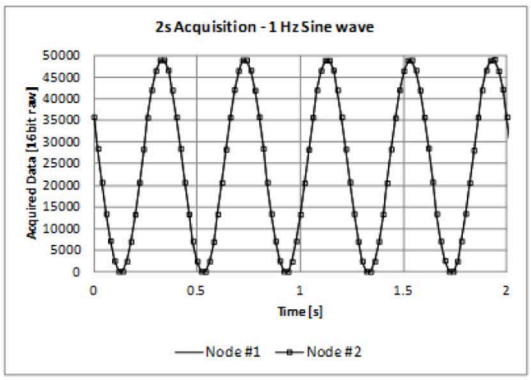

Figure 7.5 An example of signal used to assess nodes synchronization.

Figure 7.5 shows an example of time signal acquired by sensor. Data can be considered perfectly synchronized at the chosen sample rate of 1000 Hz, as explained in the procedure described in Concettoni et al 2015 [88]

Floor noise of the sensors around a value of 0g was measured putting sensors on an air suspension vibration insulation table and making an acquisition during the night, when nobody is supposed to be in the building, all machinery are stopped and road traffic close to the laboratory building has ceased.

Figure 7.6 shows noise spectral density of wireless accelerometer in comparison with a standard 1V/g MMF KF48C seismic piezoelectric accelerometer (MMF KF48C). At frequencies above 1 Hz, Loccioni nodes have a floor noise of about 160 µg/√Hz, while MMF has 40 µg/√Hz.

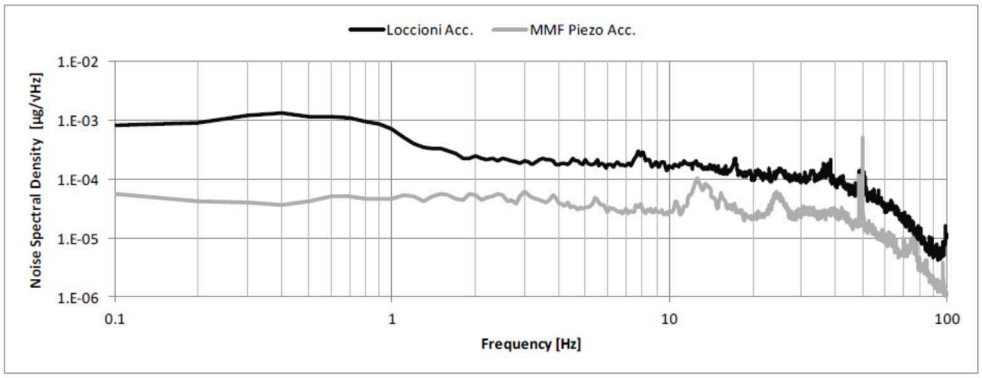

Figure 7.6 Floor noise of Loccioni nodes compared with a standard 1V/g piezoelectric seismic accelerometer

7.2.2 Sensors calibration

Each node is equipped with 2 MS9002 Colibrys MEMS capacitive accelerometers (MS9000.D, 2012), with a nominal sensitivity of 2V/g when power supply is 5V. In our case, power supply of the accelerometers is shared with other nodes' electronic components, which operates at 3.3V and as a consequence, as commonly happens with MEMS sensors, the sensitivity decreases.

The smallest amount of acceleration that a sensor can measure is determined by its sensitivity and its signal to noise ratio. The sensitivity was verified for each MEMS sensor before being placed on the scale structure, changing the orientation of the sensor in space and measuring g gravity. The accelerometer is set with the axis to be measured oriented (Fig. 7.7):

- horizontally with zero g component, so the axis measured is parallel to the force of gravity and the acceleration on that axis is zero m/s^2, which is 0g;
- vertically in the same g orientation, the acceleration on that axis is then $9.8m/s^2$ or 1g;
- vertically in the opposite g orientation, the acceleration on that axis is then $-9.8m/s^2$ or −1g.

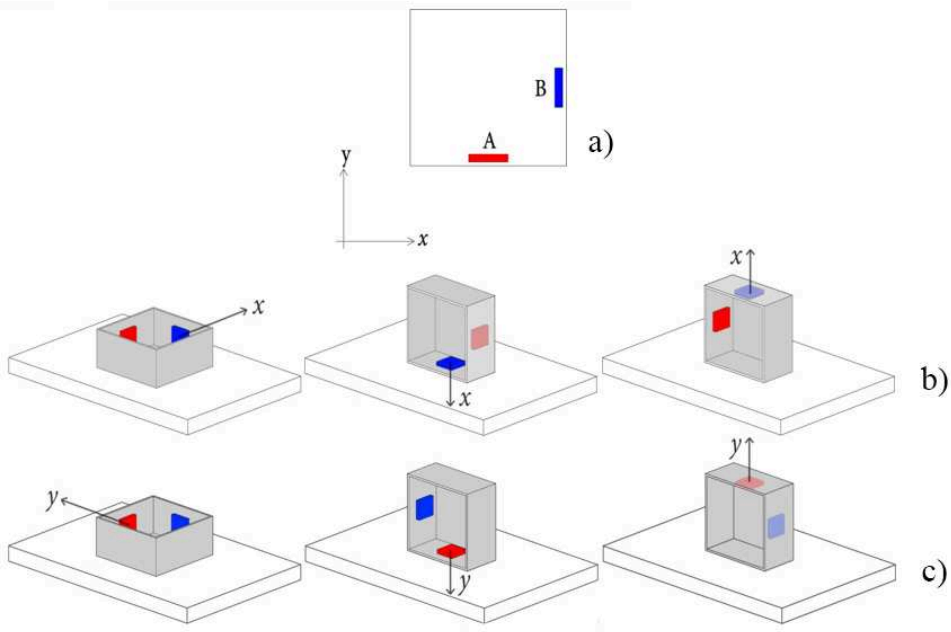

Figure 7.7 Calibration setup: (a) plan view of wireless sensor, (b) orientation of sensors for X direction, (c) orientation of sensors for Y direction

The accelerometers are connected to a data-recording device that reads the voltage signal from the accelerometer and performs an exponential moving average until the value becomes stable. Since the MEMS accelerometers are biaxial the procedure is repeated for

each direction (x and y directions) of each device (Fig. 7.7 b-c). The values obtained are shown in Table 7.1.

		NODE#1		NODE#2		NODE#3	
		x	y	x	y	X	y
"-g"	-9,81	16252,96	16203,54	16477,56	16362,28	16230,79	16138,69
“0g”	0	32494,97	32556,6	32832,7	32700,19	32606,97	32687,24
"+g"	9,81	48597,78	48589,93	49029,83	48984,27	48833,23	47595,88

		NODE#4		NODE#5		NODE#6	
		x	y	x	y	x	y
"-g"	-9,81	16466,89	16201,21	16091,41	16450,4	16056,29	16045,16
“0g”	0	32744,89	32485	32374,7	32917,1	32301,69	32312,73
"+g"	+9,81	49070,29	48779,76	48471,71	48831,51	48513,9	48470,34

Table 7.1 Calibration of wireless sensors: averaged values of voltage for each each sensor (x and y directions)

The calibration curve for each direction of each accelerometer is obtained plotting the values of voltage versus the values of gravity acceleration in g. The curves are plotted in Figure7.8.

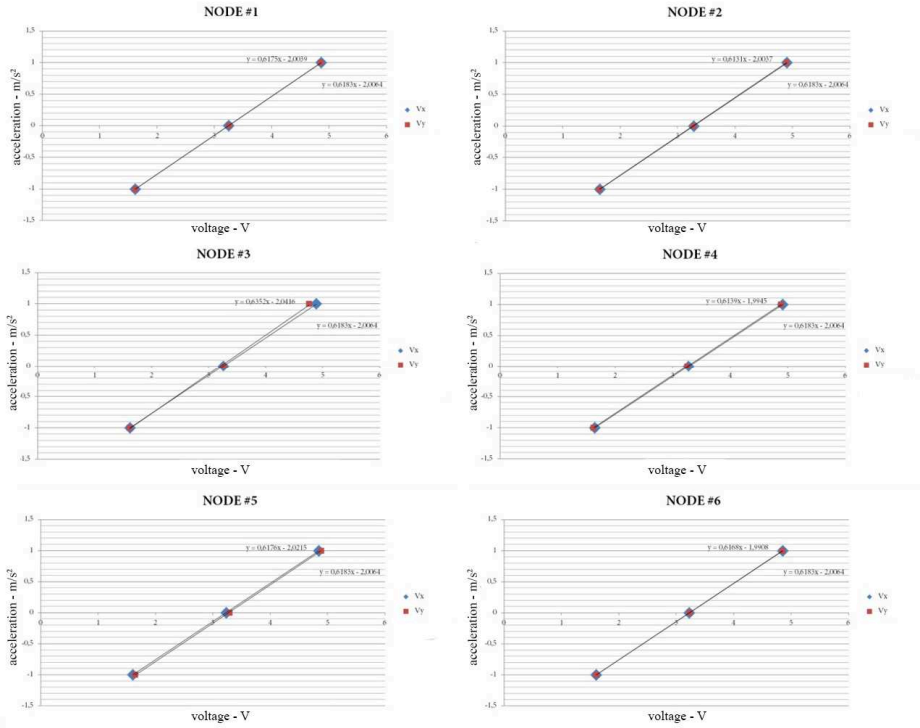

Figure 7.8 Calibration curves of each sensor

Then the value of sensitivity for each sensor and for each direction is obtained calculating the slope of the least squares linear fit of these values. The inverse of the slope coefficient is the value of the sensitivity. These are shown in Table 7.2.

Node n.	Direction	Unit of measure	Sensitivity
NODE#1	X	(mV/g)	1617,338
	Y	(mV/g)	1619,433
NODE#2	X	(mV/g)	1617,338
	Y	(mV/g)	1631,055
NODE#3	X	(mV/g)	1617,338
	Y	(mV/g)	1574,307
NODE#4	X	(mV/g)	1630,258
	Y	(mV/g)	1628,93
NODE#5	X	(mV/g)	1618,909
	Y	(mV/g)	1619,171
NODE#6	X	(mV/g)	1622,85
	Y	(mV/g)	1621,271

Table 7.2 Sensitivity of MEMS accelerometers

The acceleration time histories are calculated from voltage time histories with the equation (7.1):

$$Acc_i = V_i \frac{g}{S_i} \quad 7.1$$

where Acc_i is the i-acceleration, g is the gravity acceleration, V_i is the i-voltage signal acquired, and S_i is the corresponding sensitivity. These operations are automatically performed by the software after data acquisition before the autosaving procedure.

7.3 AVS of a historical masonry building monitored with a WSN

Seismic protection and vulnerability reduction are very relevant issues in European regions, such as Italy, characterized by the presence of a large stock of heritage structures. This increased the interest in SHM as a powerful tool to quantify and reduce uncertainties regarding the structural performance. Monitoring can be successfully implemented in some cases as an alternative to interventions or to control the medium -and long- term effectiveness of already applied strengthening solutions.

The WSN developed, after the tests conducted in laboratory environment, is used in a real SHM application. This work details the main results obtained in the context of the "Palazzo Comunale of Castelfidardo" monitoring project with WSN, with the aim of obtaining an accurate numerical model that simulates the dynamic behavior of the whole structure. An iterative approach to perform the manual tuning of the numerical model is proposed, using as calibration parameters not only mechanical entities, but also boundary conditions. Finally, a comparison between the structural responses obtained by the experimental analysis and the updated numerical model is provided. More details are available in [78].

7.3.1 Research motivation

Cultural Heritage (CH) buildings and sites represent an important historical and economic asset of European countries; in particular Italy is characterized by a large number of CH structures. The European and especially the Italian territory are moreover characterized by high seismicity and historical structures are constantly at risk; an enhanced knowledge of the dynamic behavior of structures can play a relevant role in the definition of proper countermeasures for existing buildings and historical structures. Monitoring allows preventing the execution of intrusive repair works, if they are not justified by an experimentally demonstrated worsening of the structural conditions [70,89].

In the present research an experimental and numerical methodology is proposed, in order to perform the SHM of historical buildings lying in medium seismic hazard zones using the developed WSN described in the previous paragraph.

One of the purposes of this work is the extraction of structural information about the dynamic properties. In this framework, the results of output-only modal identification tests can support the rational validation of the Numerical Model (NM); moreover, the tuning of

selected parameters makes the setting of a representative model of the structural behavior in its current state possible [70]. Finite Element (FE) techniques have been shown to be an effective tool for the interpretation of physical behavior of historic fabricæ [89,91–94]. In addition, as any damage changes the physical properties and successively the modal response changes accordingly, a dynamic survey repeated over time combined with a FE model of the structure (able to assess the sensitivity of the modal parameters according to changes in the structural system) can be used for an SHM [95–97].

Usually the updating procedure is based on a mathematical optimization problem: the differences between numerical and experimental frequencies and mode shapes should be minimized through iterative modal analyses [98]. The historical structures are usually very challenging from the scientific and technical viewpoint because of their unique structural configurations and the large modelling uncertainties; for these reasons a reliable model cannot be easily identified or cannot be identified at all [91,93,99,100]. Due to these complexities, the classical modal updating is not the best choice, and a manually iterative procedure of FE model tuning is proposed in order to have a better perception on the structural behavior alteration in the linear range.

7.3.2 Description of the structure

The seat of the Municipal Building is in the ancient priory in the center of the city of Castelfidardo (Ancona, central Italy), already used between XIV and XV centuries by the administrations of the town. In the 1567, it was decided that the old and ruined building be demolished and its reconstruction was committed to the master builder Giovanni Giacomi da Lago Maggiore. Initially the access of the structure was completely different from that used today: people entered the building through an external staircase.

The building is endowed with a belfry with Guelph-type battlements where there is also an ancient clock, bought in 1775 and decorated with circle round travertine, the bell dates back to 1803. The building was (completely) renovated in 1780 and at the beginning of XX century its bottom front was cleared of backfilling (see Figure 7.9a).

At the beginning, the building was inserted in the urban pattern and was placed side by side with other structures. In the second half of the twenties, the last two buildings were dismantled to create a new connection between the square and the street below with the market.

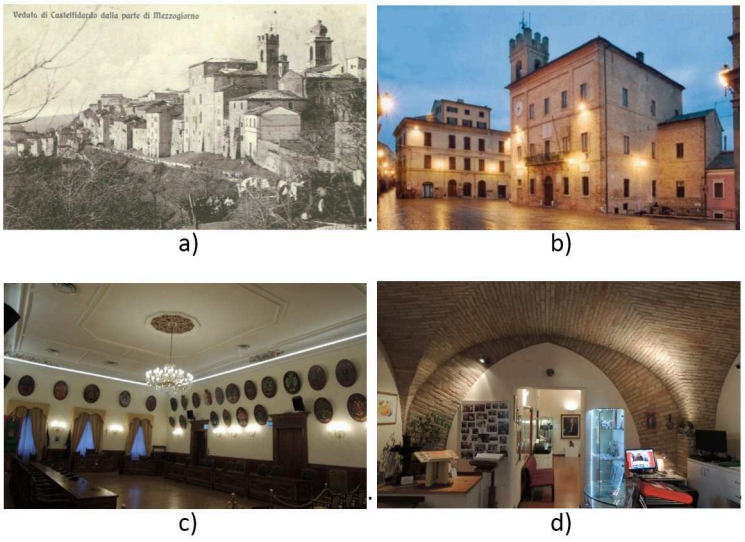

Figure 7.9 Views of: (a) the south part between years 1902-1905, (b) the actual front, (c) Salone degli Stemmi, (d) International Accordion Museum.

The building consists of five floors two of which are located below ground level. The entrance is at the same level of the main square of the town, namely "Piazza della Repubblica" (Figure 7.9b). Starting from ground level (+0.00) it is possible to reach the stairs that go to up to two more floors, housing some of the administrative offices of the town. On the top floor there is the "Salone degli Stemmi" (Figure 7.9c), once used also as a theatre for public performances. At the first basement level, there is the "International Accordion Museum" (Figure 7.9d) and in the second basement some public offices.

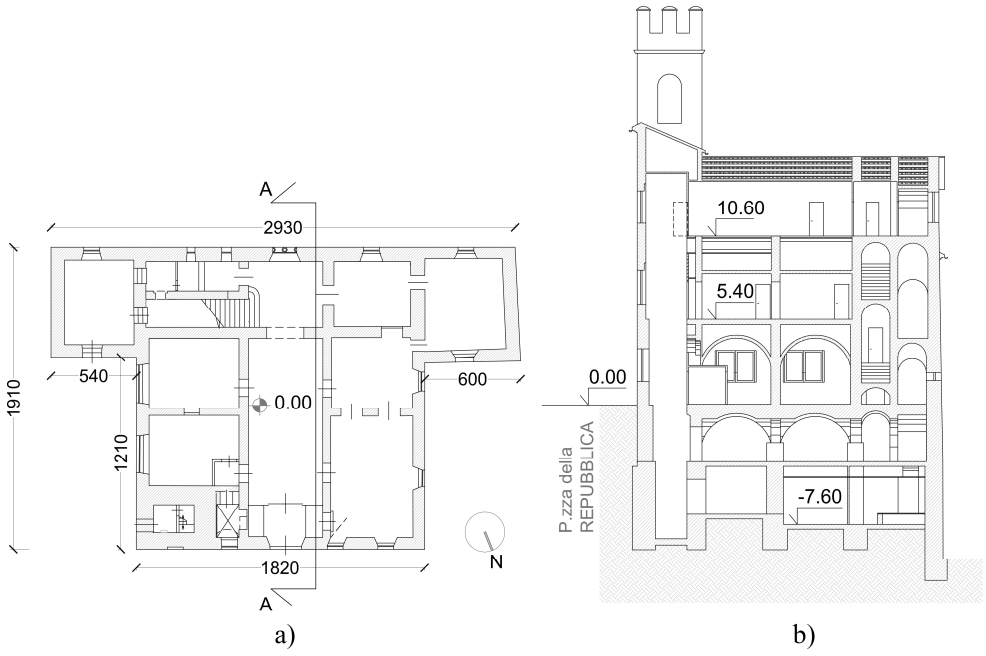

Figure 7. 10 (a) Architectural plan view of the ground floor, (b) transversal section of the building.

The building occupies an area of 23.30 x 19.10 m and has an average height of 29.5 m (Figure 7.10). The structure consists mainly of masonry walls composed of solid brick and lime mortar, and timber slabs and vault in the zero level. The thickness of the walls varies between 1 m and 0.6 m passing from the foundations to the covering floor. The floors in most cases are rigid because they have a reinforced concrete slab due to previous strengthening interventions. Deformable floors are present in some parts of the 2nd and the 4th floor (where the stairs are) and at the top of the belfry.

7.3.3 Monitoring procedures and ambient vibration tests

Due to many uncertainties associated with the construction systems, material properties, modelling techniques, analysis methods, soil interactions and successive past interventions, the evaluation of an historical structure is a difficult task. In addition, the constituting materials tend to exhibit significant variations in properties and internal structure. The damage of masonry structures mainly relates to cracks, foundation settlements, material degradation and deformations and influence significantly the structural response in the linear range.

This section resumes the major settings and the principal scope of our dynamic characterization of the monumental building “Palazzo Comunale di Castelfidardo”.

The process leading to the monitoring of historical masonry structures can be divided in different phases. A preliminary, simple and not computationally expensive, NM of the structure was set up (starting from results obtained from the geometrical and architectural survey) and it was used to locate some points on the building where the experimental tests had to be performed.

Results of the dynamic experiments are subsequently used to identify the uncertain parameters to implement in the numerical model (i.e. those parameters that are not possible to investigate during the experimental campaign). Then the uncertain parameters are selected as "updating parameters" and they are iteratively modified so that both main natural frequencies and corresponding mode shapes in the model match the recorded ones.

The ambient vibration tests were carried out with the wireless accelerometers described in this Chapter.

The use of a WSN is particular useful especially in the present case study. The massive use of cables may compromise the normal operating condition of the monitored structure, affect the quality of the signal and raise costs considerably, especially in the case of existing and historical buildings. The monitoring campaign conducted in Castelfidardo was very useful to prove and better understand the advantage of this kind of systems.

Sensor layout for the monitored building is reported in Figure 7.11.

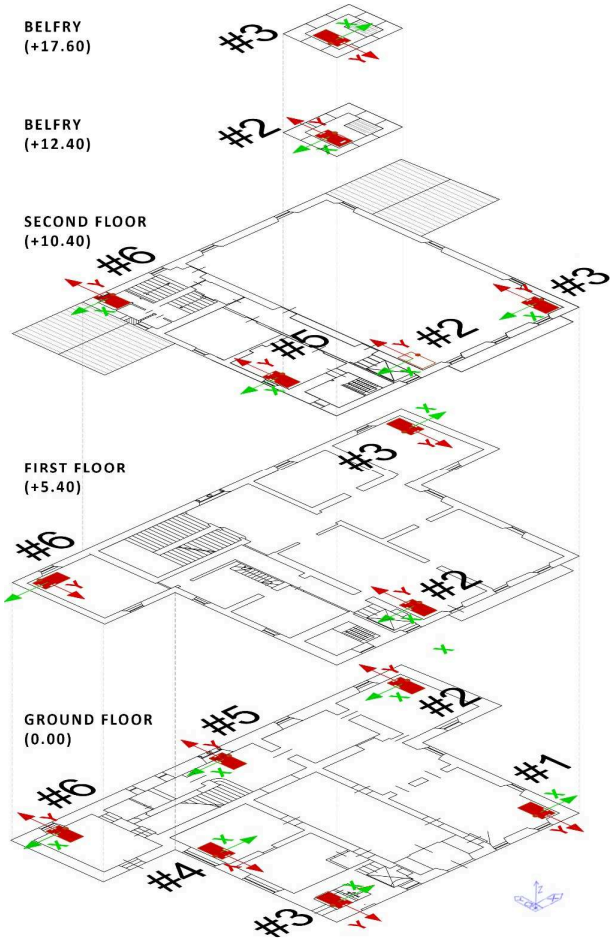

Figure 7.11 Layout of the accelerometers at each floor.

The location of the accelerometers was planned on the basis of specific considerations, using the preliminary results provided by FE equivalent frame model available, in order to catch the torsional behavior and the possible effects of the floors' rigidity. The sensors were

located, for each floor, at the extreme side of the building, as far as possible from each other to better obtain also the rotational component of the floor. The sensors were positioned along the external walls, in proximity of the windows, and also placed outside the GPS receiver in order to detect the signal and to allow the synchronization of all the nodes.

Because of the limited number of the available sensors, the structural response cannot be measured in just one test; in these cases, tests have to be repeated in different times considering different configurations, varying the position of the sensors. This method requires that a group of sensors, called reference sensors, are left in the same place for all the test configurations, so that they can be used to scale the data of different tests, acquired by the other sensors moved in different places (roving sensors) [101,102] and times.

In this case one sensor (called #1 in Figure 7.11) at the first-floor was left in the same position during each acquisition as a reference point, and it was also installed at the basement.

The duration of the recording should be long enough to eliminate the influence of possible non-stochastic excitations that may occur during the test. This recording time was set with the aid of a preliminary NM with equivalent frame method, with the aim to catch the amplitude order of the main frequencies. The main period is ~0.29 sec, and for this reason, four tests in different times were carried out, for a minimum time length of 2000 sec, i.e. 2000 times the first frequencies, and with a sample rate of 1000Hz [13].

In order to check the goodness of the acquisitions, time histories are compared with the floor noise measured in the previously tests. Fig.7.12 shows that the performed vibration measured at the ground floor is at least one order of magnitude higher than floor noise measured in laboratory.

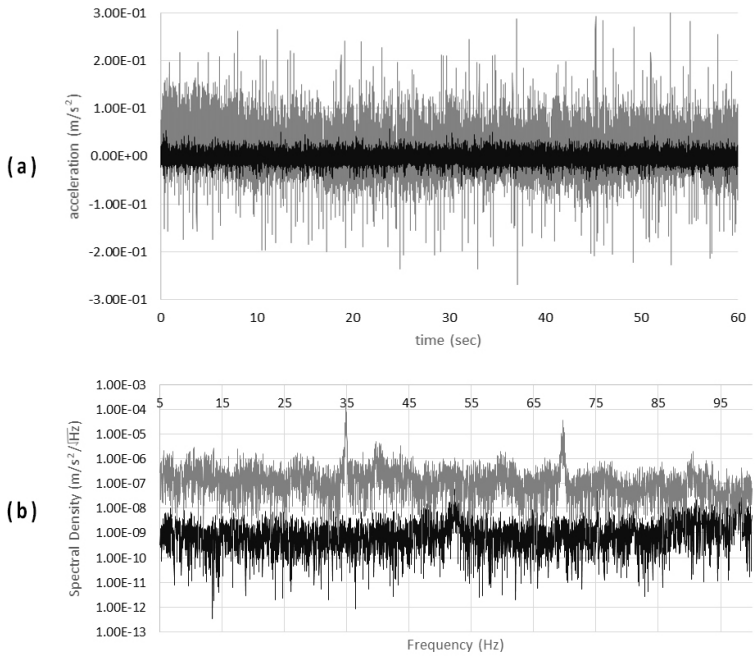

Figure 7. 12 Background noise of Loccioni™ accelerometer (black line) compared with an ambient vibration registered in one point of the structure (grey line): (a) acceleration time history, (b) PSD

Fig. 7.12 reports the comparison between background noise of LoccioniTM accelerometers and a span of 60sec ambient vibration registered from sensor #1 placed at the ground floor. The check is done in terms of acceleration (Figure 7.12a) and Power Spectral Density (PSD) (Figure 7.12b) [13]; the results are very similar for the other nodes and it confirms the good Signal to Noise Ratio (SNR).

7.3.4 Dynamic Identification and F.E. modeling of the building

The collected measurements, originally sampled at 1000Hz, were decimated by a factor of 10 before processing, in order to have the ultimate data of 100 Samples per Second (SPS); data were resampled at 25Hz [82].

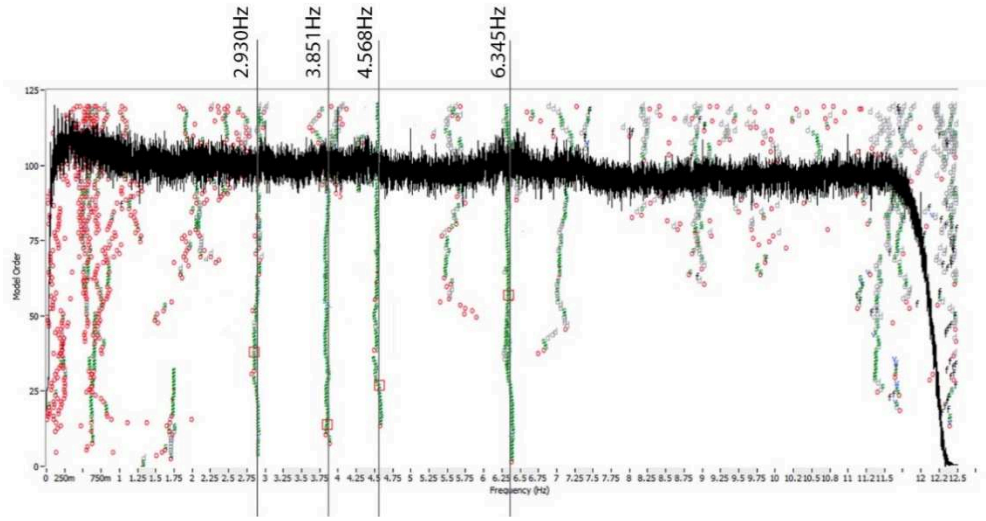

Figure 7.13 Stabilization diagram (Cov-SSI).

The stabilization diagram obtained from the analysis of the collected data through Cov-SSI is reported in Figure 7.13.

The modal identification results are reported in Table 7.3.

Mode Number	Type	Natural Frequency (Hz)	Damping Ratio (%)
1	Translational Y	2.93	8.377
2	Translational X	3.85	7.823
3	Torsional Z	4.56	6.858
4	Translational Y	6.36	5.866

Table 7.3 Modal shapes identified with Cov-SSI technique.

The damping values obtained are rather high; this can be caused by the high internal friction of the masonry-like material (see also [103]). So it is reasonable to select modes with damping values larger than 5%, but anyway smaller than 10% like those reported in [104].

The identified frequencies appear rather spaced, the relative mode shapes involve the entire structure and local modes do not appear (Figure 7.14). In fact the 1st longitudinal mode involves the Y direction, the 2nd mode is transversal along X direction with a torsional component, the 3rd mode can be assimilated to the 2nd one, but with a torsional component much more noticeable and a 4th mode that involves the Y direction of the upper floor.

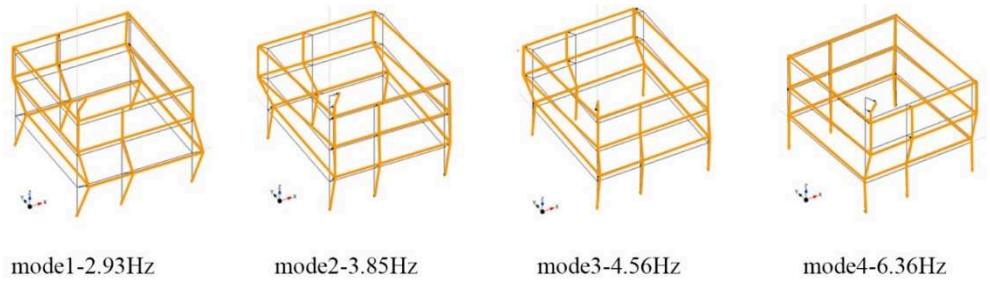

Figure 7.14 Modal shapes identified with SSI technique.

A numerical 3D Finite Element (FE) model of the structure was built by using the commercial code MIDAS GEN [56] where the geometry was based on the result of the survey., As the aim of numerical modelling is to identify the linear dynamic behavior of the building, in this study the macro-modelling approach was used, and the masonry was modelled as an isotropic continuum. Masonry walls were modelled by means of 2D shell elements paying attention to reproduce the main geometric irregularities in the wall. All the openings of the building were reproduced together with the vaults at zero levels with 2D plate elements (Figure 7.15).

The NM was developed assuming a linear behavior for masonry material because it is in our interest to know only the dynamic behavior. The final model reproduces with acceptable confidence (i.e. compared to the available data) the overall spatial configuration of masonry walls together with the entire set of architectural elements that are of structural relevance. This attention is particularly required in historic buildings where differences between architectural and structural elements are not always clear. A relatively large number of finite elements were used in the model (formed by rectangular and triangular with the maximum side equal to 0.40 m), so the model results in a total of 35902 nodes and 36993 2D elements with 162978 active degrees of freedom. A 3D view of the model is shown in Figure 10.

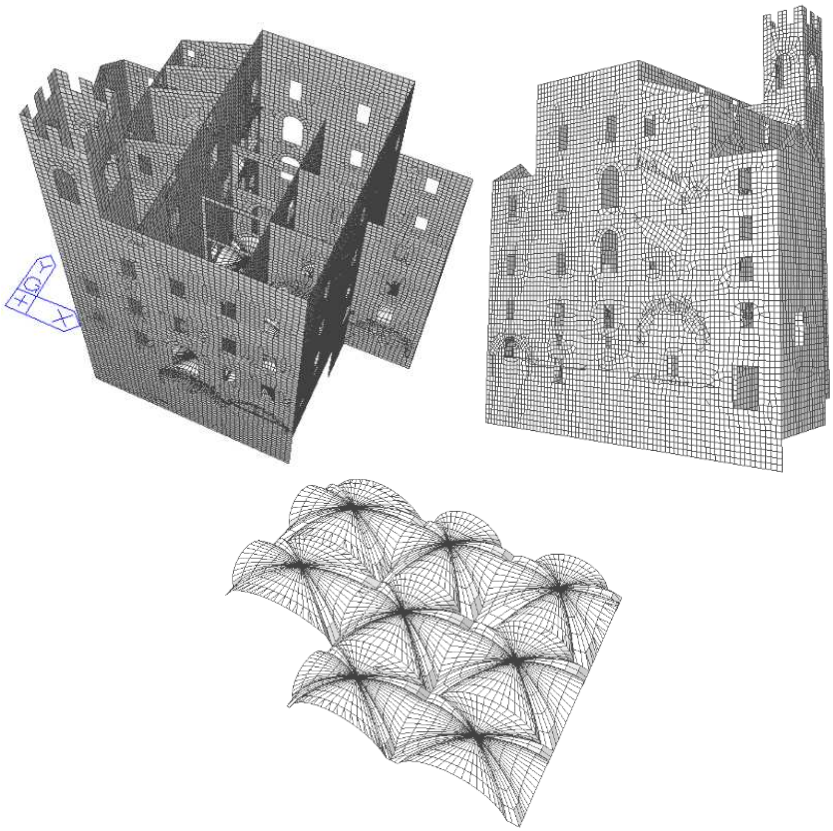

Figure 7.15 View of the FE model of the structure.

The elastic-geometric parameters like Young Modulus E, Poisson's coefficient ν, weight per unit volume γ and the thickness s of the wall at each level are reported and plotted in Figure 7.16. These values represent the starting point of our manual update analysis and they are defined on the basis of what is suggested by the Italian Code [79,105] in Annex C8A.2.

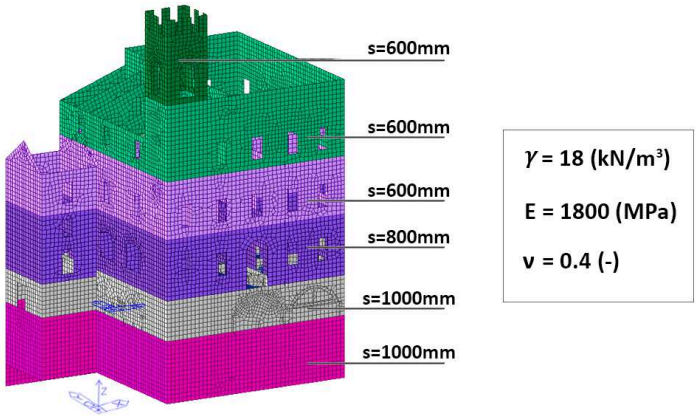

Figure 7.16 Starting point of the mechanical characteristics of the main elements.

Loads are defined according to the destination of expository space, following Italian provisions about loads [79]. Masses are uniformly distributed on the slabs. The effect of the two flights of stairs is directly modelled with plate elements.

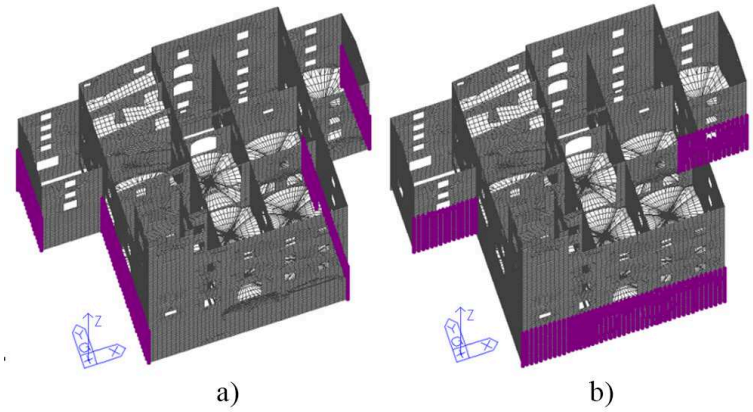

Figure 7.17 Views of boundary constraints applied in the model in (a) X-direction and (b) Y-direction.

7.3.5 Tuning of the NM

For the dynamic analysis of the "Municipio di Castelfidardo", the Lanczos method analysis was used. The mass was directly transferred to the walls and the data reported in Figure 7.16 were used. In order to obtain 95% of mass participation ratio at least 190 modes were accounted, because many modes have small mass participation and they represent local movement in the building due to lack of rigid floors in some parts.

Mode	Frequency	Period	TRAN-X		TRAN-Y		ROTN-Z	
No	(Hz)	(sec)	Mass(%)	Sum(%)	Mass(%)	Sum(%)	Mass(%)	Sum(%)
1	3.10	0.322	9.50	9.50	19.58	19.58	8.27	8.27
2	3.23	0.310	21.09	30.59	13.35	32.93	1.75	10.02
3	4.56	0.219	6.90	37.49	4.60	37.53	24.55	34.57
4	5.26	0.190	1.81	39.30	1.48	39.00	0.03	34.60

Table 7.4 Modal properties for starting Numerical Model (NM).

The dynamic properties and mode shapes of the structure, reported in Table 3 and illustrated in Figure 7.16, revealed important characteristics of the structural behavior. With the first three modes we obtain ~35% of the mass participation ratio and we can observe that the fourth is a local mode that involve only the tower. The subsequent modes, not reported in Table 7.4, are always local and involve the walls in out of plane deformations.

The major consideration is that the structure does not have a decoupled behavior in the two main horizontal directions. In fact, the first two modes of both Ambient Vibration Survey (AVS) and NM do not exhibit the same type of movement as shown in Figures 7.14 and 7.18. This is mainly due to the presence of transversal and longitudinal constraints, in the first two levels (see Figure 7.17a-b), in order to simulate the presence of interactions with the later buildings (east and west) and with underground cavities of the square (south). On the other hand, there is quite a small difference between the first period values of what is reported in Figure 7.14: of about +5% in the first mode and -19% in the second mode.

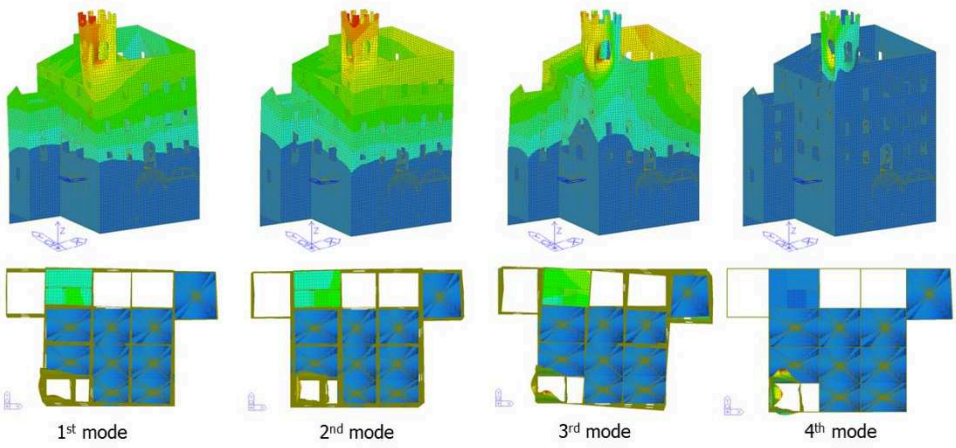

Figure 7.18 The first four modes of the Numerical Model (NM): starting point for the calibration.

Several identification methods are available to determine modal properties of the structures. In the present study the NM of "Municipio di Castelfidardo" is updated by compare-alter-check based iterative solutions like those preliminary reported in [106]. In the iteration, the mode shapes and the frequencies (or periods) of the structure, obtained by experimental and numerical surveys would be compared and the Young modulus of masonry in the required part would be altered. Young's modulus of the material was obtained starting from the indications in Table C8A.2.1 of [105] resulting in great diversity

in the model. Finally, the effect of the alteration was checked in order to define whether the mode of NM fitted the AVS mode or not.

The calibration process is explained below as a number of steps like those reported in Aras et al. [107]. In each step, mode shapes of NM are shown, calibration process is summarized and the results of the calibration are explained. It should be noted that, after each step of calibration, the model was updated and the dynamic parameters of the following steps were obtained from the updated model.

First step of calibration

From AVS two principal decoupled modes are obtained, in Y and X directions respectively. In the NM two coupled modes in X and Y direction are obtained. For this reason the absence of similarity makes the updating procedure necessary.

The first calibration aims to conceal the discrepancy between the mode shapes of the two principal modes. The first attempt is to eliminate the horizontal support in Y-direction in the two underground levels. This is due to the consideration that there are no interactions with the underground cavities of the main square, but there are only interactions in X-direction with the other buildings and the ramparts on the North front. The results in terms of frequencies, participant masses and mode shapes are reported in Table 7.5 and Figure 7.19, respectively.

Mode	Frequency	Period	TRAN-X		TRAN-Y		ROTN-Z	
No	(Hz)	(sec)	Mass (%)	Sum (%)	Mass (%)	Sum (%)	Mass (%)	Sum (%)
1	2.44	0.410	0.01	0.01	62.66	62.66	0.70	0.70
2	3.13	0.319	27.01	27.02	0.53	63.19	12.00	12.70
3	4.11	0.243	9.41	36.43	3.91	67.10	28.48	41.18
4	4.99	0.200	2.37	38.80	4.86	71.97	6.65	47.83

Table 7.5. Modal properties for starting the first calibration of NM.

On the other hand, there is a considerable difference between the frequencies with respect to the initial NM. Otherwise, a better ratio between the modes similar to those evaluated with AVS is clearly shown.

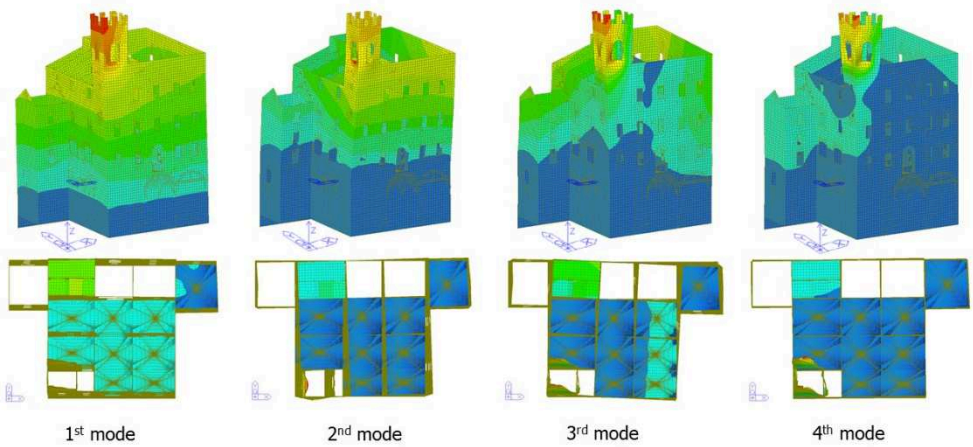

Figure 7.19 The first four modes of the NM after the first calibration.

Second step of calibration

The first consideration is that the first modes of both AVS and NM exhibit the same type of movement as shown in Figure 7.19. This similarity also shows that a well-constructed NM exists at this time. Instead, there continues to be a noticeable difference between the frequency values. The second calibration aims to conceal the discrepancy between the frequencies. This can be achieved by increasing the Young Modulus E of the building.

The calibration coefficient C is calculated as the square of the ratio of the same periods of AVS and NM [107]:

$$T = 2\pi\sqrt{\frac{M}{K}}, \tag{7.2}$$

$$C = \left(\frac{T_{NM}}{T_{AVS}}\right)^2, \tag{7.3}$$

where T is the natural period, M is the mass and K is the stiffness.

Modulus of Elasticity of the structure, E, was incremented (in all walls of the building) to C 1800 MPa = ~ 2600 MPa in order to obtain the first mode period as 0.341 s. The results of the NM are reported in Table 7.6: still present is a little discrepancy between the second mode of AVS and NM. The decoupling between modes is always present, and they are the same modes of Figure 7.19.

Mode	Frequency	Period	TRAN-X		TRAN-Y		ROTN-Z	
No	(Hz)	(sec)	Mass(%)	Sum(%)	Mass(%)	Sum(%)	Mass(%)	Sum(%)
1	2.93	0.341	0.01	0.01	62.66	62.66	0.70	0.70
2	3.76	0.266	27.01	27.02	0.53	63.19	12.00	12.70
3	4.94	0.202	9.41	36.43	3.91	67.10	28.48	41.18
4	6.00	0.167	2.37	38.80	4.86	71.97	6.65	47.83

Table 7.6 Modal properties after the second calibration of NM.

Third step of calibration

The belfry plays an important role on the third and fourth modes of NM, and the rigid diaphragm cannot be excluded a "priori" in the top of the belfry due to the presence of the system bell. In Table 7.7 the new results of the NM with the presence of a rigid floor on the top of the belfry are reported.

Mode	Frequency	Period	TRAN-X		TRAN-Y		ROTN-Z	
No	(Hz)	(sec)	Mass(%)	Sum(%)	Mass(%)	Sum(%)	Mass(%)	Sum(%)
1	2.95	0.339	0.01	0.01	63.59	63.59	0.63	0.63
2	3.79	0.264	27.80	27.81	0.44	64.02	12.08	12.71
3	5.02	0.199	10.18	37.99	2.60	66.62	33.06	45.77
4	6.66	0.150	1.02	39.01	10.53	77.16	2.99	48.76

Table 7.7 Modal properties after the third calibration of NM.

With this calibration, the major differences are noted in the 3rd and 4th modes, where a more participating mass is present.

Fourth step of calibration

The last step of the calibration problem is to introduce the corresponded mass of the system bell at the top of the belfry. This is due to the fact that the 3rd and 4th modes are prevalently at the top of the structure, and a reduction on the Modulus of Elasticity E can produce an increment of the frequencies of the first two modes on the NM.

Introducing the bell in terms of only translational masses in a node inside the rigid floor, the results reported in Table 7.8 and Figure 7.20 are obtained. From these it is possible to see that the first mode is translational with prevalence in Y direction. The second mode is prevalent to X direction with a low mass involved in the torsion, and the frequency differs by about -1.85% compared to the measured one. The last two modes, respectively the torsional and the local one of the belfry, have a difference of about +2.3% and 0% compared to the measured one.

Mode	Frequency	Period	TRAN-X		TRAN-Y		ROTN-Z	
No	(Hz)	(sec)	Mass(%)	Sum(%)	Mass(%)	Sum(%)	Mass(%)	Sum(%)
1	2.93	0.342	0.01	0.01	62.79	62.79	0.72	0.72
2	3.78	0.265	27.47	27.48	0.48	63.27	12.00	12.73
3	4.67	0.214	9.67	37.15	3.39	66.67	31.59	44.31
4	6.36	0.157	1.66	38.81	8.54	75.21	4.36	48.67

Table 7.8 Final modal properties of calibration of NM.

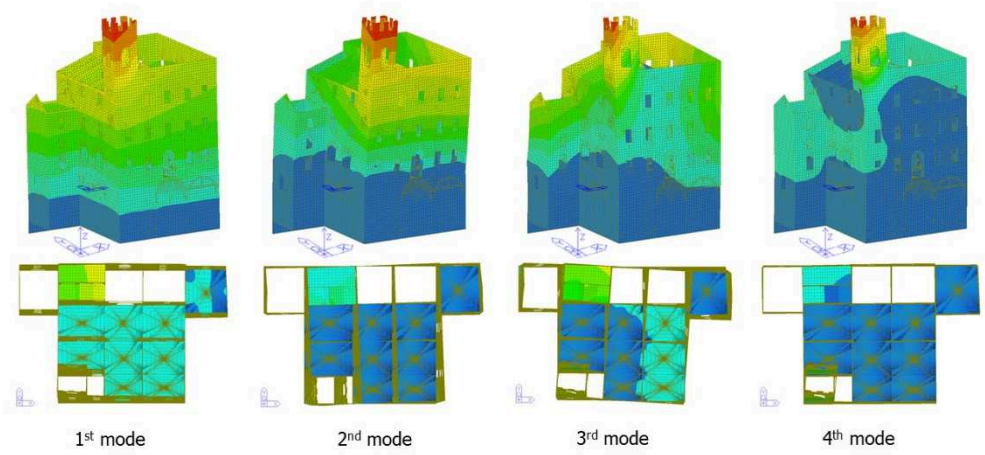

Figure 7.20 Final modal shapes after calibration.

Discussion on calibration

The performed calibration is not unique and further alterations are possible to make the modes of NM more similar to those of AVS. For example additional steps can be added to eliminate the discrepancy between the second and third modes of NM. The NM of the building was formed by 36993 shell elements with 162978 active degrees of freedom, against a limited number of AVS measurements. This prevents the perfect tuning of NM. However, it is important to emphasize the fact that the AVS mode shapes were characterized by 20 points and the 8 most important points -on the top level- were active through these modes. Finally, the explained four steps of calibration are assessed as adequate to correct the NM.

The second important parameter is the period of the modes of NM. In this case the absence of the spurious modes and the high participation mass ratio on the first four modes, gives us a good feedback on the final calibrated parameters. The correlation analysis is made in terms of the scatter between analytical and experimental values of natural frequencies:

$$\Delta f[\%] = \left|\frac{f_i^e f_i^a}{f_i^e}\right| 100 \qquad 7.4$$

where f_i^e is the experimental value and f_i^a is the analytical value of the natural frequency for the ith mode [108].

In Table 7.9 are reported the final values of the calibration process in terms of natural frequencies.

Mode No.	Experimental	Numerical							
	Frequency	Step 1	$\Delta f_{,1}$	Step 2	$\Delta f_{,2}$	Step 3	$\Delta f_{,3}$	**Step 4**	**$\Delta f_{,4}$**
	(Hz)	(Hz)	(%)	(Hz)	(%)	(Hz)	(%)	**(Hz)**	**(%)**
1	**2.93**	2.44	16.70	2.93	0.00	2.95	0.70	**2.93**	**0.00**
2	**3.85**	3.13	18.70	3.76	2.30	3.79	1.60	**3.78**	**1.85**
3	**4.56**	4.11	9.90	4.94	8.30	5.02	10.10	**4.67**	**2.40**
4	**6.36**	4.99	21.50	6.00	5.70	6.66	4.70	**6.36**	**0.00**

Table 7.9 Comparison between analytical and experimental values of natural frequencies.

7.3.7 Final remarks

Management, maintenance and preservation of heritage structures usually result in a very complex task because of the old construction techniques, unique structural schemes, the construction defect and the limited destructive investigation for structural characterization. Therefore, the availability of experimental estimates of the modal properties becomes relevant for structural and seismic assessment process.

Taking into account the increasing interest towards the opportunities provided by OMA as a tool for non-invasive techniques, the present study is intended as a contribution to the development of rational and sustainable procedures for non-destructive investigation according to the current codes for seismic protection and upgrading of heritage structures.

The modal frequencies, damping ratios and mode shapes of historical buildings in Castelfidardo were determined by the Ambient Vibration Survey. It is seen that the modes are generally formed by partial global displacements: the lack of a constant rigid floor diaphragm and the belfry explains this modal behavior.

By using the results of an experimental study, a more accurate NM is set up. Step by step, boundary conditions, modulus of elasticity of the masonry and the masses of secondary elements were altered. After four steps of NM calibration, numerical results similar to the experimental ones were obtained. In all elevations the walls have small differences in terms of elastic-geometric parameters and existing damage in the structure - through the height- should be excluded. Differently, the belfry activates a large number of local modes; this implies its strong vulnerability respect to the dynamic actions.

Dynamic measurements based on environmental vibrations, combined with appropriate model refinement procedures, definitely represent an opportunity for the minimization of the impact of structural assessment on heritage structures.

Chapter 8
Conclusions

"Unfortunately earthquakes have always been and always will be. People cannot talk about fatality. Earth shakes and nature is neither good nor bad. It is, simply and brutally, indifferent to our suffering. But we have a great power that nature has given us: intelligence. Talking about fatality is an insult to human intellect."

With these strong words the architect Renzo Piano answered the questions of journalists about the earthquake that struck the centre of Italy in August 2016.

Our heritage buildings must be protected for people's safety, ensuring an adequate level of seismic protection. It has to be done through the "*diagnosis discipline*" which is accurate, objective and scientific. Just as a good doctor makes a diagnosis before prescribing a cure, so the engineer has to monitoring buildings in order to intervene only where needed.

This thesis is in perfect accordance with these concepts. Structural Health Monitoring (SHM) is a diagnostic approach that makes it possible to leave the field of opinion and go towards the scientific one.

SHM is able to provide a deep knowledge of the monitored building, evaluating the structural health conditions and its residual life. Opportunities and effectiveness of such procedures, which do not require knowledge about the excitation that causes structural vibrations, has been demonstrated by applying them to a number of different case studies.

Classical methodologies have been carried out in several ordinary buildings, demonstrating their reliability and versatility (Chapter 6). These case studies are further examples of how monitoring techniques, in particular the Operational Modal Analysis (OMA), are an essential tool in structural diagnosis and prevention. These approaches should be applied both to existing structures, in order to obtain an evaluation of dynamic behavior before any retrofitting interventions, and to new structures as a continuous monitoring for the evaluation of natural aging.

Other applications are still in progress and are not reported in this thesis. In particular several historical masonry towers have been monitored and the identification process is now underway.

Concerning the complex SHM architecture, specific attention is focused in another important issue: damage detection. Recent seismic events have proved the high vulnerability of a large stock of existing buildings (e.g. precast structures, historical buildings, r.c. buildings, etc.). Damage estimation is one of the crucial aspects for the safety of people and for the health conditions of structures after a seismic event.

Through a numerical approach a methodology for damage localization and quantification has been developed (Chapter 5). The proposed method provides an important contribution for the prompt evacuation of the monitored building when the structural response exceeds the threshold set. Moreover it is capable of estimating the health conditions of a structure subjected to an earthquake, evaluating the potential immediate resumption of activities or if several retrofit interventions are necessary when a high-intensity seismic event occurs.

Future developments of this research consist in the implementation of damage detection approach using the updated F.E. model, carried out following the Ambient Vibration Survey (AVS) shown in Chapter 6.

Besides classical wired solutions, the advantages offered by Wireless Sensor Network (WSN) are shown (Chapter 7). These sensors represent the new frontier of SHM due to their flexibility and versatility. Typical drawbacks related to these sensors (e.g. synchronism, loss of data) are solved, but problems related to power consumption have to be considered. The latter aspect makes these devices particularly suitable for periodic monitoring, but not completely adequate for continuous monitoring.

Preliminary tests were carried out in a laboratory, then they were tested in a real case study. Despite the lower signal-to-noise ratio between piezoelectic sensors, the goodness of performed measurements allows the identification process. This research is intended as a contribution to a sustainable procedure for non-destructive investigation, a fundamental task for historical heritage structures.

This thesis attempts to help practitioners and researchers, providing useful guidelines for modal testing of civil structures and new starting points for measurement devices and diagnosis procedures. It is hoped that these techniques will be widely used as a powerful tool for increasing the level of knowledge of our heritage buildings.

References

[1] Farrar CR, Worden K. An introduction to structural health monitoring. Philos Trans R Soc A Math Phys Eng Sci 2010;365:303–15. doi:10.1098/rsta.2006.1928.

[2] Worden K, Dulieu-Barton JM. An Overview of Intelligent Fault Detection in Systems and Structures. Struct Heal Monit 2004;3:85–98. doi:10.1177/1475921704041866.

[3] Hejll A. Civil Structural Health Monitoring - Strategies, Methods and Applications. PhD Thesis, LULEÅ UNIVERSITY OF TECHNOLOGY, SWEDEN, 2007.

[4] Foti D, Gattulli V, Potenza F. Output-Only Identification and Model Updating by Dynamic Testing in Unfavorable Conditions of a Seismically Damaged Building. Comput Civ Infrastruct Eng 2014;29:659–75. doi:10.1111/mice.12071.

[5] Rytter A. VIBRATION BASED INSPECTION OF CIVIL ENGINEERING STRUCTURES,. AALBORG UNIVERSITY, DENMARK, 1993.

[6] Oliveira CS, Navarro M. Fundamental periods of vibration of RC buildings in Portugal from in-situ experimental and numerical techniques. Bull Earthq Eng 2010;8:609–42. doi:10.1007/s10518-009-9162-1.

[7] Isidori D. A LOW-COST STRUCTURAL HEALTH MONITORING SYSTEM FOR RESIDENTIAL BUILDINGS: EXPERIMENTAL TESTS ON A SCALE MODEL, PHD THESIS- POLYTECHNIC UNIVERSITY OF MARCHE, ANCONA, ITALY. 2013. doi:10.1017/CBO9781107415324.004.

[8] Hejll A. Civil Structural Health Monitoring. Strategies, Methods and Applications. 2007.

[9] Catbas, F.N., Kijewski-Correa, Aktan AE. Structural Identification of Constructed Systems: Approaches, Methods and Technologies for Effective Proactive of Structural Identification. 2013.

[10] Malekzadeh S. Structural Health Monitoring Using Novel Sensing Technologies And Data Analysis Methods - PhD Thesis. University of Central Florida, 2014.

[11] Allemang R.J BDL. A correlation coefficient for modal vector analysis. Proc. 1st SEM Int. Modal Anal. Conf., Orlando, FL, USA: 1982.

[12] G. De Roeck AT and ER. Damage Identification of Civil Engineering Structures Based on Operational Modal Data. Proceeding 1st Int. Oper. Modal Anal. Conf. (IOMAC), Copenhagen, Denmark: 2005.

[13] Ewins DJ. Modal Testing: Theory and Practice. Letchworth, England: 1984.

[14] Bendat, J. S.; Piersol AG. Engineering applications of correlation and spectral analysis. New York: Wiley-Interscience; 1980.

[15] Brincker, Rune; Zhang, L.; Andersen P. Modal Identification from Ambient Responses using Frequency Domain Decomposition. IMAC 18 Proc. Int. Modal Anal. Conf. (IMAC), San Antonio, Texas, USA: 2000.

[16] G. RCF. Operational Modal Analysis of Civil Engineering Structures. 2014.

[17] Ljung L. System Identification - Theory for the User. 1987.

[18] Van Overschee P, De Moor B. Subspace algorithms for the stochastic identification problem. Automatica 1993;29:649–60. doi:10.1016/0005-1098(93)90061-W.

[19] Van Overschee P, De Moor B. Subspace Identification for Linear Systems. Boston, MA: Springer US; 1996. doi:10.1007/978-1-4613-0465-4.

[20] Peeters B, De Roeck G. Stochastic System Identification for Operational Modal Analysis: A Review. J Dyn Syst Meas Control 2001;123:659. doi:10.1115/1.1410370.

[21] S. B. Teoria della predizione e del filtraggio. Pitagora E. 2000.
[22] Juang J. Applied System Identification. New Jersey, USA: 1994.
[23] Chopra A. DYNAMICS OF STRUCTURES, THEORY AND APPLICATIONS TO EARTHQUAKE ENGINEERING. PRENTICE H. NEW JERSEY: PRENTICE HALL, 2007, NEW JERSEY; 2007.
[24] Pastor M, Binda M, Harčarik T. Modal Assurance Criterion. Procedia Eng 2012;48:543–8. doi:10.1016/j.proeng.2012.09.551.
[25] Vives AA. Piezoelectric Transducers and Applications. Springer; 2008.
[26] http://www.ni.com/en-us.html n.d.
[27] MIHAI M. A Theoretical Review of the Damage Indices Used to Model the Dynamic Nonlinear Behavior of Reinforced Concrete Structures. Bul INSTITUTULUI Politeh DIN IAŞI 2013;LIX (LXIII:109120.
[28] Park YJ, Ang AH, Wen YK. Damage-Limiting Aseismic Design of Buildings. Earthq Spectra 1987;3:1–26. doi:10.1193/1.1585416.
[29] Bracci J.M., A.M. Reinhorn JBM and SKK. Deterministic Model for Seismic Damage Evaluation of Reinforced Concrete Structures, Technical Report NCEER-89-0033. State Univ. of New York, Buffalo: 1989.
[30] Kappos AJ. Seismic damage indices for RC buildings: evaluation of concepts and procedures. Prog Struct Eng Mater 1997;1:78–87. doi:10.1002/pse.2260010113.
[31] Hernandez M. Performance and Fragility Curves for Rinforced Concrete Frames and Shear Wall Residential Buildings in Puerto Rico - Ph.D. Thesis Univ. of Puerto Rico, 2007.
[32] Cosenza E, Manfredi G, Ramasco R. The use of damage functionals in earthquake engineering: A comparison between different methods. Earthq Eng Struct Dyn 1993;22:855–68. doi:10.1002/eqe.4290221003.
[33] Newmark N. M. and, E.H. R. FUNDAMENTALS OF EARTHQUAKE ENGINEERING. 1971.
[34] Banon H, Veneziano D. Seismic safety of reinforced concrete members and structures. Earthq Eng Struct Dyn 1982;10:179–93. doi:10.1002/eqe.4290100202.
[35] Roufaiel MSL, Meyer C. Analytical Modeling of Hysteretic Behavior of R/C Frames. J Struct Eng 1987;113:429–44. doi:10.1061/(ASCE)0733-9445(1987)113:3(429).
[36] Ladjinovic D, Radujkovic A, Raseta A. Seismic performance assessment based on damage of structures, Part 1: Theory. Facta Univ - Ser Archit Civ Eng 2011;9:77–88. doi:10.2298/FUACE1101077L.
[37] Cosenza E, Manfredi G. Indici e misure di danno nella progettazione sismica (in Italian), CNR-Gruppo Nazionale per la Difesa dai Terremoti - Roma, 2000, 125 pp. Roma: 2000.
[38] Park Y, Ang AH -S. Mechanistic Seismic Damage Model for Reinforced Concrete. J Struct Eng 1985;111:722–39. doi:10.1061/(ASCE)0733-9445(1985)111:4(722).
[39] Mehanny SSF DG. MODELING OF ASSESSMENT OF SEISMIC PERFORMANCE OF COMPOSITE FRAMESWITH REINFORCED CONCRETE COLUMNS AND STEELBEAMS, 12WCEE 2000 : 12th World Conference on Earthquake Engineering, Auckland, New Zealand. Stanford: 2000.
[40] Cosenza E, Manfredi G. Damage indices and damage measures. Prog Struct Eng Mater 2000;2:50–9. doi:10.1002/(SICI)1528-2716(200001/03)2:1<50::AID-PSE7>3.0.CO;2-S.
[41] McCabe SL, Hall WJ. Assessment of Seismic Structural Damage. J Struct Eng 1989;115:2166–83. doi:10.1061/(ASCE)0733-9445(1989)115:9(2166).

[42] Magliulo G, Ercolino M, Petrone C, Coppola O, Manfredi G. The Emilia Earthquake: Seismic Performance of Precast Reinforced Concrete Buildings. Earthq Spectra 2014;30:891–912. doi:10.1193/091012EQS285M.
[43] Belleri A, Brunesi E, Nascimbene R, Pagani M, Riva P. Seismic Performance of Precast Industrial Facilities Following Major Earthquakes in the Italian Territory. J Perform Constr Facil 2015;29:4014135. doi:10.1061/(ASCE)CF.1943-5509.0000617.
[44] Hejll A. CIVIL STRUCTURAL HEALTH MONITORING-STRATEGIES, METHODS AND APPLICATIONS. LULEÅ UNIVERSITY OF TECHNOLOGY, SWEDEN, 2007.
[45] Choi S, Park S, Yoon S, Stubbs N. Nondestructive damage identification in plate structures using changes in modal compliance. NDT E Int 2005;38:529–40. doi:10.1016/j.ndteint.2005.01.007.
[46] Chook G., Box PO, Chook G. STRUCTURAL ENGINEERS ASSOCIATION OF HAWAII ATC-20 Post-Earthquake Building Safety Evaluations Performed after the October 15 , 2006 Hawai ' i Earthquakes Summary and Recommendations for Improvements (updated), Report. October 2007.
[47] Kamat VR, El-Tawil S. Evaluation of Augmented Reality for Rapid Assessment of Earthquake-Induced Building Damage. J Comput Civ Eng 2007;21:303–10. doi:10.1061/(ASCE)0887-3801(2007)21:5(303).
[48] Paal, S., Jeon, J., Brilakis, I., and Desroches R, Paal SG, Jeon J-S, Brilakis I, DesRoches R. Automated Damage Index Estimation of Reinforced Concrete Columns for Post-Earthquake Evaluations. J Struct Eng 2015;141:4014228. doi:10.1061/(ASCE)ST.1943-541X.0001200.
[49] Casotto C, Silva V, Crowley H, Nascimbene R, Pinho R. Seismic fragility of Italian RC precast industrial structures. Eng Struct 2015;94:122–36. doi:10.1016/j.engstruct.2015.02.034.
[50] Worden K, Farrar CR, Manson G, Park G. The fundamental axioms of structural health monitoring. Proc R Soc A Math Phys Eng Sci 2007;463:1639–64. doi:10.1098/rspa.2007.1834.
[51] Isidori D, Concettoni E, Cristalli C, Soria L, Lenci S. Proof of concept of the structural health monitoring of framed structures by a novel combined experimental and theoretical approach. Struct Control Heal Monit 2015. doi:10.1002/stc.1811.
[52] Isidori D, Concettoni E, Cristalli C, Lenci S, Soria L. A combined experimental and theoretical approach to the SHM of structures subjected to seismic loading. Int. Conf. Noise Vib. Eng - ISMA 2012, Leuven: 2012.
[53] Pierdicca A, Clementi F, Maracci D, Isidori D, Lenci S. Vibration-Based SHM of ordinary Building: Detection and Quantification of Structural Damage - DETC2015-46763. Int. Des. Eng. Tech. Conf. Comput. Inf. Eng. Conf. - IDETC/CIE 2015, Boston (USA): 2015, p. 1–7.
[54] Hejll A, Hejll A. Civil Structural Health Monitoring. Strategies, Methods and Applications. PhD Thesis, LULEÅ UNIVERSITY OF TECHNOLOGY, SWEDEN; 2007.
[55] Vanmarcke E. H.; Fenton G. A.; Heredia-Zavoni E. SIMQKE-II: CONDITIONED EARTHQUAKE GROUND MOTION SIMULATOR 2011:http://dicata.ing.unibs.it/gelfi/software/simqke/s.
[56] MIDAS GEN. Analysis Manual 2015.
[57] Pierdicca A, Clementi F, Maracci D, Isidori D, Lenci S. Damage detection in a precast structure subjected to an earthquake: A numerical approach. Eng Struct 2016;127:447–58. doi:10.1016/j.engstruct.2016.08.058.
[58] CNR. Istruzioni per il progetto, l'esecuzione e il controllo delle strutture

prefabbricate in conglomerato cementizio e per le strutture costruite con sistemi industrializzati - CNR 10025/84 (in Italian) 1985:166.
[59] Magliulo G, Maddaloni G, Cosenza E. Comparison between non-linear dynamic analysis performed according to EC8 and elastic and non-linear static analyses. Eng Struct 2007;29:2893–900. doi:10.1016/j.engstruct.2007.01.027.
[60] Lenci S. GCFSA, Anis B, Börrnert F, Rümmeli MH, Kuntscher CA. Role of the pressure transmitting medium on the pressure effects in DWCNTs. Phys Status Solidi 2013;250:2616–21. doi:10.1002/pssb.201300062.
[61] Clementi F, Scalbi A, Lenci S. SEISMIC PERFORMANCE OF PRECAST REINFORCED CONCRETE BUILDINGS WITH DOWEL PIN CONNECTIONS. J Build Eng 2016. doi:10.1016/j.jobe.2016.06.013.
[62] Fragiadakis M. PM, FRAGIADAKIS M, PAPADRAKAKIS M. MODELING, ANALYSIS AND RELIABILITY OF SEISMICALLY EXCITED STRUCTURES: COMPUTATIONAL ISSUES. Int J Comput METHODS 2008;5:483–511. doi:10.1142/S0219876208001674.
[63] Filippou F.C. FGL, Fenves G.L. Methods of Analysis for Earthquake Resistant Structures. Eng. Seismol. TO PERFORMANCE-BASED, CAMBRIDGE UNIVERSITY PRESS, UNITED KINGDOM: 2004, p. 1–66.
[64] Spacone E, Ciampi V, Filippou FC. Mixed formulation of nonlinear beam finite element. Comput Struct 1996;58:71–83. doi:10.1016/0045-7949(95)00103-N.
[65] Martínez-Rueda JE, Elnashai AS. Confined concrete model under cyclic load. Mater Struct 1997;30:139–47. doi:10.1007/BF02486385.
[66] Dolce M, Kappos A, Masi A, Penelis G, Vona M. Vulnerability assessment and earthquake damage scenarios of the building stock of Potenza (Southern Italy) using Italian and Greek methodologies. Eng Struct 2006;28:357–71. doi:10.1016/j.engstruct.2005.08.009.
[67] D.C., Kent, and R., Park, Kent D.C. PR, D.C., Kent, and R., Park. FLEXURAL MEMBERS WITH CONFINED CONCRETE. J Struct Div 1971;97:1969–90.
[68] Filippou F.C., Popov E.P. BVV. EFFECTS OF BOND DETERIORATION ON HYSTERETIC BEHAVIOUR OF REINFORCED CONCRETE JOINTS - Report NO. UCB/EERC - 83/19. Earthq. Eng. Res. Cent., UNIVERSITY OF CALIFORNIA, BERKELEY: 1983.
[69] Newmark NM. A Method of Computation for Structural Dynamics. J Eng Mech Div 1959;85:67–94. doi:0.1016/j.compgeo.2015.08.008.
[70] Rainieri C, Fabbrocino G, Verderame GM. Non-destructive characterization and dynamic identification of a modern heritage building for serviceability seismic analyses. NDT E Int 2013;60:17–31. doi:10.1016/j.ndteint.2013.06.003.
[71] DM 2008, NTC2008. NTC2008, Decreto Ministeriale del 14.1.2008. Nuove Norme Tecniche per le Costruzioni (in Italian). 2008.
[72] Powell GH, Allahabadi R. Seismic damage prediction by deterministic methods: Concepts and procedures. Earthq Eng Struct Dyn 1988;16:719–34. doi:10.1002/eqe.4290160507.
[73] Cao V V, Ronagh HR, Ashraf M, Baji H. A new damage index for reinforced concrete structures. Earthquakes Struct 2014;6:581–609. doi:10.12989/eas.2014.6.6.581.
[74] Villaverde R, Villaverde R. Methods to Assess the Seismic Collapse Capacity of Building Structures: State of the Art. J Struct Eng 2007;133:57–66. doi:10.1061/(ASCE)0733-9445(2007)133:1(57).
[75] Grünthal G. European Macroseismic Scale 1998. vol. 15. 1998.
[76] Clementi F, Quagliarini E, Maracchini G, Lenci S. Post-World War II Italian school buildings: typical and specific seismic vulnerabilities. J Build Eng 2015;4:152–66.

doi:10.1016/j.jobe.2015.09.008.
[77] Luzi L, Hailemikael S, Bindi D, Pacor F, Mele F, Sabetta F. ITACA (ITalian ACcelerometric Archive): A Web Portal for the Dissemination of Italian Strong-motion Data. Seismol Res Lett 2008;79:716–22. doi:10.1785/gssrl.79.5.716.
[78] Pierdicca A, Clementi F, Isidori D, Concettoni E, Cristalli C, Lenci S. Numerical model upgrading of a historical masonry building monitored with a wireless sensor network. Int J Mason Res Innov 2016;1:74. doi:10.1504/IJMRI.2016.074748.
[79] Ministro dei Lavori e dei Trasporti. DM 14/01/2008 - Norme tecniche per le costruzioni (in Italian). Suppl. Ordin. Gazz. Uff. n. 29, 2008.
[80] D., Nayeri N. Masri F.S. CAG. Application of Structural Health Monitoring Tecniques to track structural changes in a retrofitted building based on ambien vibration. J Eng Mech 2007;133:1311–25.
[81] Rainieri C, Fabbrocino G. Automated output-only dynamic identification of civil engineering structures. Mech Syst Signal Process 2010;24:678–95. doi:10.1016/j.ymssp.2009.10.003.
[82] Singh JP, Agarwal P, Kumar A, Thakkar SK. Identification of Modal Parameters of a Multistoried RC Building Using Ambient Vibration and Strong Vibration Records of Bhuj Earthquake, 2001. J Earthq Eng 2014;18:444–57. doi:10.1080/13632469.2013.856823.
[83] Rainieri C, Fabbrocino G, Manfredi G, Dolce M. Robust output-only modal identification and monitoring of buildings in the presence of dynamic interactions for rapid post-earthquake emergency management. Eng Struct 2012;34:436–46. doi:10.1016/j.engstruct.2011.10.001.
[84] Foti D, Diaferio M, Giannoccaro NI, Mongelli M. Ambient vibration testing, dynamic identification and model updating of a historic tower. NDT E Int 2012;47:88–95. doi:10.1016/j.ndteint.2011.11.009.
[85] Di Cesare A, Ponzo FC, Vona M, Dolce M, Masi A, Gallipoli MR, et al. Identification of the structural model and analysis of the global seismic behaviour of a RC damaged building. Soil Dyn Earthq Eng 2014;65:131–41. doi:10.1016/j.soildyn.2014.06.005.
[86] Ragland W.S, Penumadu D. WRT. Finite element modeling of a full-scale five-girder bridge for structural health monitoring. Struct Heal Monit 2011:449–65.
[87] Isidori D, Concettoni E, Cristalli C, Soria L, Lenci S, Isidori D. A LOW-COST STRUCTURAL HEALTH MONITORING SYSTEM FOR RESIDENTIAL BUILDINGS: EXPERIMENTAL TESTS ON A SCALE MODEL, PHD THESIS-POLYTECHNIC UNIVERSITY OF MARCHE, ANCONA, ITALY. Polytechnic University of Marche - Ancona (Italy), 2013. doi:10.1017/CBO9781107415324.004.
[88] Concettoni E, Isidori D, Cristalli C, Giammarini M, Fioravanti M, Lenci S. Wireless sensor network for SHM system of ordinary buildings in seismic hazard zones. 7th Int. Conf. Struct. Heal. Monit. Intell. Infrastruct. - SHMII 2015, 2015.
[89] Ramos LF, Marques L, Lourenço PB, De Roeck G, Campos-Costa A, Roque J. Monitoring historical masonry structures with operational modal analysis: Two case studies. Mech Syst Signal Process 2010;24:1291–305. doi:10.1016/j.ymssp.2010.01.011.
[90] D.P.C.M. Valutazione e riduzione del rischio sismico del patrimonio culturale con riferimento alle Norme tecniche per le costruzioni di cui al decreto del Ministero delle infrastrutture e dei trasporti del 14 gennaio 2008. S.O. n. 217/L (in italian) 2011:86.

[91] Milani G, Valente M. Comparative pushover and limit analyses on seven masonry churches damaged by the 2012 Emilia-Romagna (Italy) seismic events: Possibilities of non-linear finite elements compared with pre-assigned failure mechanisms. Eng Fail Anal 2015;47:129–61. doi:10.1016/j.engfailanal.2014.09.016.
[92] Acito M, Bocciarelli M, Chesi C, Milani G. Collapse of the clock tower in Finale Emilia after the May 2012 Emilia Romagna earthquake sequence: Numerical insight. Eng Struct 2014;72:70–91. doi:10.1016/j.engstruct.2014.04.026.
[93] Betti M, Orlando M, Vignoli A. Static behaviour of an Italian Medieval Castle: Damage assessment by numerical modelling. Comput Struct 2011;89:1956–70. doi:10.1016/j.compstruc.2011.05.022.
[94] Akhaveissy a. H, Milani G. Pushover analysis of large scale unreinforced masonry structures by means of a fully 2D non-linear model. Constr Build Mater 2013;41:276–95. doi:10.1016/j.conbuildmat.2012.12.006.
[95] Alvandi A, Cremona C. Assessment of vibration-based damage identification techniques. J Sound Vib 2006;292:179–202. doi:10.1016/j.jsv.2005.07.036.
[96] ELLIS BR. Non-destructive dynamic testing of stone pinnacles on the palace of Westminster. Proc ICE - Struct Build 1998;128:300–7. doi:10.1680/istbu.1998.30464.
[97] Pieraccini M, Dei D, Betti M, Bartoli G, Tucci G, Guardini N. Dynamic identification of historic masonry towers through an expeditious and no-contact approach: Application to the “Torre del Mangia” in Siena (Italy). J Cult Herit 2014;15:275–82. doi:10.1016/j.culher.2013.07.006.
[98] Mordini A, Savov K, Wenzel H. The Finite Element Model Updating: A Powerful Tool for Structural Health Monitoring. Struct Eng Int 2007;17:352–8. doi:10.2749/101686607782359010.
[99] Betti M, Vignoli A. Modelling and analysis of a Romanesque church under earthquake loading: Assessment of seismic resistance. Eng Struct 2008;30:352–67. doi:10.1016/j.engstruct.2007.03.027.
[100] Minghini F, Milani G, Tralli A. Seismic risk assessment of a 50m high masonry chimney using advanced analysis techniques. Eng Struct 2014;69:255–70. doi:10.1016/j.engstruct.2014.03.028.
[101] Parloo E, Guillaume P, Cauberghe B. Maximum likelihood identification of non-stationary operational data. J Sound Vib 2003;268:971–91. doi:10.1016/S0022-460X(03)00377-8.
[102] Parloo E. Application of frequency-domain system identification techniques in the field of operational modal analysis. Vrije Universiteit Brussel, Belgium, 2003.
[103] Jeary a. P. Damping in structures. J Wind Eng Ind Aerodyn 1997;72:345–55. doi:10.1016/S0167-6105(97)00263-8.
[104] Bayraktar A, Türker T, Altunişik AC. Experimental frequencies and damping ratios for historical masonry arch bridges. Constr Build Mater 2015;75:234–41. doi:10.1016/j.conbuildmat.2014.10.044.
[105] Circolare Ministeriale n. 617. Cons. Sup. LL. PP., “Istruzioni per l’applicazione delle Nuove Norme Tecniche per le Costruzioni” di cui al decreto ministeriale del 14.01.2008. G.U. del 26.02.2009 n. 47, supplemento ordinario n. 27. (in Italian) 2009.
[106] Isidori D, Pierdicca A, Concettoni E, Cristalli C, Angeloni J, Clementi F, et al. Structural health monitoring applications with wireless sensors on an historical masonry building. XXII Congr. AIMETA - Assoc. Ital. di Mecc. Teor. e Appl., Genova, Italy: 2015.

[107] Aras F, Krstevska L, Altay G, Tashkov L. Experimental and numerical modal analyses of a historical masonry palace. Constr Build Mater 2011;25:81–91. doi:10.1016/j.conbuildmat.2010.06.054.
[108] Friswell MI, Mottershead JE. Finite Element Model Updating in Structural Dynamics. vol. 38. Dordrecht: Springer Netherlands; 1995. doi:10.1007/978-94-015-8508-8.

Publications

PIERDICCA A, CLEMENTI F., ISIDORI D., E. CONCETTONI, C. CRISTALLI, LENCI S. (2015).
"Numerical model upgrading of an historical masonry palace using wireless sensor network"
International Journal of Masonry Research and Innovation (IJMRI)
DOI:10.1504/IJMRI.2016.074748.

PIERDICCA A, CLEMENTI F., ISIDORI D., ANGELONI J., LENCI S. (2015).
"Structural health monitoring applications with wireless sensors on an historical masonry building"
XXII Conference - The Italian Association of Theoretical and Applied Mechanics, Polytechnic School (AIMETA)- Facilities of Architectural Science - University of Genova

PIERDICCA A, CLEMENTI F., MARACCI D., ISIDORI D., LENCI S. (2015).
"Vibration-based shm of ordinary buildings: detection and quantification of structural damage"
15th International Design Engineering Technical Conferences and Computers&Informations in Engineering Conference IDECT/CIE 2015, Boston, Massachusetts, USA

PIERDICCA A, CLEMENTI F., MARACCI D., ISIDORI D., LENCI S. (2015).
"Vibration-based shm of ordinary buildings: detection and quantification of structural damage"
7th International Conference on Structural Health Monitoring of Intelligent Infrastructure in Turin – Italy.

PIERDICCA A, CLEMENTI F., MARACCI D., ISIDORI D., LENCI S. (2016).
"Damage detection in a precast structure subjected to an earthquake: a numerical approach" Stochastic Mechanics – Meccanica Stocastica 2016, June 2016, Capri - Italy

PIERDICCA A, CLEMENTI F., MARACCI D., ISIDORI D., LENCI S. (2016).
"Damage detection in a precast structure subjected to an earthquake: a numerical approach" Engineering Structures – ENG STRUCT Elsevier
DOI 10.1016/j.engstruct.2016.08.058

PIERDICCA A, CLEMENTI F., MEZZAPELLE P., FORTUNATI A., LENCI S. (2017).
"One-year monitoring of a reinforced concrete school building: Evolution of dynamic behavior during retrofitting works" - submitted
X International Conference on Structural Dynamics, EURODYN 2017